Emergence of Spatio-Temporal Pattern Formation and Information Processing in the Brain

by

Elizabeth A. Shtrahman

A dissertation submitted in partial fulfillment
of the requirements for the degree of
Doctor of Philosophy
(Applied Physics)
in the University of Michigan
2015

Doctoral Committee:

Professor Michal R. Zochowski, Chair
Assistant Professor Sara J. Aton
Associate Professor Victoria Booth
Associate Professor Jennifer P. Ogilvie
Professor Duncan G. Steel

ACKNOWLEDGEMENTS

I would like to thank my committee for their comments and edits to my dissertation. I would also like to thank all the people who encouraged me throughout graduate school not to give up. My advisor, labmates, friends, and family were invaluable and I could not have finished if it weren't for their support and kindness. They all motivated me in different ways, and forced me to keep my stress and frustrations in perspective.

Thank you, Michal, for teaching me to look for patterns in complex data and to think about the simplest measures for quantifying those trends. From you, I learned how to approach and understand complicated problems with the simplest ideas. I think that these skills will be invaluable in my future research. I really appreciate how much you care about your students' success and future, and how you were always willing to help, even at the last minute.

Everyone in the Zochowski lab was not only a great labmate, but also a great friend. They were always happy to stop to explain something or think about a problem. I learned a lot about programming from Dan Maruyama and Chris Fink. Sarah Muldoon (Feldt) taught me how to make dissociated cultures and to run the lab. Eva Olariu helped me above and beyond to take care of the cell cultures. James Roach always provided entertainment in addition to keeping us honest with the facts from biology. Sima Mofakham, I will miss our coffee breaks. Thanks Sima, for being a true friend to confide in, and for always summarizing the trends in my life with graphical representations.

Alex Toulouse, Dave Anderson, and the many Brickhouse roommates throughout the years, you feel like family. Grad school would have be torture without you. As for my

biological family, thanks for loving me no matter what. Thanks for worrying even when you shouldn't, and for always trying to make my life as easier than yours has been.

Also I'd also like to thank Nicole, my yoga teacher, for teaching me to breathe and relax when life gets uncomfortable, and of course the baristas at Mighty Good Coffee, for making great lattés and for providing the happy environment where I wrote the majority of this dissertation.

TABLE OF CONTENTS

LIST OF FIGURES

Figure

LIST OF ABREVIATIONS

AMD	average minimum distance
AMPA	α-amino-3-hydroxy-5-methyl-4-isoxazolepropionic acid
ATP	Adenosine triphosphate
BGA	18-β glycyrrhetinic acid
Ca2+	calcium
CC	cross correlation
DIV	days in vitro
DMSO	dimethyl sulfoxide
EEG	electroencephalography
ER	endoplasmic reticulum
EPSP	excitatory postsynaptic potential
FCA	Functional clustering algorithm
fMRI	functional magnetic resonance imaging
GABA	gamma-aminobutyric acid
GFAP	glial fibrillary acidic protein
GPCRs	G protein coupled receptors
HGG	high glial groups
IPSP	inhibitory postsynaptic potential
IP3	inositol trisphosphate

LGG	low glial group
LGN	lateral geniculate nucleus
LFP	local field potentials
MEA	micro-electrode arrays
MPC	mean phase coherence
NMDA	N-methyl-D-aspartate receptor
SR101	sulforhodamine 101
TTX	tetrodotoxin

Chapter I.

Introduction-Emergence in the Brain

In many systems, complex global patterns can form and evolve from the underlying interactions between large numbers of simpler entities. This phenomenon is referred to as emergence. However, there is ambiguity in its precise definition. In general emergence is the existence of a global macroscopic property, behavior, or structure that is formed within a system as a result of interactions between its microscopic constituent parts[1–3]. These interactions are essential, and emergent phenomena cannot be understood from studying the microscopic components alone in isolation[4]. Systems exhibiting emergence typically form complex global patterns and maintain ordered structure without external manipulation or control[5]. The large-scale structures arise out of the collections of interacting components alone. The local interactions between components can be attractive (or more generally when the units tend to become more similar) or repulsive (i.e. pushing the units' state further apart) and are often nonlinear[6]. The feature of order arising without an external orchestrator is the quality of self-organization[1,7]. Unfortunately, the physics of nonlinear systems driven far from thermodynamic equilibrium, where rich emergent behavior often forms, is poorly understood[8].

While defining emergence many researchers have pointed out instead the following necessary features of a system in order for emergence to occur. The system is composed of a large number of simple units[7,9,10]. Units interact with each other through sets of local rules[7,9,10]. Each individual unit is not "aware" of the whole system; it only receives

information locally and can only function according to its interaction rules. Some have proposed that there must be some mechanisms that transcend scales, leading to nonlinear effects beyond the level of individual system components. I will argue that these mechanisms that coordinate collections of components across spatial and temporal scales are the key features to understanding emergence.

There are many examples of emergent phenomena across vastly different systems, from collections of molecules to collections of living organisms. The order can be spatial such as in the arrangement of water molecules in snowflakes, or it can be temporal such as in the flashing of fireflies in unison[8]. There are many examples of emergence and self-organization in biological systems. Colonies of ants can build underground structures and complex networks of tunnels[11]. Some species can even assemble themselves to make bridges or form rafts to escape floods. Amoeba can aggregate to form a multicellular slug, which can migrate and function as a single organism[12]. Starlings organize in flocks and form mesmerizing shapes and patterns, which evolve as the flock propagates through the sky seemingly as one cohesive unit[13].

The brain is another example of a system with emergent phenomena. The brain contains an astronomical number of components, individual discrete cells called neurons[14] and glial cells. Neurons are thought to be the main computational units in the brain. They are densely connected to each other through junctions called synapses, which couple neurons through chemical and electrical signals. Collections of neurons in the brain are the substrate for producing thoughts, perceptions, and emotions. The brain is the source of creativity to produce great works of art or calculus, and ultimately self-awareness and even consciousness. Thus here neurons form the substrate of emergent phenomena and their self-organization on a macroscopic scale that leads to cognitive phenomena is its outcome.

We now can identify specific brain regions responsible for various cognitive phenomena. Using functional magnetic resonance imaging (fMRI), which measures brain activity through detecting associated changes in blood flow, brain regions can be correlated with cognitive functions. Historically, much of our knowledge for correlating specific anatomical regions to specific cognitive functions came from patients with well-characterized lesions or injuries. A notable example is the case of patient H.M. who had his hippocampus surgically removed as a treatment for epilepsy, and as a result lost the ability to form new long-term memories. Other regions such as the visual cortex are required for visual perception, and even a particular region, the fusiform gyrus, is important for the ability to recognize faces[15]. We know that sensory information is routed and processed through different areas in the brain, and we form internal representations of the world outside of our bodies. Based on memories of previous experiences, our brain makes predictions, decisions, and coordinates all behaviors necessary for our survival.

However, we have no understanding of the mechanisms for how a particular region, or interactive regions, in the brain encodes for information and how complex information processing arises from the interactions between neurons. The intermediate scale between individual neurons and cognition is the spatio-temporal patterns of electrical activity produced by collections of interacting neurons. Thus we seem to have identified the simple building blocks for emergence, we can to some degree understand its outcome, however we do not understand the mechanisms that generate it. We are not even sure what types of mechanisms we are looking for, and in to what types of domains they fall, i.e. are they dynamical processes described by the physics of complex systems, or are they mediated by biological entities that somehow integrate the neuronal activity. Many for example have proposed the idea that the synchronization of neuronal activity is a potential mechanism to

dynamically bind together information; this is known as the correlation hypothesis.[16,17] Implementation of these mechanisms must explain how the brain can perform multiple computations simultaneously in segregated brain regions, and how this information gets routed and bound together to give rise to coherent perceptions and actions.

The focus of this dissertation is on various interactions that can facilitate emergence of higher order brain function. Mechanisms that couple and coordinate collections of neurons and their activity, potentially causing interactions across spatial and temporal scales, can underlie the powerful computational capabilities that emerge in the brain. Before I expand on these mechanisms I will discuss the major building blocks that are known to underlie brain function, and put them into context of their role in emergence.

1.1 Neurons: (Relatively) Simple Units that obey Local Rules

From the perspective of the ingredients required for emergence, the simple units in the brain are neurons. The most prominent feature of neurons relevant for understanding brain function is that they are excitable cells that can respond to stimuli with electrical signaling. Individual neurons interact with each other through propagation of these electrical signals, and obey local rules to perform computations.

The ability to connect and interact with other neurons is achieved through physical connections. Unlike other cells in an organism, the cell bodies of neurons, called somas, have processes, axons and dendrites, which physically extend across distances ranging from microns to meters and form connections to other neurons at synapses[18]. Neurons can propagate electrical spikes, called action potentials, to other neurons through changes in their membrane voltage. Action potentials are caused by voltage gated ionic channels (predominantly for sodium and potassium ions), which are present throughout neuronal

membranes, and regulate the flow of currents across their membrane[18]. The (presynaptic) neuron sends an action potential to the receiving (postsynaptic) neuron. Once it is initiated in the soma, the voltage spike travels down the axon to synapses, where vesicles containing chemical messengers are released from the presynaptic neuron[18]. The chemical messengers are called neurotransmitters, and they diffuse across the synaptic cleft, the tens of nanometer gap between neurons, and bind to receptors on the postsynaptic terminal, inducing current to flow into the dendrite of the postsynaptic neuron. The soma of the postsynaptic neuron receives current input through their dendrites, and if the voltage at the soma crosses threshold the neuron (at the hillock) will initiate an action potential to send to its synaptic connections[18]. Typically, the spike appears as a brief (approximately 1 millisecond) depolarization of about 100 mV, and is depicted in Figure 1.1. The amplitude, shape, and duration of an action potential are generally conserved for a given neuron.[18] Therefore, a spike is typically treated as an all or none event, and it is generally assumed that information is encoded in the series of action potentials over time, but the exact nature of this code is unknown and likely varies.

In contrast to synaptic interactions, where a single neuron interacts with a single post synaptic neuron, neuromodulation is the process where groups of neurons release chemical modulators that diffuse through large areas and influence the excitability of multiple specific types of neurons[18]. Where synaptic coupling between neurons elicits spiking, neuromodulation modulates the ongoing spiking in a region of the brain. Neuromodulators have diverse and sometimes multiple roles. For example, neuromodulation with dopamine has been linked to motor control, arousal, and reward.[19,20] Acetylcholine, norepinephrine and serotonin levels vary across wake and sleep states.[21] Acetylcholine has been implicated in other functions as well, such as having a role in

attention.[22–24] The ability for neurons to influence the activity in large regions is another mechanism that may link patterns of neuronal activity across spatial and temporal scales.

Through these mechanisms an individual neuron has the ability to receive current input from neurons that synapse onto its dendrites, and based on that input, send voltage spikes to the synapses it makes onto other neurons. We have understanding of the processes that allow neurons to interact and send signals to each other at synapses. In the next section, I will focus on describing the mechanisms that allow neurons to interact with each other, directly linking these interactions with the emergence of function across spatial and temporal scales.

The Synapse: Local Rules that Couple Neurons

Neurons are able to influence action potential firing in other neurons primarily through their synaptic contacts. Synapses are junctions that couple neurons, either in an excitatory or inhibitory manner, and have a strength associated with this interaction. The rules of coupling between neurons result in the effect that the presynaptic neuron can either increase or decrease the probability of the postsynaptic neuron to send an action potential[18]. The rules that determine the coupling interaction depend on the type of presynaptic neuron, neurotransmitters, and receptors of the postsynaptic neuron[18].

The type of neurotransmitters released at a synapse varies depending on the type of neuron. Excitatory neurons, express excitatory neurotransmitters such as glutamate. Inhibitory neurons release inhibitory neurotransmitters such as gamma-aminobutyric acid (GABA) and glycine. Neurotransmitters bind to particular types of receptors, and allow ions to flow into the postsynaptic dendrite. Depending on the type of neurotransmitters released and the receptors they bind, either positive or negative charged ions to flow into or out of

the postsynaptic dendrite, which causes either a depolarizing excitatory postsynaptic potential (EPSP) or hyperpolarizing inhibitory postsynaptic potential (IPSP) at the postsynaptic neuronal membrane. At rest, the voltage across a neuronal membrane is approximately -70 mV. Neurons initiate an action potential when their voltage depolarizes across a threshold, typically around -40 mV. Therefore, current that depolarizes the membrane, is excitatory, and increases the probability that the postsynaptic neuron will cross its threshold and send an action potential to its synaptic partners. Hyperpolarizing current is inhibitory, and decreases the probability the postsynaptic neuron will cross threshold and transmit information to the downstream synaptic partners[18].

Depending on the type of receptor there are two main mechanisms to achieve current influx, and each has an associated timescale. Ionotropic receptors such as (AMPA) have fast kinetics and allow ions to flow due to a conformational change in the receptor, which physically creates a channel for ions to flow across the membrane[18]. Metabotropic receptors, such as metabotropic glutamate receptors (mGluRs) have slower kinetics, and act through second messenger biochemical cascades[18]. These two receptor types control coupling over drastically different timescales, potentially providing the means to influence communication over temporal and spatial scales.

Synaptic Plasticity: Coupling Between Neurons is Dynamic

The strength of synaptic coupling, or the size of the postsynaptic potentials induced by an action potential in the presynaptic neuron is not fixed. In 1949, Hebb postulated that correlated activity between neurons leads to increased synaptic strength.[25] Years later it was found that the relative timing between presynaptic and postsynaptic spiking between pairs of neurons determined whether synapses were strengthened or weakened[26]. The change in synaptic efficacy can be caused by several cellular changes, from the probability

that neurotransmitter filled vesicles are released at a synapse to the number and density of receptors on the postsynaptic terminal[18]. Formation of new synapses can also be induced from activity, or pruning of weak synapses is possible as well[18,27]. This change in strength of the coupling between neurons is referred to as synaptic plasticity, and it is thought to be the cellular mechanism underlying learning and memory.

1.2 The Brain as a Complex Network: Structural and Functional Connectivity

As I have described in the previous sections, the brain is composed of dynamical units (neurons), whose strength of interactions (synaptic coupling) is irregular and dynamically evolving in time (plasticity). The human brain has approximately 10^{11} neurons, and each neuron make approximately 10^{4} synapses onto other neurons, forming a complex network[18]. One can think of networks as the first emergent layer in the brain, as their properties cannot be directly derived form the properties of their constituents. Network properties can be described both structurally, by the statistics of the physical connections, and also functionally, by the correlations between network components and their emergent properties.

The structural network topology is the arrangement of physical connections between neurons. Functional connectivity is based purely on the coincidence of firing and is defined by statistical correlations in the activity patterns. Therefore, two neurons that are not synaptically coupled may still be functionally correlated and these functional relationships can be transient and dynamic. Network structures, as I will describe in the following section, determine pattern formation and the synchronization properties among the network components. Functional network properties are emergent from the time evolution of the activity patterns in the network and synchrony or coordination of patterns.

Network Structures and Pattern Formation

The structure of a network plays a crucial role in determining the emergence of pattern formation and complex dynamics. Network structure affects the propagation of activity between neurons, and the resulting spatio-temporal activity patterns[28,29]. Network dynamics can transition between various regimes based on changes in network topology alone, for example it can evolve from wave propagation to network wide synchrony due to varying the connectivity from purely local to purely random[29]. Therefore, the physical network structure influences the spatio-temporal patterns of activity.

To quantify network structures, it is useful to apply concepts from graph theory, a field of mathematics, which describes networks as composed of nodes and connections between nodes, called edges. Different network topologies have been shown to be more effective at routing and transmitting information. For example, the small-world topology[30] refers to networks in which the average shortest path length (number of edges) between nodes increases proportionally to the logarithm of the number of nodes in the network. The small world connectivity implies that there is no singular region where all information converges and could orchestrate the network activity. Another type of network structure is scale free topology[31], where the fraction of nodes with k edges is proportional to a power law dependence of k. Thus, scale free topology implies the presence of few highly connected nodes in the network called hubs, which could result in an effective design to orchestrate synchronization.

In the human brain, we have understanding of the gross anatomical regions and pathways, but the exact structural connectivity of the human brain and that of other

mammals remains largely unknown. It is not even clear on what scale the details of network connectivity are most pertinent (i.e. individual neurons, individual layers, individual modalities). The nervous systems of simpler organisms have been studied and the connections have been mapped for the 302 neurons in the roundworm Caenorhabditis elegans. The neural network of the roundworm has been shown to be a small-world network[30]. Whether or not the connectivity of neuronal networks of more complex organisms is also small-world is controversial. There has been competing evidence in several in vitro studies that brain networks may follow a scale-free topology[32,33]. However it remains to be verified which topologies are actually present in the exact anatomical connectivity in vivo of complex brains.

Functional Cell Assemblies

The central question becomes: How are the large scale patterns formed? The timescale for anatomical changes in the network connectivity due to plasticity are on the order of minutes[34], while the timescale for forming perceptions is on the order of hundreds of milliseconds[35]. Therefore the neural substrates of representations cannot rely on purely anatomical connectivity changes in the network. The aspects of the representation must be transient, dynamic, and able to adapt to changing information. A possible coding strategy is that neural dynamics allow for self-organization of the spatio-temporally evolving activity patterns of functional cell assemblies on an anatomically fixed network. Learning modifies the physical network but functional ensembles dynamically arise on shorter time scales. Donald Hebb was one of the first to propose that the spatio-temporal activity patterns in groups of brain cells form the representations of information in the nervous system[25]. Growing evidence supports this theory that emergent functional neuronal circuits underlie the computational abilities of the brain[36]. Recent work has found that cortical activity is

dominated by coactive groups of neuronal ensembles, and this has been shown for V1 an area of the visual cortex in both the presences and absence of visual input.[36] The members of these functional assemblies are flexible and cannot be accounted for by the independent firing properties of individual neurons.[36] Understanding how the firing properties of individual neurons and collections of neurons in functional assemblies code for information will be explored in the following section.

1.3 From Networks to Emergent Functions: Neural Coding

Networks of neurons and, possibly, glia self organize to form the complex spatio-temporal patterns that underlie cognitive functions. Information about a stimulus is encoded in the patterns of action potentials over time. We have some understanding on how networks of various cell types facilitate pattern formation in the brain. However, what aspects of this patterning represent the information content? Two main theories on neural coding dominate: rate coding and temporal coding.

Rate Code vs. Temporal code

The activity of individual neurons and groups of neurons has a quantifiable relationship to sensory representations and behavioral outputs. In rate coding, the sequence of action potentials encodes information based on increases in the number of spikes per time window or spike rate. This is most easily observed in experiments where neurons increase their firing rate in response to a salient aspect of sensory input or motor outputs, and this has been recorded in many experimental paradigms. For example, single neurons in the visual system increase their firing rates in response to specific spatial orientations of a visual bar, or the velocity of a moving visual grating in specific regions of the visual field[37]. Auditory neurons are tuned to respond to particular frequencies of sound[38].. Place cells in the rodent hippocampus increase their firing rate when the animal is

traversing in a particular spatial location[39]. Motor neurons control the movement of muscles and do so using a rate code, where the strength at which the innervated muscle is flexed depends on the firing rate of the motor neuron[40]. These examples show there are numerous observations to supports that information can be encoded in the mean firing rates of neurons, however there could also be information encoded in more complex statistical features of the patterns of action potentials.

In a temporal coding scheme, on the other hand, the coding is based on the precise timing of single action potentials within a sequence. Single neurons have been shown to temporally encode information in the primary visual system encoding complex visual patterns[41,42], and in the auditory cortex of cats encoding sound source localization[43]. Temporal encoding has been observed across small ensembles of neurons in the frontal cortical areas of the primate brain, where very precise patterns on the timescale of a few milliseconds were shown to correlate with specific behavioral situations.[44] Even larger assemblies of neurons have been shown to have complex response patterns. For example in the olfactory bulb of the rabbit, dynamical patterns of ensembles of neurons were correlated with the perception of different odorants.[45] These larger ensemble patterns were obtained through electroencephalography (EEG) recordings. The fact that coordinated activity can be recorded extracranially implies a high degree of synchrony in the activity of neurons to produce the signals observed. Large populations of neurons must act together in time to generate outputs synchronously.

Our perceptions that emerge out of these distributed activity patterns tend to group and interpret objects as related if they have similar features or are contiguous in space or time[46]. In the Temporal Correlation hypothesis, the functional role of synchrony has been proposed as mechanism to bind neuronal activity, and underlie feature binding and

perceptual grouping[16,47]. This theory does not rule out the relevance of both a rate and temporal coding scheme. The increased firing rates of individual neurons can be dynamically modulated in their synchrony within different cell assemblies over time.

We still do not understand the anatomical and physiological constraints that enable these codes to propagate through networks and form the basis for computations. However the exact nature of patterns of spikes encodes for information, the information needs to be interpreted and transmitted to downstream synaptic connections. How do neurons respond to increased firing rate or temporal coordination? What is the biological implementation of these coding schemes and how it propagates? Organisms must interpret information from these coding schemes. How do downstream neurons to which the population projects, read and encode information? One must be able to explain how the organism could estimate these input firing rates from observation of the action potential patterns in real time of its own neurons.

Combining rate and timing: a role of Resonance?

How neurons respond to rate or temporal structure of its inputs is dependent on the biophysical properties of individual neurons. In the central nervous system, neuronal spiking is generally not the result of a single synaptic event. A typical excitatory postsynaptic depolarization is on average 0.55 mV,[48] while the depolarization required to cross threshold is on the order of 10s of millivolts. Therefore, whether a neuron fires an action potential reflects a spatiotemporal integration over a range of inputs.

So far we have considered neurons as simple components that integrate input from their presynaptic connections, and send action potentials when their membrane voltage depolarizes across a threshold. The spike is a simple all or none and discrete event.

However, as I already mentioned before, individual neurons have complex dynamics governed by the specific expressions of ion channels, and the integration of input to reach threshold can be complex. Neurons are capable of more than a simple input-output relationship of increasing their firing rate with stronger stimulus strength. The specific current and governed by channels expressed lead to active membrane properties, and give the neurons the ability to shape incoming stimuli. Therefore, how a neuron responds to input depends on intrinsic electroresponsive properties of that neuron, and will affect whether a neuron will depolarize to cross threshold for a particular input.

There are two types of intrinsic electroresponsive properties: integrators and resonators, shown in Figure 1.2. After an integrator receives an input pulse, the voltage exponentially converges back to the rest state. If a second pulse is received, the shorter the distance between the two pulses is, the more likely the neuron is to reach threshold and fire an action potential. Therefore, integrators perform temporal integration of inputs and respond preferentially to higher frequency input[49].

Resonators have oscillating membrane potential, which gives them sensitivity to the timing of input. An oscillator will resonate or increase its amplitude when the driving frequency matches its intrinsic oscillatory frequency[49]. The ability to resonate is a familiar phenomenon in the physical systems of driven oscillators. The only required components are an oscillator and a driving input, which are both found in the brain. Neurons can have subthreshold oscillatory membrane pontentials[50,51] and can be driving by oscillatory synaptic input.

During the oscillation the distance to threshold is changing. Therefore, the timing of an input pulse relative to the phase of the membrane oscillation will determine if the cell

reaches threshold and fires a spike. Therefore, resonators are sensitive to the timing of a stimulus, and respond to inputs whose frequency is in resonance with the frequency of the sub-threshold membrane oscillation[49]. Both integrator and resonators have been observed in cortical neurons. For example, some cortical fast spiking interneurons have resonator properties and some cortical regular spiking neurons have integrator properties[52]. Additionally, individual neurons have been shown to switch between types[53].

The presence of sub-threshold membrane oscillations is due to multiple possible ionic mechanisms that are responsible for compensating changes in current flow. Additionally, the frequency of which neurons can oscillate and therefore resonate can vary based on the voltage across the membrane[54,55]. The mechanisms underlying voltage dependent resonance shifts are not completely understood. However in some cell types they have been linked to particular currents[54,55]. The voltage dependence of resonance frequency preference is a feature of neurons that I will expand on in Chapter V. There, I will show work that links single neuron resonance shift properties and network connectivity to propose a potential mechanisms to coordinate groups of neurons in their spatio-temporal activity patterns, which could bind populations of neurons while segmenting them from the rest of network they are embedded in.

Astrocyte Networks: Another Layer of Network Complexity

Another potential source involved in coordinating activity of neurons is through interactions with another type of cell in the brain. Neurons are outnumbered by glial cells, whose exact function remains controversial[56]. Unlike neurons, early experiments on glial cells found only passive membrane currents[57]. This lead to the view that due to their excitability, neurons are the computational units of the brain, while silent glial cells were

thought to provide primarily structural and metabolic support for neurons. However, recent work suggests that glia may be active participants in brain information processing.

Findings that glial cells contain G protein coupled receptors (GPCRs) enable a wide array of intracellular signaling pathways in glia[57]. GPCRs are transmembrane protein receptors that bind molecules outside of the cell to activate intracellular cascades, which lead to a variety of glial cell responses. One of the most studied downstream effects of GPCR activation is the elevation of intracellular calcium (Ca^{2+}) concentration. Calcium is involved in many pathways such as the release of various signaling molecules, a process called gliotransmission[57].

Astrocytes are the most predominant type of glial cell in the central nervous system, and their morphology allows them to contact neurons. It has been estimated that one astrocyte cell can contact up to 10^5 synapses[57], and they physically ensheathe and wrap their processes around the synapses between neurons. Neurotransmitters released from neurons have been shown to activate GPCRs in astrocytes[58]. Through calcium-mediated excitability, astrocytes can release signaling molecules, which can feedback to interact with neurons, modulating neuronal excitability and synaptic plasticity. This leads to a new notion of a synapse, named the tripartite synapse,[59] depicted in Figure 1.3. A synapse is not just the connection between a presynaptic and a postsynaptic neuron, but also interaction with an astrocyte must be considered in order to understand plasticity on the cellular and network levels.

Not only do astrocytes interact with neurons and potential play crucial roles in modulating individual synapses, but also astrocytes are able to interact with other astrocytes. Astrocytes couple to adjacent astrocytes through direct connections called gap

junctions, and form a cellular network of glial cells. Small molecules can diffuse passively through gap junction, and it has been shown that calcium activated release of the molecule inositol trisphosphate (IP_3) is involved in the communication between gap junction coupled astrocytes[60]. Gliotransmission from astrocytes not only interacts with neurons, but can also activate GPCRs on other astrocytes. This signaling between astrocyte networks results in a complex and poorly understood set of interactions between astrocytes themselves and with neuronal networks. Moreover, the timescale for an action potential in a neuron is on the order of milliseconds, while the timescale for calcium signaling in an astrocyte is on the order of seconds. Therefore interactions with astrocyte networks provide a potential mechanism to integrate and modulate activity in large populations of neurons transcending across time scales, which potentially has a role in understanding computation in the brain.

1.4 Outline

The following chapters will expand on mechanisms that can facilitate the emergence of network-wide activity patterns that potentially underlie information processing in the brain. First in Chapter II, I will describe the experimental and computational methods utilized in this work to probe the coordination of spatio-temporal network activity patterns. I will discuss using dissociated cell cultures as an experimental system to study network dynamics, and the electrophysiological and imaging techniques that will be implemented in the following chapters. I will also describe computational approaches for simulating neurons and networks in order to study emergence of spatio-temporal activity patterns.

In Chapter III, I will investigate communication in networks of dissociated cultured cells of neurons and glia. I will show results from calcium-imaging experiments, where we study the coupling in glial network, specifically between astrocytes a type of glia, and quantifiy how perturbing the coupling between astrocytes influences the astrocytic activity

patterns. To gain insight into understanding the emergence of spatiotemporal pattern formation in astrocyte network signaling, we compare several properties of the network patterning with a simple model that incorporates the two mechanisms of astrocyte coupling: gap junction coupling (active coupling) and diffusive coupling of extracellular chemical release (passive coupling). We showed that gap junctions and extracellular chemical release interact in astrocyte networks to modulate the spatial temporal patterns of their calcium dynamics and reproduce patterning results with the simple model. This work is currently prepared for publication.

In Chapter IV, I will go on to study the interaction between neurons and glial cell networks and how glial networks modulate neuronal dynamics and synchrony over network development. I will discuss experiments where we applied large-scale pharmacological manipulations of glial networks in dissociated primary neuronal and glial co-cultures grown on microelectrode arrays. To identify the effect of glial networks on neuronal activity, we quantified changes in the functional connectivity of the neuronal network activity by implementing a novel clustering algorithm (FCA) which groups neurons with statistically correlated activity patterns. We show an interaction between the glial and neuronal networks present in dissociated cultures, and that glial networks influence the coordination and synchrony among populations of neurons. This work[61] was published in Physical Biology in 2010.

Both chapters III and IV, are projects where the interactions that facilitate emergence of neuronal functional assemblies are provided by coupling with glial cell networks, and particularly with calcium signaling in astrocytes. In chapter V, I investigate an entirely different mechanism for coordinating ensembles of neurons. I will show results of a computational model that shows how biophysical resonance shifts in individual

neurons can interact with the network topology to influence pattern formation and separation. We show that sub-threshold neuronal depolarization can shift neurons into and out of resonance with specific bands of existing extracellular oscillations, and this can act as a dynamic readout mechanism during information storage and retrieval. We propose this resonance shift is a possible mechanism for the selective activation of regions of a network, necessary for neuronal information processing. This work was submitted for publication to Nature Scientific Reports and is currently under review after resubmitting with revisions.

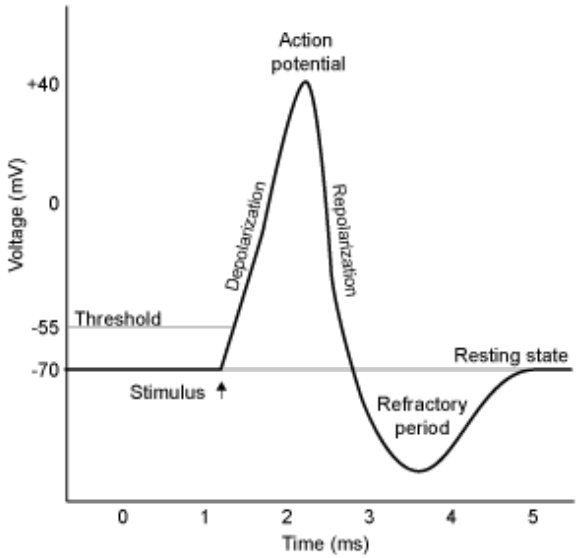

Figure 1.1 Schematic of the voltage over time for an action potential. The action potential is initiated when the stimulus depolarizes the resting state voltage across threshold. Voltage gated ion channels regulate the flow of ions across the membrane, and cause the further depolarization of the membrane followed by a repolarization of the membrane, hyperpolarization refractory period during which the neuron cannot initiate another action potential.

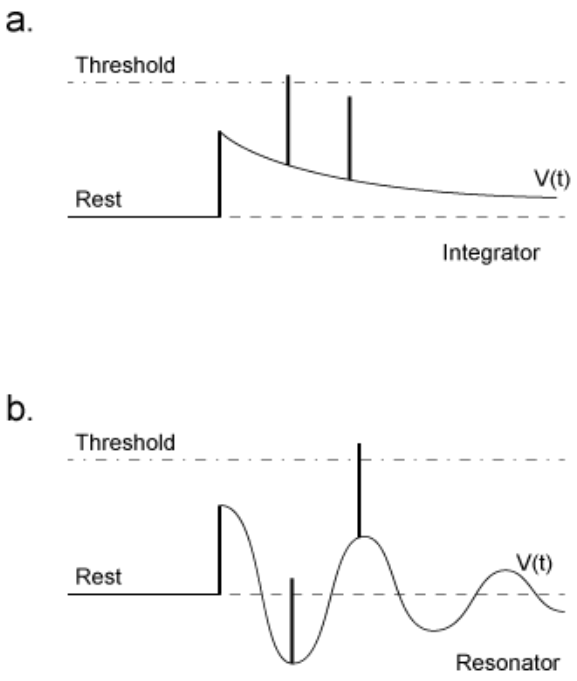

Figure 1.2 Sub-threshold voltage dynamics for an integrator vs. resonator. The membrane voltage V(t) for an integrator exponential decays to rest following an input pulse, therefore high frequency input will cause the voltage to cross threshold. The membrane voltage V(t) for a resonator follows a damped oscillatory decay to rest following an input pulse, leading sensitivity for particular frequencies of input pulse. (Image modified from [49])

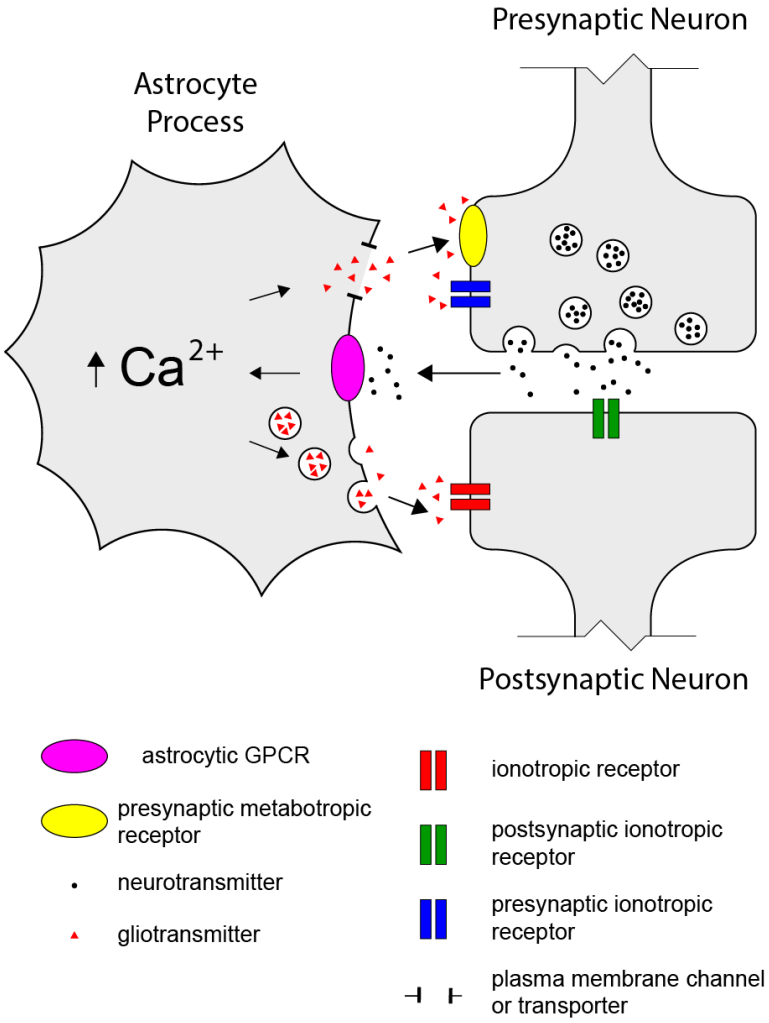

Figure 1.3. Cartoon of the tripartite synapse. Neurotransmitter from the synapse binds to GCPRs on the astrocyte process, activates Ca^{2+} influx into the cytosol from intracellular stores. Ca2+ activates release of gliotransmitters that bind to receptors on both the presynaptic and postsynaptic terminals, modulating synaptic currents, which can affect neuronal excitability and plasticity. (Image modified from [57])

Chapter II.

Methods- Identifying Universal Cellular and Network Properties

Here I will discuss methods to study the mechanisms that facilitate the formation of neuronal and glial network patterns. Ultimately, to understand how the spatiotemporal patterns of activity of neurons and glia underlie brain functions such as memory formation and retrieval, one would like to probe the activity in a human as these functions are performed. It is not possible to record invasively in humans with the rare exceptions of patients undergoing surgery to localize and remove the brain tissue responsible for intractable epilepsy. However, the sampling is sparse and data is scarce. Electric fields can be recorded outside of the skull through Electroencephalography (EEG) recordings. However, the electric field from single neurons is too small to be recorded by EEG. The signals measured are spatially averaged synchronous activity of thousands or millions of neurons that have similar spatial orientation. Techniques such as functional magnetic resonance imaging (fMRI) measure brain activity through detecting associated changes in blood flow, and give spatial information of regions with enhanced activity, but with poor temporal resolution. In order to gain information about the detailed spatio-temporal patterning of the brain, we must pick a model system. From in vivo animal models of various complexities, to in vitro tissue extracted from animal brains, to in silico computer simulation, each model has advantages and limitations.

2.1 Experimental Approach: Dissociated Primary Cultures

Dissociated cell cultures provide a reduced experimental model for studying network dynamics. Dissociated cultures are prepared by surgically removing regions of brain tissue from sacrificed (typically rodent) animal models. Under carefully controlled conditions, the connections between neurons are broken through both chemical and physical perturbation. This process leaves the majority of cell bodies of both neurons and glia in tact. Cells are plated on chemically treated and coated dishes, which allow for cells to adhere and grow. Cells are submerged in nutrient containing media, and kept in an incubator under temperature and pH control. If cultures are healthy, over time glial cells will continue to multiply and neurons will regrow their axons and dendrites, making synapses and forming networks[62]. The network connectivity from the intact brain tissue is not preserved, and the patterns of activity cannot be linked to behavioral outputs. However, cultures are an advantageous model for several reasons. They retain many properties of the in vivo networks such as complex patterns of spontaneous activity, cultured networks can be monitored long term, and are amendable for pharmacological intervention and accessible to both electrophysiological and optical approaches for reporting neuronal activity[63,64].

Recording Network Activity

One of the biggest limitations in understanding the spatio-temporal pattern formation of activity in neuronal networks is the lack of techniques available for measuring simultaneous activity of many cells. Extracellular electrodes measure the local field potentials and action potentials, with sub-millisecond temporal resolution. Using algorithms that triangulate to sort action potentials, one can resolve single action potentials in individual neurons. However, they sample the network sparsely. Dissociated cultures can be

grown on micro-electrode arrays (MEAs), which are dishes with embedded planar electrodes arrays to measure the local field potentials at multiple locations (Fig. 2.1). MEA's can provide sub millisecond temporal resolution of neuronal activity and are available with transparent dishes to allow for imaging.

Fluorescence calcium imaging provides an optical method to measure activity in defined cell types including both neurons and astrocytes. It utilizes fluorescent dye molecules whose absorption spectrums shift upon binding to calcium (Fig. 2.2.). This ion flows into the cell during an action potential, and therefore acts as an indirect measure of neuronal electrical activity. However, elimination of intracellular calcium is slow and the dyes have a limited dynamic range, resulting in saturation during sustained activity in neurons. Calcium concentration is also a reporter for activity in astrocytes, as elevated concentrations of calcium in the cytosol activate the release of signaling molecules extracellularly. Calcium imaging can be performed in individual cells and therefore offers excellent spatial resolution, and the dynamics of astrocyte calcium signaling are on the order of seconds and can be temporally resolved with calcium indicator kinetics.

2.2 Computational Approach

Some of the limitations of experimental techniques can be overcome by performing simulations. The spatial and temporal resolution of observations is limited by the level of detail within the model, but in principle a simulated network can provide the activity with single action potential resolution and from every neuron in the network. In addition the exact connectivity is known and easily perturbed to study its influence on dynamics.

Neuron Model

The choice of which neuron model to implement depends on the question one aims to understand. Biologically realistic models such as Hodgkin-Huxley neurons model how action potentials propagate, incorporating the conductance of specific ion channels. Multi-compartmental models can account for cell morphology and influenced how currents propagate integrate input. However, the level of detail chosen comes at a computational cost and it is challenging to implement for large networks.

There are other simpler spiking neuron models that capture prominent features of biological neurons, while having greater computational efficiency making them amendable for larger network simulations. For example the integrate-and-fire[65] and the resonate-and-fire[49] models produce behaviors of biological neurons, such as their response to simple pulses of dc current or sub-threshold oscillatory dynamics. One can isolate effects such as coincidence detection or frequency preference of input with the appropriate neuron model choice.

Network Connectivity Model

How spiking neurons are connected to each other will affect the network spatio-temporal patterns. Watts and Strogatz proposed a novel graph model that generates a family of toy networks with small world connectivity. Briefly the algorithm starts with a ring lattice with n vertices and k edges per vertex, one rewires each edge from local connectivity with random probability p (Fig 2.3). By tuning the parameter p, the graph has local connectivity (p=0), to random connectivity (p=1), and the intermediate region (0<p<1). Small world properties arise in a range of p near p=0.1.

The small world network paradigm offers an extremely useful tool to perturb the connectivity in a network model from local to random with one parameter. Whether brain networks in fact have small world topology remains to be determined (see section 1.2a), but the paradigm from a modeling standpoint is an extremely useful approach and will be utilized in later chapters.

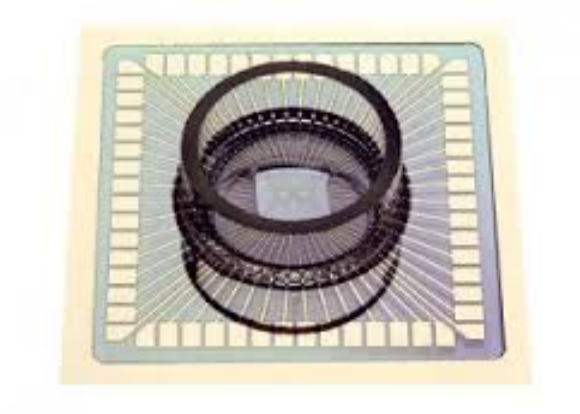

Figure 2.1 Microelectrode array. Dissociated cultures are grown in the dish. 60 electrodes arranged in an 8x8 grid are in the center of the well with spacing 200 μm apart. Contact pads and tracks are transparent to allow for optical imaging. Microelectrode arrays and amplifier are commercially available through Multichannel Systems. (image from: http://www.multichannelsystems.com/sites/multichannelsystems.com/files/styles/grid-4-normal/public/images/product/MEA_front.jpg?itok=ht3HhL-x).

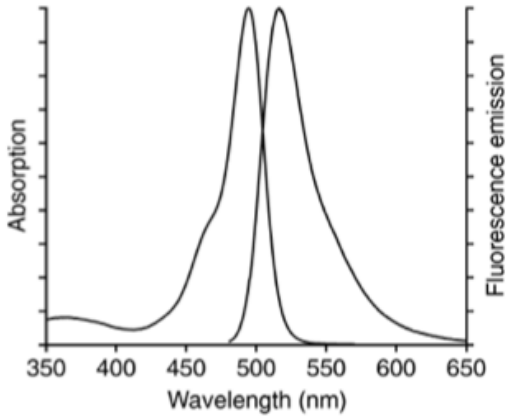

Figure 2.2 Fluorescence imaging with calcium indicators. Upon binding to Ca2+ ions the absorption spectra of calcium indicators shifts and there is an observed increase in fluorescence than from unbound indicator. (image modified from http://www.hexec.it/tesi/img68.png)

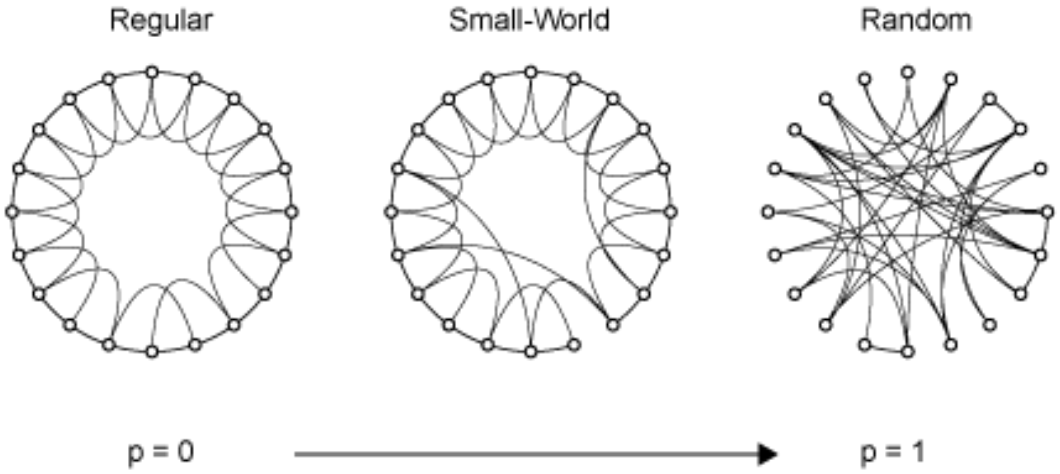

Figure 2.3 Small world network paradigm. Nodes are connected in a 1-dimensional ring, with local connections of radius r. The regular network is rewired, for every edge with probability p to breaking the existing connection and rewire the edge to a randomly chosen node. Probably p=0 is local connectivity, p=1 is random connectivity, and the small-world regime is for intermediate values of p. (Image modified from [30].)

Chapter III.

Spatial and temporal patterning of astrocyte calcium transients explained by active and passive coupling in a simple network model

3.1 Introduction

Networks of interacting components are known to self organize and form complex macroscopic processes, which emerge from local coupling between individual network components[66,67]. The brain is an example of a system with self-organizing dynamics; it contains an astronomical number of neurons and glia that interact over multiple spatial and temporal scales. Patterns of brain activity within these interacting networks underlie our thoughts and memories, and drive behavior. These interactions happen on multiple temporal and spatial time scales, are mediated through different cell populations and through various transport mechanisms. The most researched types of interactions in the brain are those mediated by neurons. Traditionally, glial cells were thought to provide primarily structural and metabolic support for neurons[68]. However, recent work suggests that glia may be active participants in brain information processing. Within the last decade it became clear that astrocytes, a sub-population of glial cells, play an important role as modulators of neural activity.

Astrocytes have been shown to display dynamic calcium transients in both *in vitro* and *in vivo* preparations[69–71]. Astrocyte calcium signaling is involved in many processes

including biochemical pathways that activate the extracellular release of a variety of transmitter molecules, which can interact with other astrocytes and also with neurons. For example, the release of ATP or glutamate from a single astrocyte has been shown to activate calcium transients in other astrocytes[58,72,73]. Moreover, It has been shown that a single astrocyte can envelope up to 140,000 neuronal synapses, putting it in a unique position to control neuronal domains[57]. These astrocytic processes are endowed with various G-protein coupled receptors that, among others, evoke the cell's calcium responses[56]. Thus it became clear that there is a bidirectional communication between the neurons and astrocytes, and this notion led to the formulation of a "tripartite" synapse concept, in which astrocytes play a prominent role in regulating neuronal signaling at a synapse level[74]. Therefore, patterns of calcium signaling in astrocytes can be important for shaping neuronal network formation and development. Even though the functional effect of astrocytes on neurons is complex and poorly understood, it is clear that astrocytes have a role in brain function that needs further study.

The research done on the involvement of astrocytes in modulating these neuronal processes has mainly focused on the single astrocyte level. However, these local interactions are embedded in complex network interactions. Astrocytes couple to each other through direct connections called gap junctions, and form a cellular network of interacting cells[75]. At the same time they secrete and uptake signaling molecules from the extracellular space. These molecules can diffuse forming another class of signaling pathways. The interaction of these two coupling mechanisms, diffusion of extracellular chemical signaling and the direct gap junction coupling, can lead to complex spatial temporal patterning of the network activity has been demonstrated in recent work[76]. Here, we studied the network dynamics of spontaneous calcium signaling formed in dissociated cultured astrocyte networks to

investigate the interaction of the passive and active transport mechanisms. We show that reduction of active, gap junction coupling changes the interaction patterns in a way predicted from the reduced model.

3.2 Methods

Dissociated cell cultures

We prepared hippocampal cell cultures from Wistar rats on postnatal day 1 using a protocol modified from[62]. Tissue was digested with %0.5 Trypsin-EDTA (Invitrogen) diluted in Hanks Balanced Salt Solution (Invitrogen) and then dissociated by titration with a pastueur pipette. Cells were centrifuged and re-suspended in Neurobasal-A medium (Gibco) supplemented with 2% B-27 (Gibco), 5% heat-inactivated horse serum (Gibco), 0.5 mM L-glutamine (Sigma-Aldrich), 0.5 mM pen-strep (Sigma-Aldrich) and 10 mM HEPES (Sigma-Aldrich). The cell density was adjusted to a final plating density of 1500 cells/ mm^2.

Micro-electrode Arrays

Dissociated cells were plated on microelectrode arrays (Multi Channel Systems, Reutlingen, Germany), with 60 electrodes in an 8 by 8 grid, with 200 μm spacing between electrodes and 30 μm in diameter. Contact pads and tracks were transparent to allow for optical imaging. Microelectrode arrays were cleaned and treated with 0.05% poly-ethylene-imine (Sigma-Aldrich) in borate buffer followed by the 20 μg mL−1 laminin (Roche Applied Science) solution in media following the protocol[62].

Calcium imaging

Cultures were imaged at 5 days in vitro using calcium indicator Fluo 4-AM (Invitrogen) and astrocyte marker[77] sulforhodamine 101 (Invitrogen). Fluo 4-AM and

sulforhodamine 101 were diluted to final concentrations in HEPES-buffered saline containing the following: 119 mM NaCl, 5 mM KCl, 2 mM CaCl2, 2 mM MgCl2, 30 mM Glucose, 10 mM HEPES, and pH adjusted to 7.4. Culture medium was replaced by 5μg/mL fluo4-am and incubated for 40 minutes at room temperature, following a second incubation with 5 μM sulforhodamine 101 for 20 minutes at room temperature. Cultures were gently washed with HEPES-buffered saline 3 times following incubations. Cultures were maintained at 35 degrees Celsius during imaging. Olympus microscope IX71 was used for wide-field fluorescence imaging, and recorded with Hamamatsu Digital CCD camera C10600 at (6.4 Hz frame rate). MetaMorph software was used for data collection, all further analysis was done with Matlab.

Pharmacological Treatment

18-β glycyrrhetinic acid (BGA) (Sigma-Aldrich) was dissolved in dimethyl sulfoxide (DMSO) into 1000x stocks and stored at -20°C. Before treating the culture, BGA stock was diluted in HEPES buffered saline to a final concentration of 25 μm and incubated for 15 minutes

Cell detection and event detection

Fluorescent imaging was acquired with commercially available MetaMorph Microscopy Software for Olympus Basic and imported into MATLAB for semi-automatic cell contour detection using custom software[78] modified from the Rosa Cossart lab. All subsequent analysis was performed with custom programs in MATLAB. Astrocyte somas were detecting in the SR101 image, and the fluo4-am fluorescence signals were processed by wavelet filtering of the raw signal and event detection was determined by thresholding

the signal above baseline. Each fluorescence signal was examined and any false positives and negatives in the event detection were corrected.

Measures

Fractional change was calculated for various quantities as the value after condition (A) minus the value before condition (B), and normalized by their sum (A+B).

$$\Delta = \frac{A - B}{A + B} \tag{3.1}$$

Spatial clustering

We defined the spatial clustering distance as the average closest distance between all closest pairs of astrocytes with calcium events during an imaging experiment (D_{exp}). To compare between experimental conditions with varying number of active astrocytes, we compared D_{exp} to the value of the spatial clustering distance for randomized networks (D_{sim}). Namely we randomized locations of active astrocytes distributing them randomly among experimentally identified locations (as measured with sulfarodamine 101) of all astrocytes. The average distance between active cells, D_{sim}, was computed for over 50 sets of randomizations and compared to that observed experimentally. To quantify the spatial clustering we define the spatial clustering measure C given by,

$$C = \frac{D_{sim} - D_{\exp}}{D_{sim} + D_{\exp}} \tag{3.2}$$

where C is the ratio change of the spatial clustering distance for experimental data (D_{exp}) with the spatial clustering distance for simulated networks (D_{sim}).

Autocorrelation Widths

The autocorrelation function was calculated of each astrocyte calcium fluorescence signal. To determine a measure of the autocorrelation signal width, we calculated the time lag at a half maximum of the autocorrelation, where the total height is determined by the peak of the autocorrelation and the first derivative of the autocorrelation crossing zero. Using the time lag at the autocorrelation half maximum as an indicator for the timescale of astrocyte calcium signal duration, we computed the average time lag for all signals in an imaging experiment and the ratio change for before and after pharmacological treatments.

Cross Correlations

The cross correlation function was calculated pairwise between all pairs of astrocytes in a network for time lag shifts between -90 seconds and 90 seconds. Pairs of astrocytes with distances were binned and the average cross correlation functions was computed for pairs within distance ranges. The temporal ordering is not relevant for obtaining a measure of total average correlation at a distance. Therefore we utilized the following strategy to avoid averaging out correlations that are maximal for either positive or negative time lags. Any correlation functions whose global maximum occured for a negative time lag value, we reflected the cross correlation function across the y=0 axis, so that only the magnitude of the time lag information is averaged over pairs. The pairs of astrocytes with maximal cross correlation functions at negative time lag values are equivalent to the cross correlation function between the same pair of signals with the ordering switched.

Model Network

The astrocyte network model is a two process modified integrate and fire model, and follows the description in reference[79]. The key components of the model are that it contains a direct coupling interaction, gap junctions, and an indirect coupling term, representing diffusive extracellular coupling. Astrocytes are represented as the nodes of the network and nodal activity is driven by random noise and extra-cellular excitation from other active astrocytes. An integrate-and-fire model was chosen as the basis for the nodal dynamics for its simplicity and its ability to grossly encapsulate the desired pathways. The release of Ca^{2+} from the endoplasmic reticulum (ER) is represented by an internal flush of nodal agent upon exceeding a charging threshold. This internal concentration is allowed to interact with other connected astrocytes through gap junctions via an equilibrating term (see equation 3.3 below). In addition to the internal release, breaching the charging threshold is accompanied by a diffusive flush of signaling into the extracellular space, which allows astrocytes to passively influence neighboring astrocytes. While it is clear that these two pathways are mediated by (many) other signaling molecules, here we assumed for simplicity that the extracellular signaling will inadvertently affect the calcium levels in an astrocyte by activating G protein coupled receptors.

Thus, the full equation describing the dynamics is as follows:

$$\tau_E \frac{dX_i}{dt} = -\alpha X_i + I_{noise,i}(t) + I_{flush,i}(t) + \beta \sum_j A_{ij}(X_j - X_i) + \gamma \sum_j D_{ij}(r, t - \tau_j) \qquad (3.3)$$

We also changed the parameters for slow diffusion. Variables are the same as in the published model paper[79], with the following exceptions, leak constant (α=0.5), speed of diffusion (D*=0.001), and amplitude of diffusion release(N=1000).

Here X_i denotes the concentration of Ca^{2+} present in the i^{th} astrocyte. α is the leak constant controlling the auto-decay of calcium levels in the cell (α=.5). I_{noise} describes random excitation experienced separately by each astrocyte. The random excitation occurring with a probability p=.01 and is represented by short stimulation pulse. I_{flush}, on the other hand, represents the release of Ca^{2+} from the ER into the interior of the cell. The form of the release is modeled as an exponential decay in order too capture experimental timescales:

$$I_{flush,i}(t) = I_{amp}(e^{\frac{-(t-\tau_i)}{C_1}} - e^{\frac{-(t-\tau_i)}{C_2}}) \tag{3.4}$$

Astrocytes form a 2D lattice to match experimental observations. The next term on the RHS of Equation (3.3) describes the active network coupling term. The parameter β denotes efficacy of coupling. The range of gap-junction strengths is limited by the overall amount of agent (Ca^{2+}) an astrocyte can send out. Higher values indicate a greater sharing of agent amongst astrocytes and less retention of their individual concentration level. The A_{ij} represents the adjacency matrix of astrocytes, A_{ij}=1 if cells i and j are directly coupled and A_{ij}=0 otherwise . The gap junction coupling, $X_j - X_i$, is a standard term describing gap junctions that allows for rapid equilibration of Ca^{2+} concentrations at different sites. Astrocytes are initially coupled via gap-junctions to all neighbors within a radius, R=2. A small portion of the connections, ~10% of them, are selected to be randomly rewired.

The last term on the RHS of Equation (3.3) represents the extracellular diffusive coupling of astrocytic transmitters. The function:

$$D_{ij}(r, t-\tau_j) = \frac{N}{4\pi D^*(t-\tau_j)} e^{\frac{-r^2}{4D^*(t-\tau_j)}} e^{-\zeta(t-\tau_j)} \tag{3.5}$$

reflects the distance and time based effect a cell j will have on cell i given the distance between cells is r, and the time since j had a Ca^{2+} event , τ_j. This term is the solution of a 2D diffusion equation in open space. The strength of this extracellular diffusion is controlled by the coupling parameter γ. The gap junction and diffusive coupling parameters are both set to the range of values from quiescence to dominating network dynamics in bursting behavior.

Simulation Details

Simulations were run on a 40x40 grid of astrocytes. The cells were evolved, via Euler's method, for 10,000 timesteps to effectively randomize the starting condition before simulating for another 40,000 timesteps in which the network is closely followed. The figures displayed represent the averages over 4 simulations.

3.3 Results

We have grown mixed hippocampal cell networks in primary cultures and measured astrocytic activity utilizing optical imaging with calcium sensor Fluo-4AM, while neuronal electrical activity was monitored using microelectrode arrays (see methods section 3.2 for detailed description). Here we are interested in early development of the networks during the first week in vitro. During the early development, astrocytes form a network and display spontaneous calcium signaling while there is no electrical neuronal activity. However this is an active period for synapto-genesis and it is known that neurons release various signaling molecules at that time[80]. We observed robust patterns of calcium activity during the first week in culture before spontaneous action potentials in neurons were observed on the microelectrode arrays. The neurons became subsequently electrically

active after 7 DIV (days in vitro). We imaged the spontaneous astrocyte calcium transients of hundreds of astrocytes over several minutes (Fig. 3.1). To identify individual astrocyte somas, we used concurrent staining with sulforhodamine 101 which selectively labels astrocytes[77]. The astrocytes were identified as the cells that were co-labeled with both markers.

In parallel we have constructed a reduced model of astrocyte-astrocyte interactions. Based on the known experimental results[57] we simulated two major means of signal transduction: active transport through astrocytic gap junctions, and passive transport through diffusion in extracellular space. The reduced cellular activity is modeled through integrate-and-release dynamics. In short based on the incoming signal the Ca^{2+} is released from the internal stores and propagates through out the cell, and the associated network. While it is clear that astrocyte signaling is multimodal and extremely complex we implicitly assumed that the extracellular agents act directly on calcium concentration within a cell and we modeled it as one species. The properties of this model were extensively studied in recent work[79]. We have shown that depending on connectivity properties of gap junctions the two processes (active network transport and passive diffusion) can cooperate, strengthening the network activity, or they can compete inhibiting each other and subsequently lowering the network response. Here we assumed that astrocytic connectivity is primarily local as there are no long-distance connections between astrocytic processes[81].

Figure 2a shows an example raster plot of the fluorescence intensity over time for an astrocyte network during four minutes of imaging. Each row displays the changes in calcium fluorescence over time for individual astrocytes rescaled between the fluorescence intensity signal's minimum (black) and maximum (white). To better understand the effects

of calcium signaling on astrocytic network, we perturbed these spontaneous Ca^{2+} patterns by pharmacological disruption of the gap junction coupling strength between astrocytes. We found that the number of astrocytes with spontaneous calcium transients is dependent on gap junctional coupling strength between cells (Fig 3.2b). Following incubation with gap junction blocker BGA (n=2 cultures), the number of astrocytes with spontaneous calcium events during imaging decreases relative to the vehicle control (n=3 cultures). We quantified this effect by calculating the ratio change in number of astrocytes with spontaneous calcium transients between before and after BGA treatment. We measured a negative value in the fractional change in number of astrocytes with spontaneous calcium transients for BGA treatment, and no significant ratio change for vehicle control (Fig 3.2b). This indicates that astrocytic gap junctions play an important role in network signaling.

Similarly, we lowered the conductance of gap junction coupling, β, in our model. The simulated astrocyte network shows a decrease in activity for weaker gap junction coupling parameter values (Fig 3.2c). Fig 3.2c depicts the frequency of astrocytic calcium events as a function of both gap junction coupling and the interaction strength between the extracellular signaling in astrocytes. In the presence of local gap junction coupling the astrocytic activity scales monotonically (columns decrease in activity amplitude for smaller gap junction coupling) with strength of β. Thus, in this case, weakening gap junctions always results in decrease on astrocytic activity independent of extracellular signaling strength. These effects change dramatically for different network connectivity parameters[79].

After weakening gap junction coupling in the astrocyte network, in addition to fewer astrocytes with spontaneous calcium transients, we also observed significant changes in the distribution of active cells in cultures. The spatial distribution of the remaining active astrocytes stopped being uniform, but formed locally clustered domains (Fig. 3.3a,b). To

quantify this effect we defined the clustering measure C (see methods section 3.2) as a fractional change of Euclidian distance between locations of observed active astrocytes and the randomized ones. The higher value of C indicates more clustered groups of astrocytes were active. We observed that for control conditions the spatial distribution of active astrocytes is only minimally different from randomized locations, indicating only a small propensity for clustering. However, the clustering coefficient increased significantly when cultures were treated with BGA. This effect is again not present for the vehicle control (Fig. 3.3e). This indicates that blocking gap junction obliterates one mode of coupling, leaving the other still intact. We hypothesize that the remaining coupling mechanism is linked to extracellular signaling and diffusion transport.

To support this hypothesis we conducted similar in silico experiments using the developed model. Similarly to the experimental results, we observe that in networks with strong gap junction coupling large numbers of cells activate, forming randomly distributed activity domains (Fig 3.3c). Spatial randomization of active sites yields no measurable effect in this case. However, when the network coupling is lowered, the large domains do not form and we observe formation of small clusters of active cells (Fig. 3.3d) with high clustering coefficient. These observations are summarized on Fig. 3.3f.

We also wanted to investigate what effect network coupling can have on the shape of calcium signaling in an individual astrocyte. Gap junction coupling is a bi-directional coupling that rapidly equilibrates the Ca^{2+} levels among the coupled cells. Assuming that a relatively stereotypic amount of calcium is released from the ER into the cytosol during the calcium event, the duration of event and the time evolution of the event may be strongly depend on the gap junction strength.

We measured the time course of calcium responses of individual astrocytes in the absence and in the presence of gap junctions coupling (Fig. 3.4). Our simulations indicated that the duration of elevated calcium (the width of the calcium event) is strongly dependent on both the strength of gap junctions and the efficacy of extracellular signaling (Fig 3.4F). For low β and low γ (strength of effect of extracellular signal on an individual astrocyte) the width of the calcium event initially decreases as gap junction coupling grows. This is due to the equilibration effect discussed above. For strong β and even low γ, however, we observe subsequent broadening of the event width. This is due to the fact that the extracellular signaling together with strong network coupling equilibrates Ca^{2+} network levels away from resting value leading to a slower time decay of the Ca^{2+} levels after the event. For high values of γ on the other hand the change of event width is largely independent of β. This is due to the fact that extracellular transport dominates network dynamics raising the resting calcium concentrations away from the original value.

Similarly, we investigated the time course of single astrocytic calcium events experimentally. Figure 3.4a and 3.4b shows an example of calcium fluorescence transients of an astrocyte before and after weakening gap junction coupling in the astrocyte network. We find that the duration of astrocyte calcium transients increases after BGA treatment. To quantify the change in timescale of calcium events, we computed the width of the autocorrelation of fluorescence signal of every astrocyte Ca^{2+} event (see Methods) as a measure for the time duration of calcium fluctuations in astrocytes (Fig. 3.4c,d). We find a significant increase in the width of the autocorrelation after decoupling gap junctions with BGA, seen as an increase in the fractional change compared to control (Figure 3.4e). We also plot the change of the calcium event time course for the vehicle, but here we do not observe significant change. These results are consistent with our simulations for relatively

weak gap junctional and extracellular coupling, possibly providing constraints on the biological values of the coupling parameters.

Finally, we wanted to disambiguate the role of both coupling mechanisms in mediating formation of temporal correlations between the astrocytes. To study the network level spatio-temporal patterning of spontaneous calcium activity in cultured astrocyte networks, we measured how correlated are calcium events as a function of spatial distance between the cells, when gap junctions are left intact and when they are disrupted by BGA (Fig. 3.5). We plot an example of evolution of cross correlation (CC) as a function of time lag for all astrocyte pairs falling into given distance range. Fig 3.5a depicts control condition, while Fig 3.5b shows BGA treated culture. We observe a significant change in the shape of the CC at all distances. For the controls there tends to be a peak in CC at relatively small lag. The lag increases significantly for cells that are located at a greater distance from each other. For the BGA treated astrocytes the peak of cross correlations is significantly shifted at all distances. However, notably there is not a big difference in the magnitude of cross correlation. These results are summarized in Fig. 3.5e. We see that the lag values at which maximal CC is observed are significantly larger for the BGA treated cultures as compared to controls and vehicle treatment. It is interesting to see that the changes in the lag within the treatment group are only observed at shortest distances ($r < 50$ and $50 < r < 150$). The lags at which maximum CC happen are not significantly changing for longer distances between astrocytes. This is probably due to intrinsic timescales connected with calcium events of individual astrocytes.

We observe very similar effects in our simulations. When gap junctions are present we observe much smaller lags at which maximal CC happens (Fig 5c). Lowering β, on the other hand, leads to much larger lags (Fig. 3.5d and Fig. 3.5f) that stabilize at larger cell

distances (cell distances are calculated here in terms of lattice length). At the same time however we also observe a significant decrease in the cross correlation amplitude. This is a significant departure from our experimental findings. This might indicate that the extracellular coupling is stronger than we assumed in the model.

3.4 Discussion

To gain insight into mechanisms mediating pattern formation in astrocyte networks, we experimentally monitored astrocytic Ca^{2+} activity in mixed culture settings. We have also created a computational model that takes into account two major types of signaling pathways in astrocytes: active transport through astrocytic gap junction coupling and diffusion in extracellular space. In terms of experiments, we perturbed the first pathway by blocking gap junctions using BGA. The extracellular pathway, on the other hand, is mediated by a host of signaling molecules, and therefore we were not able to successfully regulate it. We quantified the number of spontaneously active astrocyte cells, spatial clustering, temporal duration of calcium transients, and the dependence of temporal signal correlations on the spatial distance between cells. We show that the experimentally observed changes after the BGA treatment agree with our modeling results, providing credence to the hypothesis that both of these types of signaling pathways play an important role in network signaling. Furthermore, changes in spatio-temporal patterning observed in our model when we were changing the relative coupling strength of both mechanisms provide general constraints on the biological values of these parameters.

The unanswered question remains whether, and to what extent, changes in astrocytic spatio-temporal activity patterns affect activity patterns of neurons, and subsequently the pathological and cognitive function of the brain. However there is experimental evidence linking astrocytic activity to brain wide pathologies[82,83].

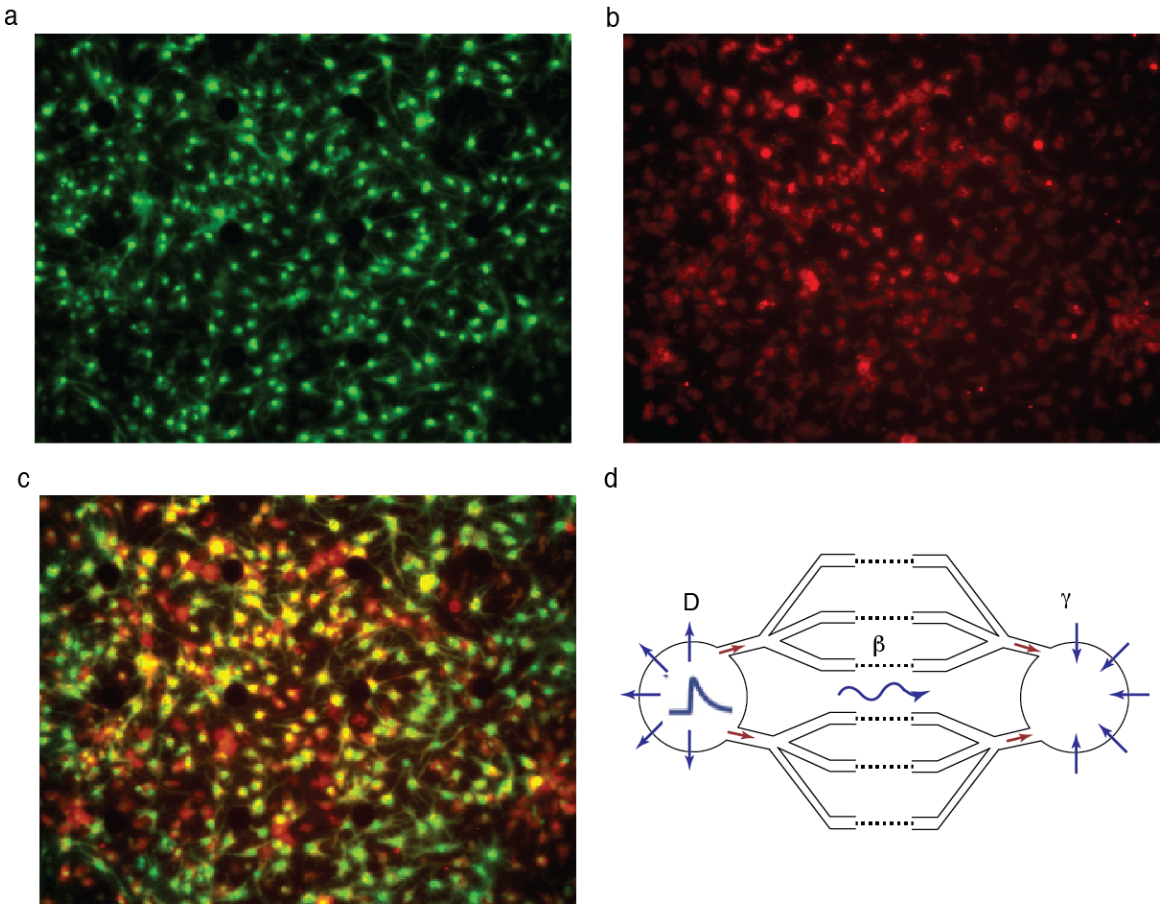

Figure 3.1 Fluorescence imaging of spontaneous astrocyte calcium transients in dissociated hippocampal cultures. (a) Example fluorescence image of calcium indicator fluo-4am. (b) Example fluorescence image of astrocyte marker sulforhodamine 101. (c) Overlay of fluo-4am and sulforhodamine 101 images, yellow marks astrocytes co-labeled with both dyes. (d) Schematic of model shows the active and passive pathways of astrocyte coupling.

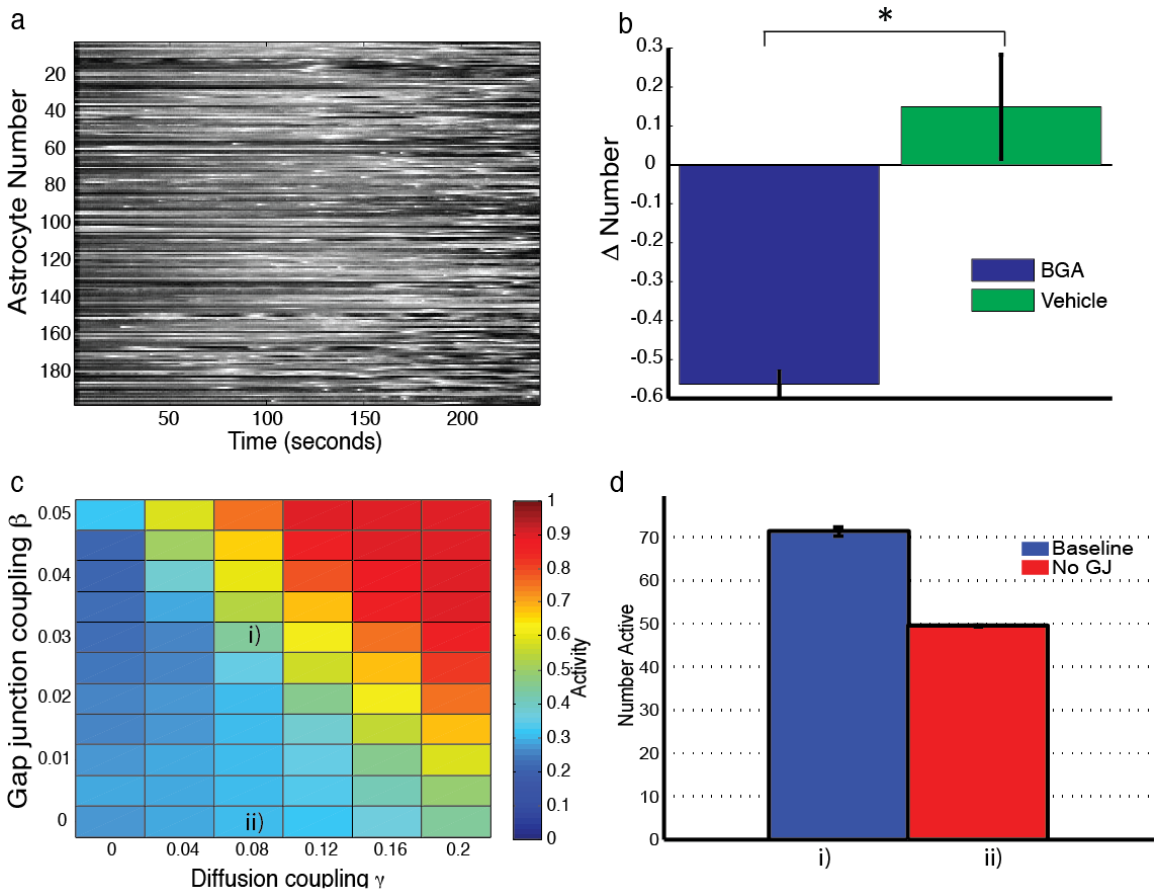

Figure 3.2. Cultured astrocyte networks display spontaneous calcium transients mediated through gap junction coupling. (a) Example raster plot of spontaneous astrocyte network activity. Florescence intensity is rescaled between 0 and 1, where maximum intensity (1) is white and minimum intensity (0) is black. (b) The number of astrocytes with spontaneous calcium transients is dependent upon gap junction coupling in the network. Gap junction blocker BGA decreases the number of astrocytes with spontaneous calcium transients relative to the vehicle control (p-value=0.027). Δ Number is the ratio change in number after-before/after+before BGA (n=2) or vehicle treatments (n=3). (c) Simulated astrocyte network shows similar dependence on gap junction coupling strength. For decreasing gap junction coupling, activity decreases across various diffusion coupling strengths. Color bar defines activity as the average duration active/total simulation length * refractory period (refractory period=1000). (d) Example simulation for parameters in regions (i) and (ii) of (c) shows decreased activity for weaker gap junction coupling. Activity units are the number of active cells within 100 timesteps at point i) and ii) in (c).

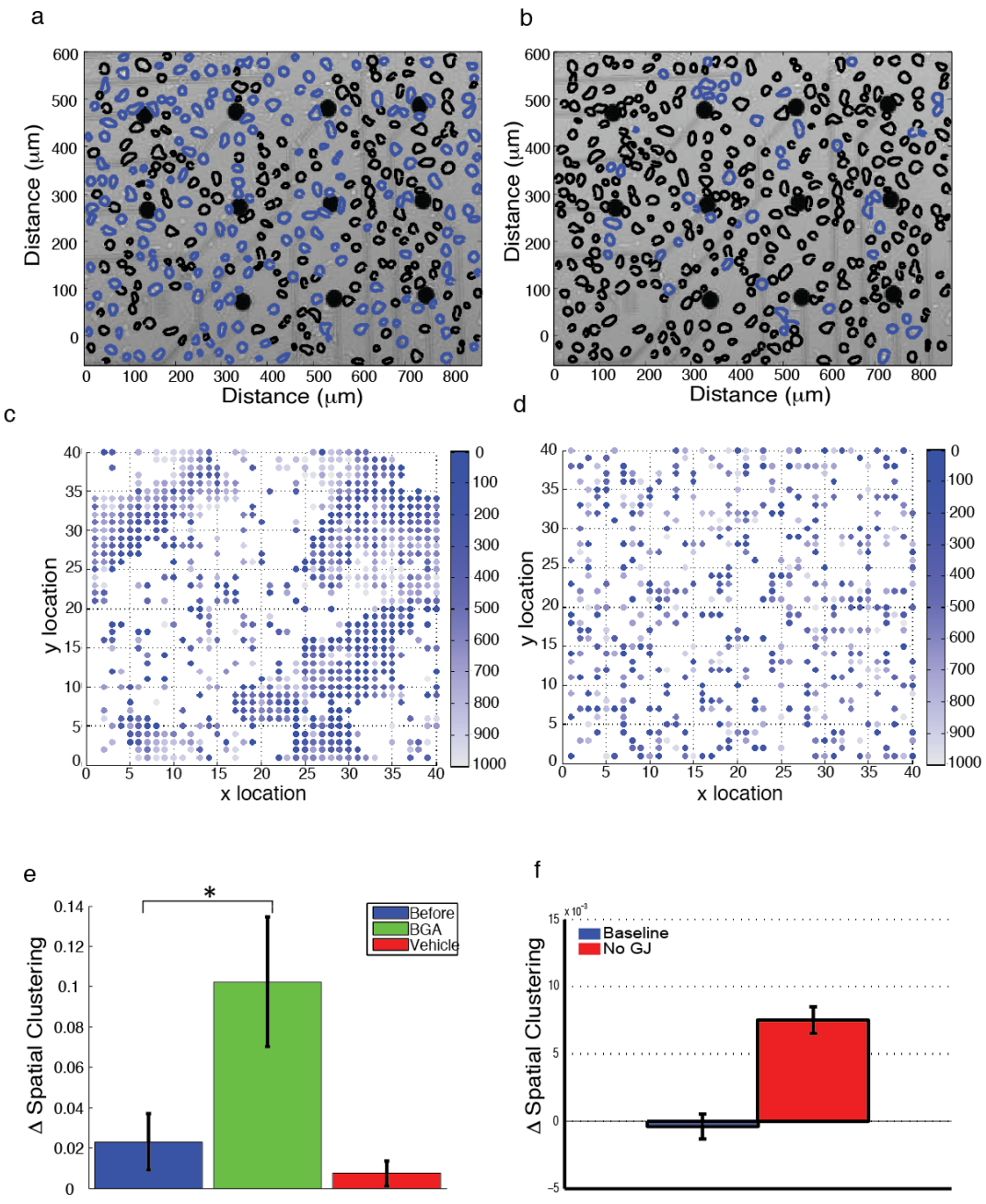

Figure 3.3. Decoupling gap junctions reveals underlying spatial clustering within astrocyte networks. (a,b) Example bright-field image of a cultured network before (a) and after (b) BGA treatment. Spatial locations of astrocytes are outlined, where blue regions displayed calcium transients during the experiment and black regions had no spontaneous activity. (c,d) Simulated astrocyte networks have similar spatial clustering before(c) and after (d) gap junction coupling. (e) Disruption of gap junction coupling with BGA enhances spatially clustering of astrocyte network activity (p-value=0.05). Δ Spatial Clustering is the ratio change in spatial clustering between experimental and random networks of the same spatial locations (see methods). (f) Simulated astrocyte network producing similar spatial clustering. Nearest neighbor distance ratio measured as (random-real)/(random+real).

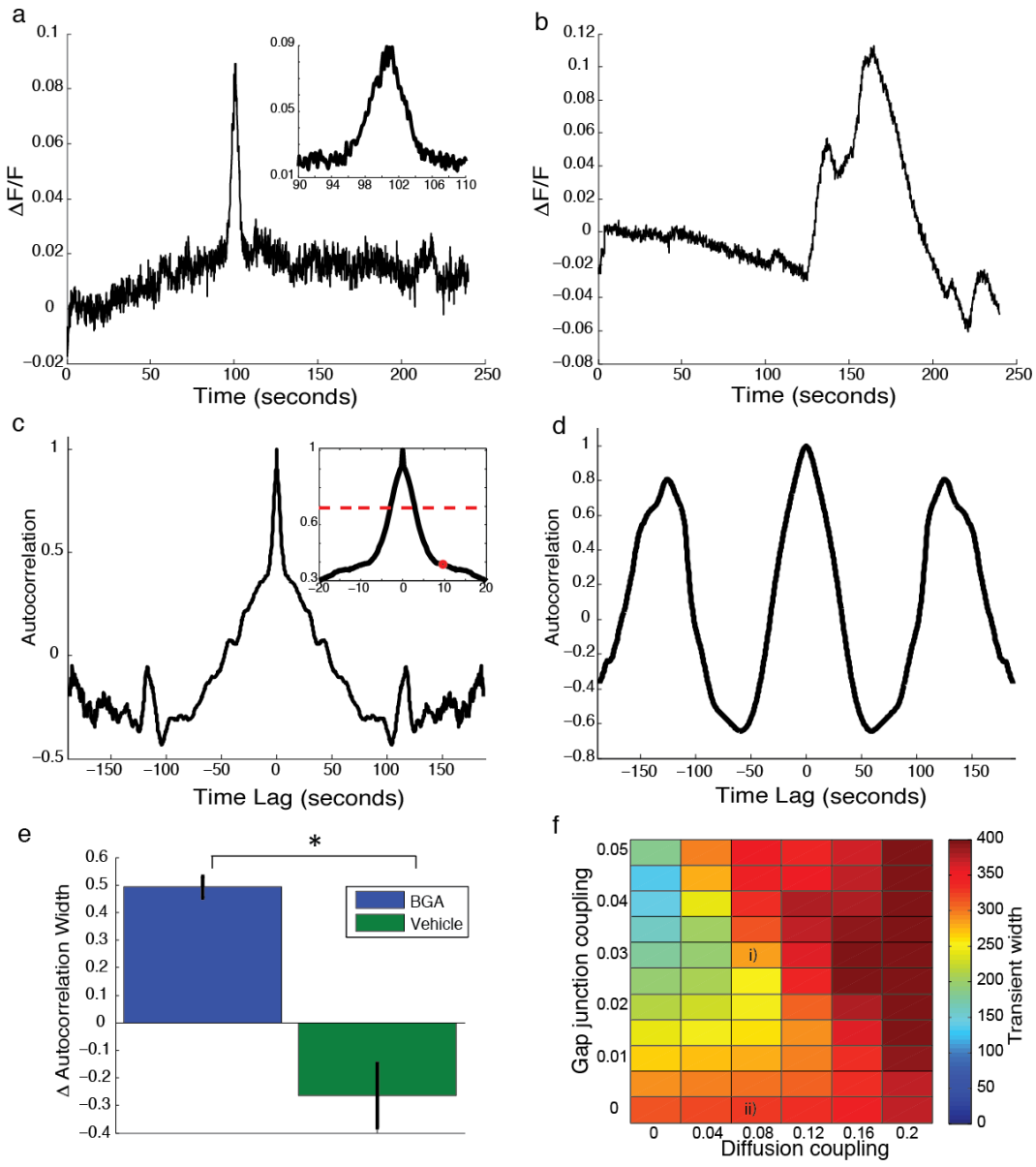

Figure 3.4. Weakening network wide gap junction coupling affects the timescale of calcium transients in individual astrocytes. (a,b) Example calcium fluorescence transients of an astrocyte before (a) and after (b) treatment with BGA. (c,d) Corresponding autocorrelation of the fluorescence trace. Insets are zoomed in to show timescale. Red dot marks the first local minimum of the slope of the autocorrelation (see methods) and the dashed red line marks the half maximum. (e) An increase in the width of the autocorrelation at half maximum shows an increased duration of calcium transient after BGA (p-value=0.02). Δ Autocorrelation width is the ratio change in transient width after-before/after+before BGA or vehicle treatments. (f) Simulated astrocyte network shows similar timescale of calcium transients. Weaker gap junction coupling (ii) has increased transient width than stronger gap junction coupling (i). Color bar represents the width of the transient in number of timesteps.

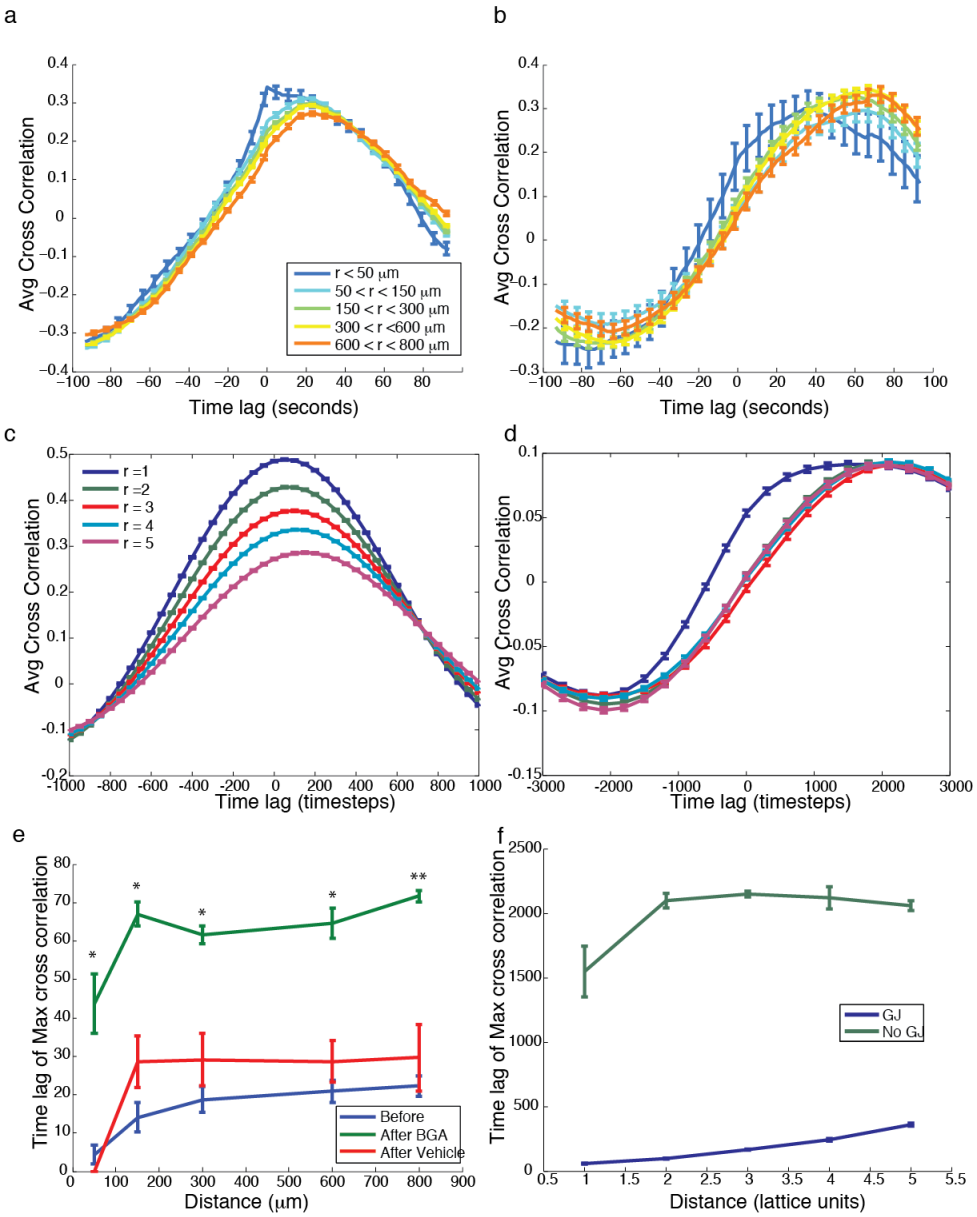

Figure 3.5. Spatio-temporal correlations between pairs of astrocyte calcium transients are mediated by gap junction communication. (a,b) Example cross correlations of calcium transients between all pairs of astrocytes within the network before (a) and after (b) BGA treatment across distances between all pairs of astrocytes. (c,d) Simulation results for cross correlations of calcium transients before(c) and after blocking gap junctions. Time lags are in number of timesteps. (e,f) Maximum cross correlation between pairs of astrocytes occurs at longer time lags as a function of distance between pairs of astrocytes for both experiments (e) and simulations (f). Weakening gap junction coupling with BGA increased the time lag for maximum cross correlation across distances (r=50, 150, 300, 600, and 800 μm) between all pairs of astrocytes (p-values=0.03, 0.03, 0.04, 0.02, 0.01, respectively).

Chapter IV.

Functional clustering in hippocampal cultures: relating network structure and dynamics

4.1 Introduction

The study of networks and their role in social, technological, and biological settings has recently been realized to be of great importance in understanding these complex systems. However, much work has focused on the study of the structural properties of static networks in which the nodes and edges of the network remain constant over time or are examined over a snapshot or time window during which they are effectively static[30,31,84–86]. While this work has contributed much to our understanding of networks, it fails to recognize that many types of networks are composed of dynamic elements, which are connected to form a specific function. In these dynamic networks, we can define a new type of structure called functional structure. Here connections between nodes are derived from a functional relationship between their dynamics.

The brain is a specific example of a dynamic network in which functional structure has gained a great deal of attention[87–90]. When studying the brain, one can examine the relationship between the anatomical network structure of the neurons and the resulting dynamics, which define the functional network structure. The availability of new data from large scale brain imaging techniques such as fMRI has allowed for the large scale studies of the relationship between structure and dynamics of different brain regions, and often one

finds a correlation between the anatomical connections between brain regions and the resulting functional structure[91–94]. At the same time, recent advances in technology allow for the recording from multiple single neurons in vivo, but the complex connectivity of the brain makes it difficult to simultaneously study the underlying structure of the brain on this smaller scale. Modeling can provide valuable insights intothe relationship between neuronal connectivity and dynamics, but does not provide experimental evidence for these relationships. It is therefore imperative to develop an experimental model in which structural network properties can be directly compared with neuronal dynamics. Dissociated cultures are a good reduced system in which to study neuronal dynamics because they maintain many properties of neuronal interactions, but also have the advantage of the relative ease of structural and pharmacological manipulation[63,95–97]. The gross structural properties of the culture can be observed using labeling techniques and dynamics of single neurons can be electrically recorded. They are therefore a useful tool to simultaneously study how anatomical connectivity, functional structure, and brain dynamics relate.

In this type of culture preparation, a single cell suspension of hippocampal cells is plated onto a culture dish. The neurons attach to the surface of the dish and start to grow processes, forming synapses with other neurons and creating a two-dimensional network of neurons. After 3-7 days, these neurons will begin to spontaneously fire action potentials, and as the cultures age, the neural activity evolves into highly synchronous activity in the form of network bursts, during which almost all neurons will fire action potentials[64,98]. The dynamics of these network bursts have been studied to examine burst patterning[99–103], learning[96,100,104,105],and with pharmacological manipulation as a model of epilepsy[106–108].

An often overlooked feature of these cultures is that they are composed of both neural and glial cells, and in fact, the neurons require the presence of glial cells to survive. While neurons do not proliferate in the culture, the glial cells do, and thus the number of glial cells in the culture will quickly multiply, creating a confluent layer of support cells for the neurons. However, it is possible to inhibit the division of these cells through the addition of chemical blockers[109] or type of media used[110]. Different groups have studied the dynamics of the neurons in cultures grown under both types of conditions, although many studies allow the glial cells to multiply in order to provide a continuous layer of support for the neurons[64,101].

While the dynamics of the network bursts produced by the neurons in these cultures are often investigated, the impact of the glial network on the neuronal dynamics is less studied. However, recent work suggests that glial cells, and specifically astrocytes (a certain type of glial cell), can have numerous impacts on neuronal networks[56]. The presence of glial cells is known to impact the development of neurons[111], which will certainly affect their dynamics, but astrocytes have also been shown to exhibit calcium oscillations which can affect intracellular calcium dynamics in neurons[112–115]. Calcium plays multiple roles in neuronal signaling, so these calcium oscillations likely contribute to the activity of the neurons. Additionally, astrocytes have been shown to mediate calcium waves during the developmental stage (first two weeks) of dissociated cortical networks, and the presence of these waves influences the dynamics and maturation of the culture[70]. Recent work has also shown that astrocytes modulate slow oscillations in cortical networks through the regulation of synaptic receptors[116]. We therefore expect that changes in the glia network should impact the dynamics of the neuronal network.

We are interested in studying differences in the functional structure derived from the dynamics of the neuronal network in the presence of either a low or high density of glial cells. We investigate dissociated hippocampal cultures and examine the underlying anatomical network structure of both neurons and glial cells and how these networks interact to influence the resulting functional network structure. The cultures are grown on multi-electrode arrays (MEAs) which allow for the recording of individual action potentials from cells near the electrodes. We analyzed the formation of spatio-temporal activity patterns using a new clustering technique (functional clustering algorithm) to determine the resulting functional network structure. We then relate this functional structure to gross anatomical network properties obtained through immunolabeling and DiI staining.

This chapter is organized as follows: Section 4.2 describes the experimental methods and analysis. The results describing the anatomical structure, the resulting functional network structure, and how this structure changes over time and between groups of the cultures are presented in Sections 4.3. The relationship between functional and anatomical network structure is discussed in Section 4.4, where we further describe how the structure of the glial and neuronal networks influences the dynamics and resulting functional structure of the neuronal network.

4.2 Methods

Cell Culture Preparation

Dissociated cell cultures were prepared from neurons (and glia) obtained from the hippocampus of P1 Wistar rats using a protocol modified from[96]. Briefly, hippocampi were first chemically digested in a trypsin solution followed by mechanical titration with a flamed pasteur pipette. Cells were centrifuged and re-suspended in Neurobasal-A Medium

supplemented with B-27, 5% heat activated horse serum, 0.5mM L-Glutamine, 0.5mM pen-strep, and 10mM HEPES. The cell density was adjusted by the addition of media such that the density upon plating would be ~1400 cells/m^2.

The cell suspension was plated on MEAs (Multi Channel Systems, Reutlingen, Germany) which had previously been coated with 0.05% poly-ethylene-imine in borate buffer followed by 20 µg/mL laminin solution in media. Cultures were maintained in a humidified incubator with a 95%O_2/5%CO_2 saturated atmosphere at 37°C.

Between 24-36 hours after plating, cultures were split into high and low glial groups (HGG) and (LGG) respectively. Neurobasal-A media supplemented with horse serum as described above was added to cultures in the high glial group to allow for the proliferation of glial cells, while the media of the low glial group was replaced with Neurobasal-A media that had not been supplemented with horse serum. The sera-free media environment keeps the number of glia cells in these cultures constant by inhibiting their division. Following this, half of the media was replaced with the appropriate fresh media once each week.

MEA recordings

Cultures were recorded at 8, 11, and 13 days *in vitro* (DIV) for N=5 cultures in the high glial group and N=4 cultures in the low glial group. For recordings, media was replaced with a recording buffer to maintain the pH of the culture. Cultures were recorded at 25 kHz using a Multi Channel Systems data acquisition card and MC-Rack software. During the recordings, cultures were maintained at 37°C and each recording lasted 5 minutes.

Cell fixation and staining

Cultures used in staining studies were grown on culture dishes following the same protocol as those used for recordings. The cultures were fixed using 4% paraformaldehyde in PBS at either 8, 11, or 13 DIV to correspond to the days of recordings. DiI crystals were dissolved to a saturated solution in cold liver oil and micro-droplets of the solution were placed on neuronal cell bodies, allowing the dye to dissolve through the cell. After 5 days, the neurons were imaged using an Olympus IX71 microscope.

After DiI staining and imaging, cultures were immunolabeled for synapses by standard immunocytochemical techniques. Samples were blocked with blocking solution, followed first by incubation with monoclonal anti-synaptophysin primary antibody, and then by a fluorescein-conjugated secondary antibody. Cultures were then imaged on a Zeiss LSM 510-META laser-scanning confocal microscope with a 63x objective. After imaging, samples were labeled for glial cells using an anti-glial fibrillary acidic protein (GFAP) primary antibody followed by an AMCA-conjugated secondary antibody. Cultures were then imaged on a Deltavision-RT fluorescent microscope with a 10x objective.

Process length/form

Sholl analysis was performed on the arborization of imaged neurons by counting the number of process crossings with concentric circles of increasing radii centered on the soma. The median crossing distance, total number of crossings, and longest process length was then computed from the distribution of process crossings. For cultures in the high glial group, this analysis was done on N=9,11,14 randomly chosen neurons for DIV 8,11,13 respectively and on N=10,12,13 neurons for DIV 8,11,13 in the low glial group.

Synaptic density

DiI-synaptophysin labeled images were analyzed using ImageJ software for synaptic density along neuronal processes. Images were normalized for contrast and each channel was thresholded to distinguish signal from background. The density of synapses was calculated by dividing the number of co-localized areas of synapse and process by the total area encompassed by processes, resulting in the number of synapses per unit area of processes stained by DiI.

Glial cell density

GFAP labeled images were analyzed using ImageJ software to determine the glial cell density. Images were thresholded to separate signal from background and the percentage of the image covered in glial cells, P was measured. In order to compare between the different culture conditions, we compute the normalized difference of P between the high and low glial groups denoted as P_H and P_L respectively:

$$D = \frac{P_H - P_L}{P_H + P_L} \tag{4.1}$$

Spike detection

The local field potential recorded from each electrode was assessed for spiking activity and active channels were selected for spike detection. Signals were first filtered through a high pass Butterworth filter at 250 Hz. Spike detection was done using a thresholding method, using 5 standard deviations of the baseline noise as the threshold value. No attempt was made to distinguish between single neurons recorded by the same electrode.

4.3 Results

We analyze structural and functional connectivity in dissociated hippocampal cultures grown in conditions which allow for the proliferation of glial cells (high glial group - HGG) or inhibit the division of glial cells (low glial group - LGG). Cultures were grown either on culture dishes and used for immuolabeling/staining studies (Fig. 4.1(a-b)) or on microelectrode arrays (MEAs) for the recording of neuronal dynamics (Fig. 4.1(c-d)).

Anatomical Network Structure

We first examined the anatomic structural properties of the cultures. Although it is not feasible to determine the exact connectivity structure of the cultures (despite the reduction of the system, the resulting network is still quite complex), we are capable of studying gross properties of the network structure which could lead to differences in dynamics and functional structure. As discussed previously, we control the proliferation of the glial cells such that, over time, we obtain a high glial group (HGG) and a low glial group (LGG). Although the neurons do not proliferate over time, they do grow processes and synapses, changing the neuronal network structure as the cultures age.

In order to quantify the differences in the glial network between the two culture groups, we labeled astrocytes as previously described and computed the normalized difference between the percentage of area covered by astrocytes for cultures in the HGG and LGG. This quantity is plotted as a function of DIV in figure 4.2. The measure shows that, as expected, the area covered by astrocytes is higher for the HGG, and that the ratio of coverage between the culture groups remains fairly constant over time (due to the fact that astrocytes do not proliferate in the LGG and have already formed a confluent layer by 8 DIV in the HGG).

We then studied the structure of the neuronal network for the two culture groups using a Sholl analysis (see methods). From the distribution of the number of process crossings as a function of radii, we computed the median crossing distance, total number of crossings, and longest process length for each neuron. These results are presented as a function of DIV in figure 4.3(a-c) for each culture group. We see changes as the cultures age and in certain cases between groups for these measures. The median crossing distance (a) and longest process length (c) increase as a function of time for neurons in the HGG, but both measures show a slight decrease for 13 DIV cultures in the LGG. This represents a re-organizing of the distribution over time since the total number of crossings increases as the cultures age as depicted in figure 4.3(b). Neurons in the LGG are growing more local arborizations, as compared to those in the HGG whose processes continuously increase in length over time. However, it should be noted that the density of synapses along these processes is similar over time between the two culture groups, although it is slightly higher for neurons in the HGG initially (figure 4.3(d)). Together, these labeling results indicate that neurons in the LGG are involved in more local signaling, while those in the HGG are developing more long-range connections.

Dynamics

We studied the dynamics of the cultures as a function of age to determine the effects of the changing glial network and growth of neuronal processes. Cultures were recorded from at 8, 11, and 13 DIV as described in section 4.2. Spike detection was done on the recorded signals and the resulting spike activity was analyzed as follows.

Visual observation of the recording sessions shows that cultures in the high glial group tend to persistently fire in network bursts with short silences in between bursts,

while those in the low glial group tend to fire in longer bursts with longer quiescent periods between bursting events. These quiescent periods grow in length over time. We show these differences in dynamics by examining the interspike interval (ISI) as calculated for the net spiking activity in each culture (Fig. 4.4(a)). In this plot, we examine the interspike interval of cultures as a function of DIV. The width of the ISI distribution for each culture group was increased for visualization purposes. Cultures from the high glial group are plotted in shades of red (light gray), and cultures from the low glial group are plotted in shades of blue (dark gray). The shade of the dot indicates data from a specific culture within the respective group. Note the semi-log scale for visualization purposes of longer ISI events. Initially, the distributions are uniform, showing a mix of short and long ISI values. However, over time, one can see that in the low glial group (blue/dark gray shades), the distribution becomes increasingly bi-modal. This indicates that firing events are consistently occurring within the bursts on short time scales, while the time between bursting events is becoming more polarized, with either short or long intervals between bursts and few quiescent periods of medium length. The cultures in the high glial group maintain a more evenly distributed arrangement of ISI times, although some polarization begins to appear at 13 DIV. Examples of raster plots showing this difference in dynamics over time and between culture groups can be seen in Fig. 4.4 for a cultures in the HGG (Fig. 4.4(b)) and LGG (Fig. 4.4(c)).

We then investigated the number of active electrode channels as a function of DIV. An active electrode was defined as a channel from which reliable spiking activity could be detected using the thresholding method. It should be noted that in order to record the activity from a neuron, the neuron must lie very near to the electrode and be well attached to the surface of the dish. As the network ages, some neurons die and others begin to fire,

meaning that the active electrodes can change over time. However, one expects the overall number of active electrodes to increase over time as the neuronal processes grow, allowing for more neurons to be recruited into spontaneous activity. The number of active electrodes is plotted for both the high and low glial groups in Fig. 4.5(a). In both groups this number increases over time, yet is consistently higher for the high glial group. This indicates that the higher number of glial cells allows for the recruitment of more spatially separated sites into the bursting activity.

In Fig. 4.5(b), we plot the average number of spikes per active electrode as a function of time. We see that the number of spikes per channel is lower for cultures in the low glial group, but both groups follow the same general trend of increasing numbers of spikes. This corresponds to the changes in neuronal network re-organization through the growth of neuronal processes.

Determination of functional clusters

Functional clustering was determined from the obtained spike train data using a clustering method developed in our laboratory called the functional clustering algorithm[117]. Advantages of using this algorithm include that the clustering is determined directly from the dynamics of the recorded neurons through a comparison to surrogate data, meaning that clustering is based on statistically significant similarities between firing patterns. The use of statistical significance to determine clustering also means that the algorithm has a natural stopping point and no *a priori* knowledge of the number of functional groupings is required. We briefly describe the algorithm below, and for a complete description of the algorithm, please refer to reference[117] .

The FCA can be summarized in the following 5 steps:

1. Choose a similarity metric and create a matrix of pairwise similarity values between all spike trains.

2. Use surrogate data sets (see below) to calculate 95% confidence intervals for each pairwise similarity. Use this to determine the level of statistical significance for each pairwise relationship.

3. Choose the pair of trains with the highest significance and group these trains together, recording the significance between the trains. When grouping the two spike trains, create a new train representing the joint activity by merging the spikes into a single train.

4. Remove the trains which were joined from the data set, and recalculate the similarity matrix for the new set of trains. Create new surrogate data sets, and re-calculate the pairwise statistical significances.

5. Repeat the joining steps (3-4), recording the statistical significance used in each step of the algorithm until no pairwise similarity is statistically significant, indicating that the next joining step is not statistically meaningful. At this point, determine the resultant functional groupings by observing which spike trains have been combined during the algorithm. The results of the clustering algorithm are depicted using a dendrogram where the dashed line denotes the cutoff point of the algorithm.

In order to asses similarities between firing patterns, we used the average minimum distance (AMD) which is a new measure designed to detect synchronous events in discrete event data[117]. To compute the AMD between two spike trains S_i and S_j, we calculate the distance Δt_k^i from each firing event in S_i to the closest firing event in S_j. We then define

$$D_{ij/ji} = \frac{1}{N_{i/j}} \sum_{k} \Delta t_k^{ij} \tag{4.2}$$

where $N_{i/j}$ is the total number of spikes in S_i or S_j respectively. Finally, we define the AMD to be

$$\theta_{ij/ji} = \frac{D_{ij} + D_{ji}}{2} \tag{4.3}$$

Surrogate data sets used in the calculation of significance were created through the addition of jitter to spikes (also known as dithering or teetering). The jitter is drawn from a uniform distribution over a given window. Here we used a jitter window of 70ms, centered on each spike. This time scale allows us to examine synchronization at the level of network bursts in the culture.

To asses the level of statistical significance, we used 10,000 surrogate data sets to create cumulative distribution functions (CDF) of AMD values and determine 95% pairwise significance levels. The scaled significance (Fig. 4.8) is measured in units defined as the distance from the midpoint of the CDF to the 95% significance cutoff. Thus, a scaled significance greater or equal to 1 is deemed to be statistically significant, while values below 1 are not.

The FCA was applied to the spike train data recorded from cultures in both groups at 8, 11, and 13 DIV. In order to keep the total number of spikes used in the algorithm below 50,000, a 3 minute window of data was used, with the exception of one 13 DIV culture in the LGG for which a 1 minute time window was used.

Since we observe difference in dynamics as a function of DIV as well as between culture groups, it is interesting to ask how these differences will be embodied in the

functional structure of the network. To study the functional groupings of active sites, we implemented the FCA as described above.

We first explore the functional clustering as a function of time for cultures within each group. In Fig. 4.6(a),(c) we show examples of the spatial layout of the functional groupings over time for the two culture groups. In this figure, each square represents the spatial location of an electrode on the culture. The spatial layout of the squares here corresponds to the spatial layout of the MEAs as seen in Fig. 4.1. Colored squares represent active electrodes, and squares of the same color belong to the same functional group. The dendrograms corresponding to the spatial clustering shown for the the plots in (a) and (c) at 8 and 13 DIV are shown in Fig. 4.6(b,c) respectively. For the case of the high glial group, we see that, initially, the culture contains multiple groups that largely represent local regions of the MEA. This indicates that only local groups of neurons are involved in synchronous activity during network bursts. However, as the culture ages, the synchronization becomes increasingly global, and more neurons are recruited into the largest cluster. To quantify this effect, we plotted the percentage of electrodes that participate in the largest cluster as a function of DIV in Fig. 4.7.

Interestingly, we do not see this increase in cluster size in the case of cultures from the low glial group, as the clustering instead remains fragmented over time as seen in Fig. 4.6. This fragmentation corresponds to the lack of change over time in the percentage of electrodes that participate in the largest cluster seen in Fig. 4.7.

Finally, we were interested in quantifying the level of synchronization present in the detected functional groupings. This was done through the examination of the scaled significance used in the joining steps of the FCA. An example of the scaled significance and

the significant clustering steps for a 11 DIV culture is shown in Fig. 4.8(a). Note that a higher scaled significance indicates a tighter relationship between spikes of electrodes. We then calculated the average value of the scaled significance for the statistically significant steps for each culture. In Fig. 4.8(b) we show the average scaled significance used in the significant clustering steps as a function of DIV for both the high and low glial groups. The average scaled significance is greater for the high glial group on each recording day, indicating that the high glial cultures show a tighter relationship between firing events during the bursts. However, the average scaled significance grows over time for cultures from both groups, indicating that the firing becomes more synchronous as all cultures age.

4.4 Discussion

While previous work has studied either structural properties of cultured networks or analyzed the dynamics of these cultures, there is little work, which attempts to link changes in structural network properties to the resulting dynamics and functional interactions. The work that has been done has focused on the effects of different substrates used to coat the dishes[118] or on patterned plating of cultures[100,119]. Here we studied cultures grown with either a high density of glial cells or a low density of glial cells in order to relate the influence of the glial network on neuronal dynamics as a function of time (and therefore increasing density of glial cells). It is known that the presence of glial cells shapes neuronal development[111], and Sholl analysis on the arborization of neuronal processes revealed that cultures in the high glial group contained neurons whose processes grew globally over time, while cultures in the low glial group grew increasingly local processes. Study of synchronization in coupled oscillators has shown that the addition of global connections (such as in a small-world network) leads to greater synchronization[120,121]. Additionally, astrocytes have been shown to mediate spontaneous calcium waves which correspond to

the presence of synchronized activity in dissociated cortical cultures[70]. Astrocytes are also responsible for the modulation of slow oscillations in *in vivo* cortical networks through the regulation of synaptic receptors[116]. It is therefore reasonable to conclude that the observed differences in neuronal dynamics between the high and low glial groups is likely due to the influence of the glial network on the neuronal network.

Both culture groups displayed synchronized activity in the form of network bursts, but the specific form of these bursts varied between the two groups. The high glial cultures had more active electrodes, however, the total number of spikes per electrode was similar between the two groups for each recording session. As shown in previous studies[64], the cultures became increasingly active over time as seen in the rise of active electrodes and total spikes per electrode. However, the cultures from the high glial group displayed persistent bursting activity with a varied distribution of interspike intervals. Cultures from the low glial group displayed spiking patterns that became increasingly polarized towards either short or long intervals between spiking events, corresponding to an increase in the spiking frequency during a burst with larger intervals between bursting events.

The changes in neuronal dynamics over time led to a difference in functional classifications. We applied the FCA to detect functional clusters and examined the spatial aspect of the resultant clusters. Cultures from the high glial group initially showed the formation of local clustering which became more global over time. However, cultures in the low glial group showed a different behavior as the groupings remained fragmented over time. These functional differences indicate that the cultures from the high glial group display bursting events which become increasingly globally synchronous while bursting events are consistently composed of smaller groups of synchronous activity in the low glial

culture. Thus the functional structure detected by the FCA reflects the expected changes due to the differences in anatomical structure discussed above.

We also quantified the amount of synchronization present within the functional clusters by comparing the scaled significance used in the joining steps of the FCA. Cultures from the high glial group showed greater values of significance indicating that the firing events within the bursts are more highly synchronized. The fact that these cultures have a higher glial density indicates that the glial network aids in the synchronization of the neuronal network, which is again consistent with what we expected from structural observations. The significance used in clustering increased as a function of DIV in both groups indicating that as the neuronal networks evolve, the firing events become increasingly correlated. Thus the overall observed synchronization of bursts is the result of changes in both the neuronal network and the underlying glial network.

Despite the fact that dissociated neuronal cultures are a simplified system and their structure and dynamics cannot be directly linked to brain dynamics, we have shown that they are a good reduced system in which to study the interplay of structure and dynamics in neuronal networks. Unlike neuronal data recorded from the intact brain of humans or animals where it is difficult to study the properties of the underlying network structure, we are able to manipulate gross properties of the anatomical network structure and observe how these changes affect neuronal dynamics. We can then apply methods developed to detect functional structure (such as the FCA) and relate the differences in the obtained clusterings to the known structural changes. This allows for the discovery of the important parameters that affect the relationships between structure and dynamics, which can later be used to make inferences about network properties that can direct research in more complicated systems such as the brain.

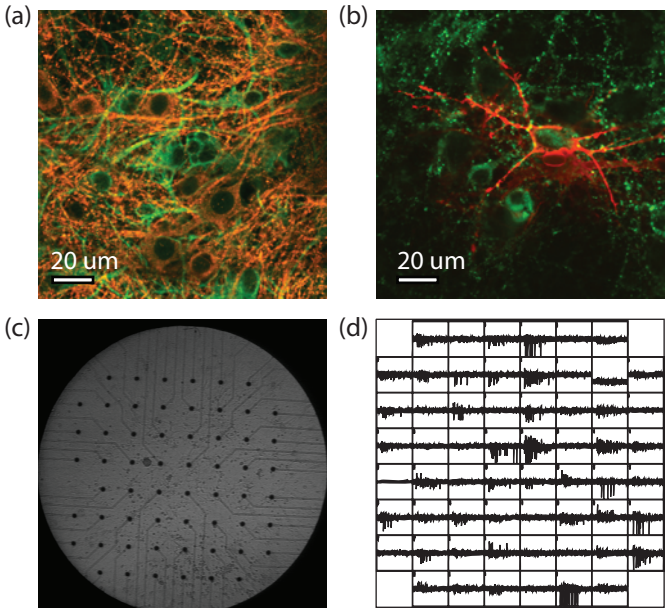

Figure 4.1 (a) Immunocytochemical labeling of neurons and astrocytes showing morphology. Neurons are immunolabeled for beta-III tubulin (red), while astrocytes are immunolabeled for GFAP (green). (b) Example of an isolated neuron stained with DiI (red). Synapses are immunolabeled for synaptophysin (green). (c) Example of a culture grown on an MEA showing the spatial layout of the electrodes (black dots) The distance between electrodes is 200 μm. (d) Example of recorded activity from a culture displaying bursting dynamics. The spatial layout of the activity traces corresponds to the spatial layout of the electrodes shown in (c). Each window represents a 500 ms time window during which the synchronous firing of neurons can be seen.

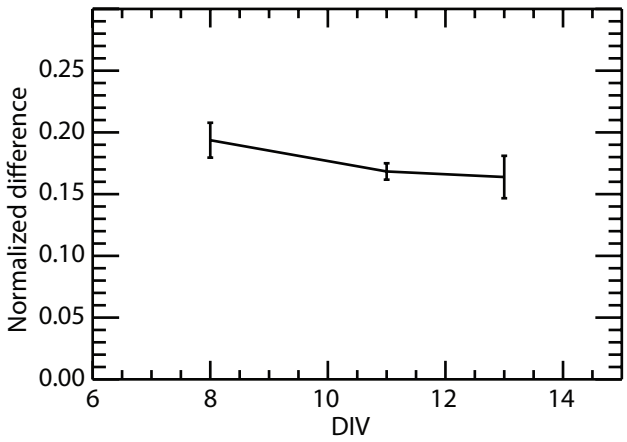

Figure 4.2. The normalized difference calculated between the percentage of coverage of glial cells in the high and low glial groups (Eqn. 4.1). This measure remains approximately constant over time due to the fact that the glial cells do not multiply in the low glial group and have already covered the culture dish by 8 DIV in the high glial group.

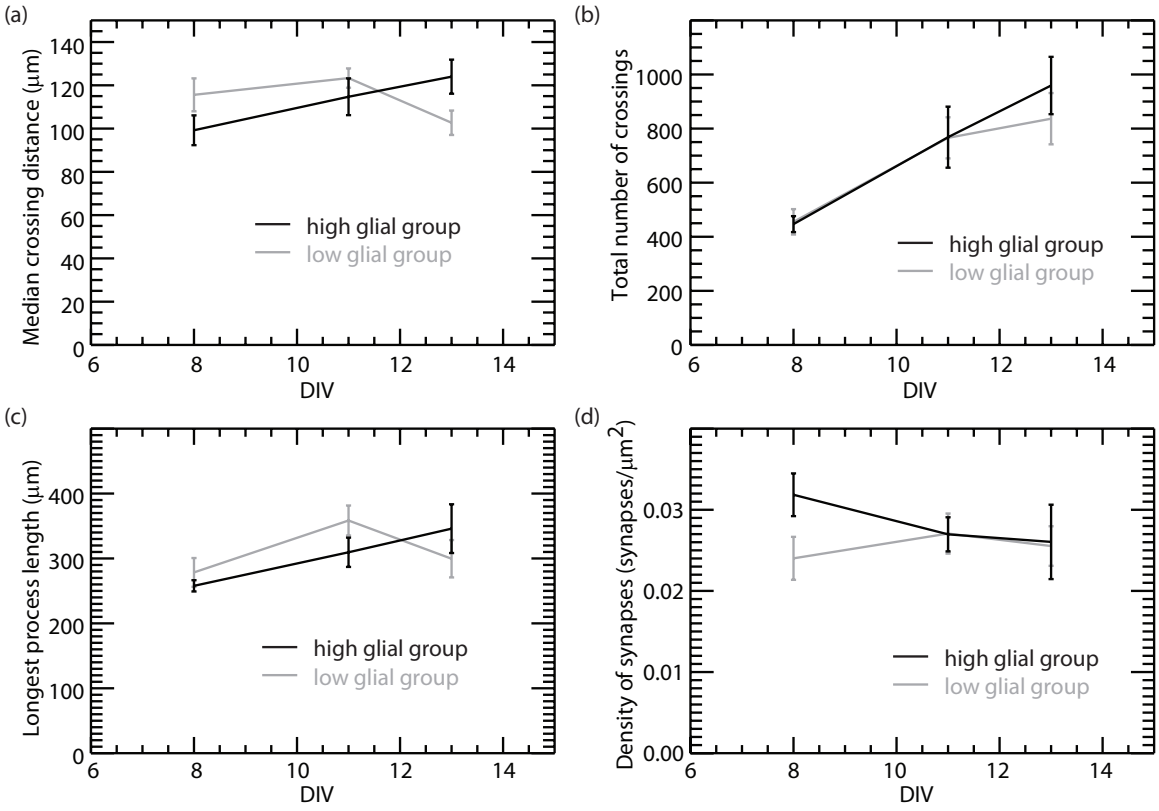

Figure 4.3. Neuronal process morphology and synapses. (a-c)Properties of the distribution derived by a Sholl analysis conducted on DiI labeled neurons (see Sect. II D). (a) Median crossing radius as a function of DIV. (b) Total number of crossings. (c) Longest process length. (d) Density of synapses co-localized with DiI stained neuronal process, as a function of DIV.

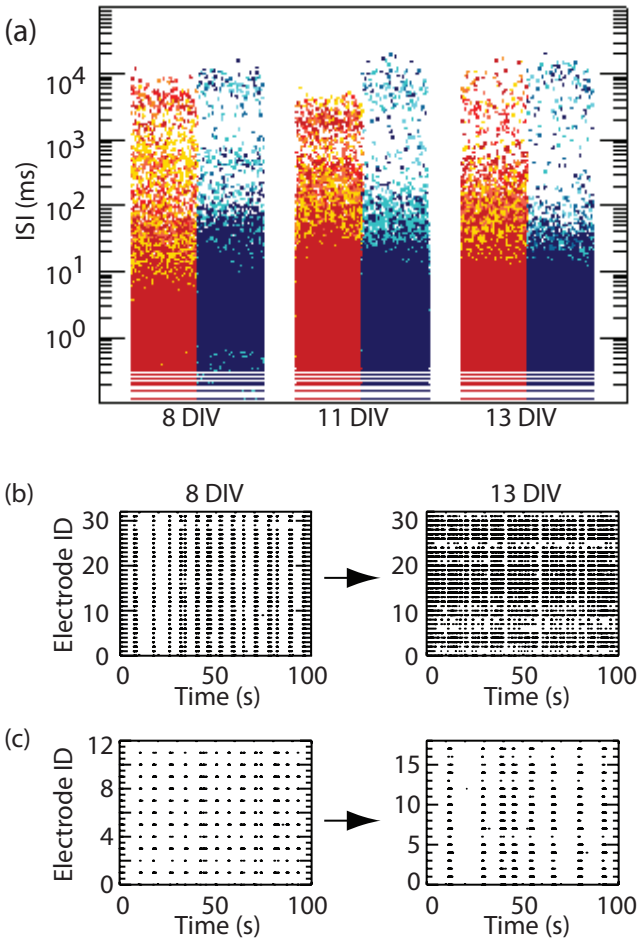

Figure 4.4. (a) ISIs plotted as a function of DIV for high and low glial groups. The width of the distributions was increased for visualization purposes. Shades of red (light grays) indicate data from the high glial group while blues (dark grays) denote the low glial group. The specific shade denotes data from a given culture in the group. (b) Example raster plots for a culture in the high glial group at 8 and 13 DIV. (c) Example raster plots for a culture in the low glial group at 8 and 13 DIV. One can see that the cultures in the low glial group show an increasingly polarized distribution of ISI indicating the development of long quiescent periods in between bursting events.

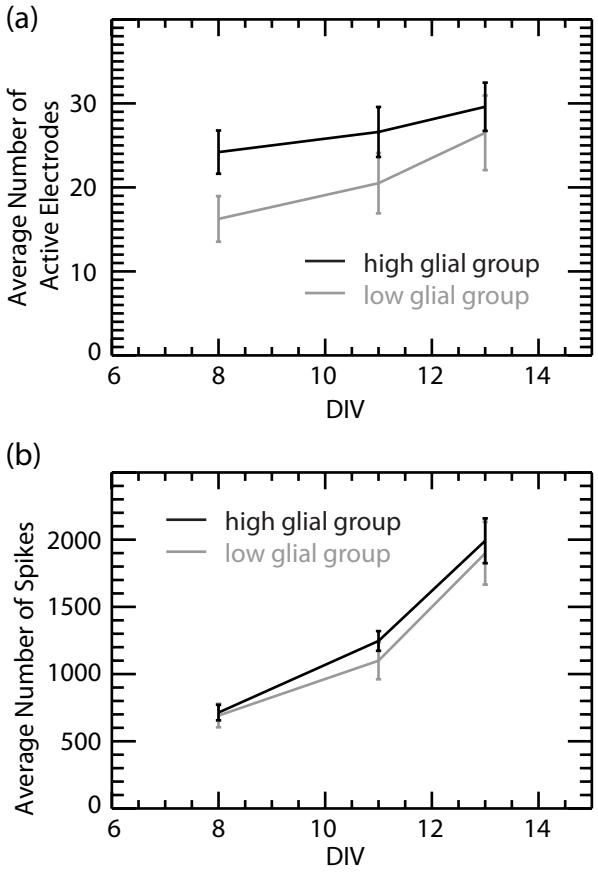

Figure 4.5. (a) Number of active electrodes as a function of DIV for both high and low glial groups. While this number grows over time for both groups, it remains smaller for cultures in the low glial group indicating that the glial network seems to influence the recruitment of sites in the neuronal network. (b) Average number of spikes per active electrode as a function of DIV. This number is similar and grows for both culture groups as the cultures become more active over time, corresponding to changes in the neuronal networks.

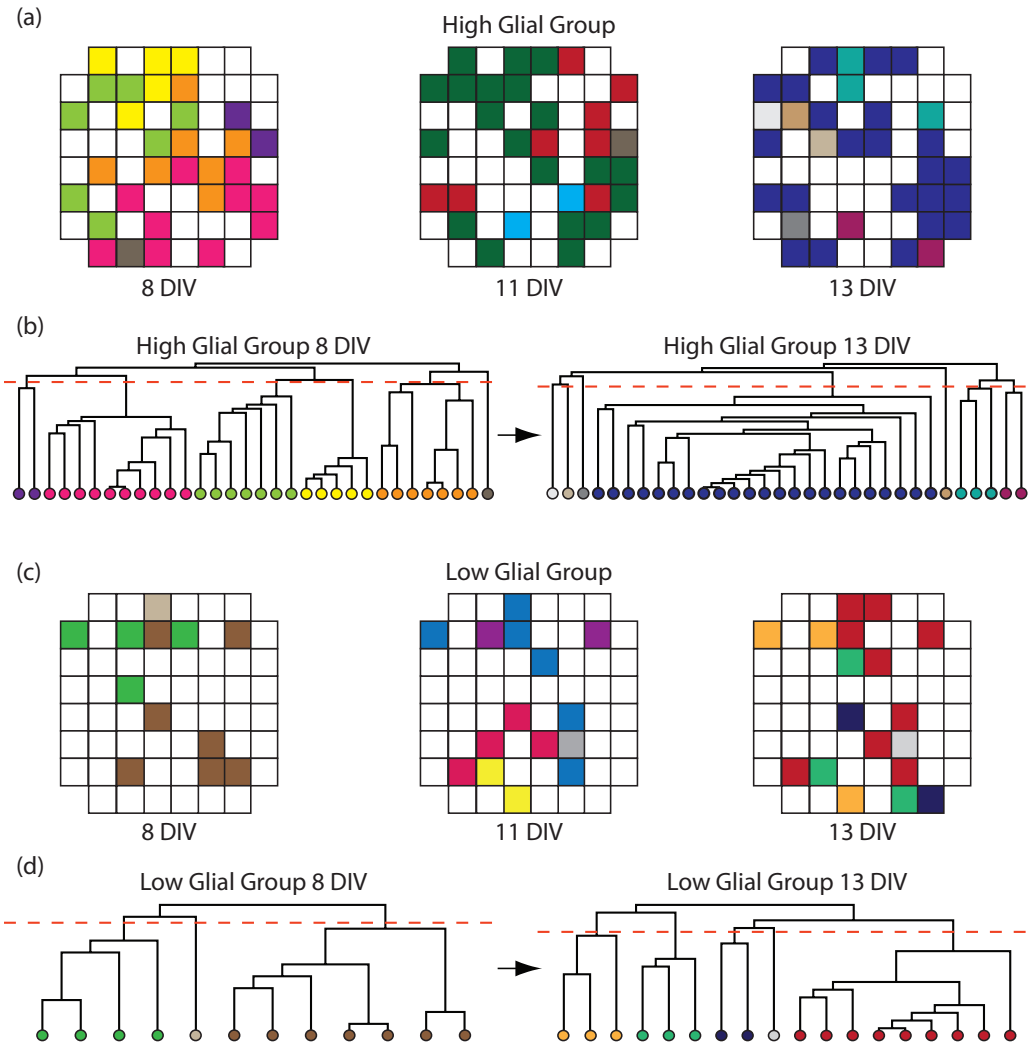

Figure 4.6. Examples of functional groupings obtained from the application of the FCA to culture data. (a,c) Spatial representation of functional clusters. Colored squares indicate active electrodes and squares of the same color belong to the same functional group. (a) High glial group. (c) Low glial group. The clustering becomes increasingly global over time for the high glial culture, while the clustering of the low glial culture becomes increasingly fragmented. (b,d) Examples of the dendrogram corresponding to the spatial maps in (a) and (c) at 8 DIV and 13 DIV.

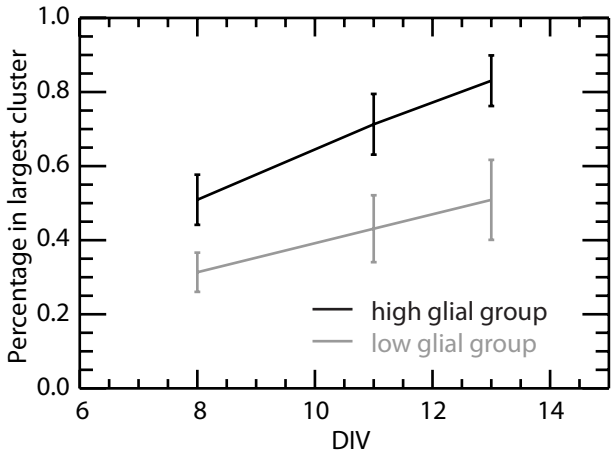

Figure 4.7. Percentage of electrodes participating in the largest functional cluster as a function of DIV. The percentage increases over time for the high glial group indicating the spread of global synchronization. Although we also see an increase in this number for cultures in the the low glial group, the percentage remains smaller, as these groupings remain fragmented.

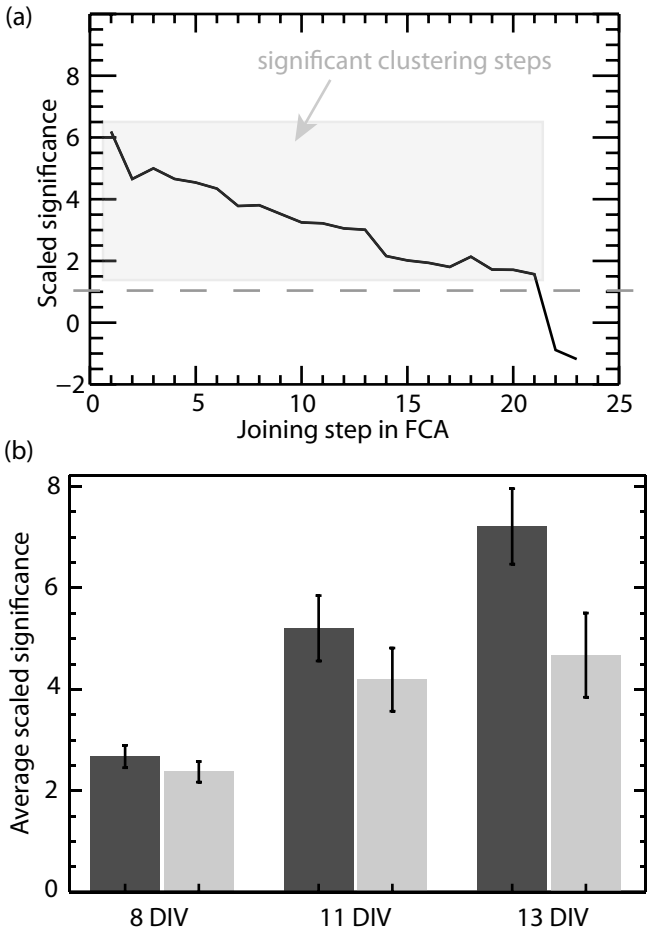

Figure 4.8. (a) Example of the scaled significance used in each step of the FCA for an 11 DIV culture from the HGG. The dashed line denotes the clustering cutoff, and steps above this line (enclosed in the gray box) are statistically significant. (b)The average scaled significance used in the significant clustering steps. This value was averaged over cultures from the HGG and LGG and calculated as a function of DIV. The significance increases as a function of time, indicating an increase in the synchronization of spiking within network bursts. The high glial cultures also show increased significance (synchronization) compared to the low glial cultures.

Chapter V.

Pattern Segmentation with activity dependent natural frequency shift and sub-threshold resonance

5.1 Introduction

The brain forms a complex interconnected network in which spatio-temporal patterns of neuronal activity are thought to underlie its information processing. However, basic questions remain unanswered. What aspects of this patterning represent the information content? How do these network wide representations robustly emerge out of the dynamical properties of individual neurons? How are distributed features dynamically bound together, while at the same time segmented out from the rest of the network, to form a coherent representation? These questions not only pertain to the brain, but also to the formation of distributed representations in any network. In terms of neuronal processing, many proposed coding schemes are based on either the firing rate or the temporal structure of spikes in response to a stimulus[37,39,122]. Correlations within these activity patterns lead to network rewiring, where the connections between neurons encoding the same functional pattern are strengthened. However, it is unclear how these regions of enhanced connectivity or biased input can lead to virtually instantaneous, dynamically evolving, and robust separation of activity patterns, which in turn encode for functionally diverse information content, while embedded within the same interconnected group of neurons.

Single neurons integrate input to generate action potentials, however they can also

display damped sub-threshold oscillations giving them complex dynamics and sensitivity to temporal patterns of input. The ability to resonate at particular frequencies has been observed in many experimental preparations[51,123]. The natural frequency has been shown to be voltage dependent and it can shift at both depolarized and hyperpolarized membrane potentials[50,54,55]. This phenomenon was reported in various cell populations such as hippocampal pyramidal neurons[6,7]and pyramidal cells of the amygdala olfactory cortex[8]. In the case of hippocampal pyramidal cells, the underlying ionic mechanisms are related to a slow hyperpolarization-activated cation current (often referred to as I_h current), a slow activating potassium current (so called M-current as it acts through muscarinic receptors), and an instantaneously activating, inwardly rectifying potassium current. Interestingly, these mechanisms are activated differentially when a cell is hyperpolarized (I_h is activated) or depolarized (I_M is activated). In all cases, however, voltage gated sodium channels played a central role, as application of tetrodotoxin (TTX) abolished the sub-threshold oscillations[6,8]. The observed resonance shifts range from a couple of Hz to more then 10Hz.

At the same time oscillations of large neuronal populations have been observed with local field potentials (LFP) or EEG measurements[124–126], and these oscillations are classified into discrete frequency bands spanning single to tens of Hertz. These brain rhythms have been implicated in various cognitive functions[127,128]. However, the influence of these oscillations on individual neuronal activity patterns or network wide activity has remained unclear[129]. Sub-threshold oscillatory input through synaptic or ephaptic coupling provides feedback between brain oscillations in the local field potential and individual neurons[130]. This idea is experimentally supported by findings that oscillations in the visual system can affect downstream processing, as seen in the phase locking of neurons in the

lateral geniculate nucleus (LGN) to the 50 Hz oscillations in the input received from the retina[131].

We propose a novel mechanism that links the voltage-dependent resonance frequency shifts of individual neurons with the large-scale oscillatory rhythms observed in the brain to selectively activate neuronal ensembles. We hypothesize that sub-threshold depolarization from synaptic coupling or external input can shift neurons into and out of resonance with specific bands of extracellular oscillations and this resonance shift can act as a mechanism to selectively activate functionally diverse neural populations. Thus a given oscillatory band acts as a readout carrier for neurons that are selectively depolarized and shifts their resonance frequency into that band. We investigate this mechanism for memory storage and retrieval but it could also pertain to rapid attention switching[22–24]. We show that this is a robust mechanism that works within broadly defined known biological constraints[129,132] and can explain experimentally observed neuronal dynamics during the storage and retrieval processes[133–135]. It also provides a mechanism for dynamic signal separation within a network that can change rapidly as a function of external input and network structure, or both. It provides flexibility and easily combines patterns of external stimuli with intrinsic structure for emergent readout of activity patterns. The proposed mechanism is not limited to neuronal networks but it is a universal dynamical mechanism that can be more generally applied to other networks. As we show below, the only two required features are that the network is composed of oscillatory nodes whose natural frequencies vary as a function of the input magnitude and a readout frequency.

5.2 Methods

Network of Modified Resonate-and-Fire Neurons

The dynamics of each neuron is described by Resonate-and-Fire Neurons[49] modified with a current dependent resonance frequency with the following equations:

$$\frac{dx^i}{dt} = bx^i(t) - \omega^i(t)y^i(t) + I^i_{ext}(t) \tag{5.1}$$

$$\frac{dy^i}{dt} = \omega^i(t)x^i(t) - by^i(t)$$

where

$$\omega^i(t) = \omega^i_o + \delta I^i_s(t) \tag{5.2}$$

and

$$I^i_s(t+1) = \frac{\alpha I^i_s(t) + I^i_{ext}}{1+\alpha} \tag{5.3}$$

Here x^i is the internal current and y is the voltage of i^{th} neuron in the network and ω^i is the resonance frequency (or eigenfrequency) of the i^{th} neuron. It shifts from its intrinsic value $\omega_o{}^i$ and is proportional to the current input $I_s{}^i$, with proportionality constant δ (Eq. (5.2)). $I_s{}^i$ is a slowly changing function ($\alpha=10^5$) of the current input term $I_{ext}{}^i$ in Eq. (5.1), which in

turn is defined as the sum of the synaptic coupling and sub-threshold oscillatory input current:

$$I_{ext}^{i}(t) = \sigma C_{syn} \sum_{j} S^{ij} I_{syn}^{j}(t) + I_{input} \tag{5.4}$$

where

$$I_{input}(t) = A\sin(ft) + I_{sub} \tag{5.5}$$

Here C_{syn} is the strength of synaptic coupling, σ is an additional weight multiplier to represent heterogeneities in network connectivity strength, S^{ij} is the adjacency matrix, and I_{syn}^{j} is excitatory post-synaptic current input. We model I_{syn}^{j} with a double exponential pulse that lasts approximately 15 ms. Eq. (5.5) describes the sub-threshold oscillatory input current, where A is the amplitude of oscillations, f is the driving frequency, and I_{sub} is sub-threshold external current. When the voltage reaches threshold, the current and voltage variables are reset to 0, and the neuron cannot receive input for a 5ms refractory period. The neurons are additionally driven by noise; we set the voltage variable y^i above threshold with a given probability p_N. For all simulations unless otherwise stated, the parameters are b = -1, ω_o = 100 (corresponds to ~16 Hz), δ = 40, σ=4, C_{syn} =5, A=3, I_{sub}=10, α=10^5. Eq. (5.1) is integrated using Euler's method, with a time step of h=10^{-5}. Four hundred neurons are connected into a 1D sparsely connected networks using the Small-World[136] framework, with connectivity radius R=3 and rewiring probability p=0.1 unless otherwise stated.

Modeling the Inhibitory Network

To study the potential impact of inhibitory neurons on the proposed pattern separation mechanism, we coupled an inhibitory network of 400 integrate-and-fire[65] neurons to the excitatory resonate-and-fire networks. For simplicity we chose to use the integrate-and-fire model, where the dynamics of inhibitory neurons are given by:

$$\frac{dv^k}{dt} = -Rv^k + C_{syn}\sum_j S_{kj} I_{syn}^j(t) \tag{5.6}$$

Where v^k is the voltage of the k^{th} inhibitory neuron, R is the membrane leak constant, C_{syn} is the strength of synaptic coupling, S_{kj} is the adjacency matrix between the k^{th} inhibitory neurons and the j^{th} other neurons in the network (where j spans both excitatory and inhibitory neurons) and I_{syn}^j is the input current received. All parameters are the same as for the excitatory network with the following exceptions. C_{syn} is negative for inhibitory synapses. Network connectivity between inhibitory neurons is random, excitatory to inhibitory connections are local, and inhibitory to excitatory connections target randomly the whole network except the heterogeneity itself. To identify to what degree the excitation and inhibition are balanced in the network, we quantify the inhibitory network strength as a ratio of the average inhibitory synaptic input to average excitatory synaptic input that excitatory neurons receive integrated over a 3 second time window of the simulation.

Targeted Inhibition

For the simulations on dynamic switching between competing heterogeneities, the effect of inhibition was modeled with direct, targeted inhibitory connectivity between the cells belonging to different heterogeneities. That is, all neurons within one heterogeneity

had weak, targeted inhibitory connections, of strength C_{syn}=2.5, to all cells within the second heterogeneity.

Calculation of Phase and Mean Phase Coherence

We created continuous signals of the network activity within and outside of the heterogeneity, by collapsing all spike trains within given region into one aggregate spike train and convolving each signal with a Gaussian function of 10 millisecond width. To quantify the phase locking we computed the instantaneous phases of the network activity and the sub-threshold oscillatory input using the equation:

$$\phi(t) = \arctan(\frac{\tilde{s}(t)}{s(t)}) \tag{5.7}$$

where the instantaneous phase ϕ(t) for each signal is found using the Hilbert transform $\tilde{s}$(t) of the signal s(t) defined as:

$$\tilde{s}(t) = \frac{1}{\pi} p.v. \int_{-\infty}^{+\infty} \frac{s(t)}{t-\tau} d\tau \tag{5.8}$$

The p.v. denotes the Cauchy principal value. The Mean Phase Coherence (MPC) is given by:

$$MPC = \left| \frac{1}{N} \sum_{j=0}^{N-1} e^{i\Delta\phi(j\Delta t)} \right| \tag{5.9}$$

where Δϕ is the phase difference between the instantaneous phase of the network activity signal and the instantaneous phase of the sub-threshold oscillatory input current, N is the number of timesteps in the simulation, and Δt is the step size.

Calculation of Firing Rate Response Time

Neurons were driven with a subthreshold oscillatory input with constant frequency and given an additional subthreshold current step 10 seconds into the simulation to shift their resonance. To quantify the onset of firing, we calculated the average firing rate over a moving time window of 500 ms. Similar results were observed for 250 and 750 ms time-windows.

5.3 Results

To explore this pattern separation mechanism in the brain context, we investigated maximally reduced neuronal networks fitting the above criteria. Namely, we constructed networks composed of 400 Resonate-and-Fire neurons[49]. These neurons are essentially damped oscillators that emit an action potential when the voltage reaches a threshold. In addition, the neurons have a current dependent resonance frequency and are driven by a weak (sub-threshold) external oscillatory current (see methods section 5.2).

We impose the experimentally observed voltage dependent resonance frequency shift[50,54,55] by Eq. (5.2), (see methods section 5.2) and observe the resonance phenomena as we vary the driving frequency of the sub-threshold oscillatory input current (Fig. 5.1). The firing frequency of neurons preferentially increases when the driving frequency matches the resonance frequency of the neuron. The cells shift their resonance in response to the applied current input (Fig 5.1a). In a network, this additional current input to a single neuron can arise from co-activation of the neurons having higher synaptic coupling. We refer to regions of the network containing additional synaptic connectivity as network heterogeneities. Neurons within network heterogeneities receive additional sub-threshold

current input from their synaptic connections. This current shifts the resonance frequencies of neurons within the heterogeneity to higher frequencies (Fig. 5.1b), separating the response frequencies of the heterogeneity from rest of the network (Fig. 5.1c), and thus allowing for selective activation of the heterogeneity for matching driving frequencies (Fig. 5.1d). Thus, even though all neurons in the network are driven with the same sub-threshold oscillatory input current representing ongoing brain rhythms, the resonance frequency shift allows higher connectivity regions to separate out from the rest of network in their firing rate profiles.

Figure 5.1c depicts the network wide resonance curves (i.e. mean firing frequency within the given neural population) when there is no cellular resonance frequency shift ($\delta=0$) and with current dependent resonance frequency shift ($\delta=40$) for two different coupling strengths (coupling multipliers $\sigma=1$ and $\sigma=4$, please refer to methods section). We observe a significant shift of the network response towards higher driving frequencies with increased coupling strength, when the neuronal resonance frequency is current-dependent. At the same time the shape of the resonance curves changes significantly, and can be understood by considering the distribution of resonance frequencies in the network. The response of the network region with lower coupling is narrower but taller indicating, on one hand, higher response specificity to the frequency of the driving oscillation, and at the same time an increased network response magnitude in terms of an elevated mean network firing frequency. This is due to the fact the variance in the resonance frequencies of the network of neurons increases significantly with network coupling strength (error bars on Fig. 5.1b) because of the higher variability in the total input the neurons receive. This in turn causes some neurons to be in resonance with the driving current while others remain out of resonance, which makes the network response as a whole change gradually and

achieve lower overall values. The network achieves maximal response when the driving frequency matches the resonance frequency of most neurons in the network. This variation in the resonance frequencies of neurons in the network also explains the asymmetry in the resonance peak. When the driving frequency is high there are fewer neurons that resonate with the driving oscillatory current (note the widest distribution of resonance frequencies is at the falling phase of the network resonance curve, Fig. 5.1b). Their number quickly increases as the driving frequency is lowered. For intermediate values of driving frequency there is a finite pool of neurons that resonate and activate the network-wide response.

This separation mechanism is robust across a wide range of parameters. We quantified the separation mechanism with two metrics, the peak-to-peak distance ΔP and the resonance firing frequency difference ΔF (please refer to Figure 5.1c). We explored the separation of network activation for various network connectivity strengths as a function of the network topology, strength and frequency of external oscillatory current, noise level and magnitude of activity dependent resonance shift. The network topology is varied using the small world network paradigm[136], with additional network heterogeneities added in the coupling weight within neuronal subgroups of the network.

To better understand the workings of the proposed mechanism, we quantify the signal separation, both ΔP and ΔF, for various system parameters (Fig 5.2). To investigate the sole effect of synaptic strength on signal separation for different simulation parameters, we eliminated the connections between the heterogeneity and the rest of the network, which we refer to as disconnected networks. For both metrics (ΔP and ΔF), values above zero denote significant separation; all error bars represent 1 standard error of the mean, and all means are averaged over 4 simulations. As expected, the peak-to-peak separation increases with larger values of the resonance frequency shift δ (not shown). Both measures

report separations of several Hz for varying values of δ. Results presented in Figure 5.2 are for disconnected networks, therefore the effects on separation are due to disparate connectivity strengths alone. The separation mechanism is not limited to particular resonance frequencies of the neurons. However, the measures report weaker separation at higher resonance frequencies (Fig 5.2a). The peak-to-peak distance increases while the resonance firing frequency difference decreases (Fig 5.2b, c) for higher coupling weight within the network heterogeneity or higher driving noise. The first is due to the fact that both of these quantities provide additional activity levels (or current) to recipient neurons increasingly shifting their resonant frequency away from the baseline. However since neurons can have a variable number of inputs, stronger coupling increases the spread of instantaneous resonance frequencies, which widens but reduces the height of the resonance peak. We have also investigated the size of the external oscillatory current required to observe signal separation. We report its magnitude (Fig 5.2d) as a ratio to a minimal constant threshold current needed to generate a spike. Robust signal separation appears for oscillatory amplitude as low as 0.1 of the threshold current, well within those observed experimentally[130,137] (Fig 5.2d).

We then investigated how the signal separation changes for two interconnected regions as a function of the network topology and the number of connections (Fig. 5.3). We vary the network topology from local to random coupling by changing the connection rewiring probability[136]. We find that this separation mechanism is effective across various network connectivity parameters. Both separation measures are only marginally influenced by the rewiring probability, showing a small decrease of separation for increasingly random networks. This is due to the fact that for more random networks there are relatively fewer connections within the functional subgroups while the subgroups are more tightly

interconnected. At the same time, peak-to-peak separation increases for a higher radius of connectivity, as it provides additional input variance between the neurons within the heterogeneity and outside of it.

The above results indicate that we see a robust separation in the frequency response of the neurons forming the network heterogeneity from the rest of the network. It has been shown that hippocampal memory formation both in animals and humans is accompanied by increased power in the theta band oscillation as well as phase coherence of neuronal activity with oscillations at that frequency[133–135]. We hypothesize that the experimentally observed increase in power, for example of theta during memory consolidation, as well as the increased phase coherence of neuronal activities with that band, can be explained by our resonance readout mechanism, as it is well established that the resonating oscillators lock to driving oscillatory signals[138]. To that effect we investigated the difference in the power spectrum of the average activity within and outside of network heterogeneities. We compared the power spectrum of the average activity within the network heterogeneity to the rest of the network and found a notable increase in power when the driving oscillation is in resonance with the network heterogeneity (Fig 5.4a). To better understand the increase of power around the driving frequency, we measured changes in the phase locking between the neurons within and outside of the heterogeneity as a function of driving frequency. To quantify the phase locking we computed the instantaneous phase of the network activity. Using the phase difference between the network activity and the sub-threshold driving oscillation, we calculated the Mean Phase Coherence (MPC)[139], and found a substantial increase in mean phase coherence between the driving oscillation and the heterogeneity at its resonant peak (Fig 5.4b). Here we depicted the mean phase coherence as a function of the driving frequency for the heterogeneity (blue

line), for the rest of the network (green line), and for the difference between the two (black line). We observe that the mean phase coherence between the network firing and the driving oscillation is relatively highest at the raising phase of the network resonance curve peaks for both the heterogeneity and the rest of the network. Thus the proposed resonance frequency shift mechanism separates out the cell activities within a network heterogeneity for a significant range of driving frequencies in both their firing rate and phase coherence with ongoing oscillations. It is interesting to note that the mean phase coherence drops rapidly on the falling phase of the resonance curve. This again can be attributed to the large heterogeneity in cellular resonance frequencies, with relatively few neurons driving the network-wide response.

We have shown that current dependent resonance shifts can separate out regions of a network with higher coupling in both their firing frequency and phase locking to sub-threshold oscillatory input. We then investigated the response time of the network to new patterns of input in order to understand how long the network takes to form separated representations in response to shifting resonances. Here the timescale is set by the frequency of the oscillatory input and can potentially be directly compared with experimental findings measuring response time to the incoming stimulus[140–142]. We investigated the timescale of pattern formation by observing the response time required to reach the significantly elevated firing rates observed in the resonance curves. Specifically, to probe this onset time of enhanced resonant firing, we applied an additional sub-threshold current input during the simulation and measured the time delay between this input and the significant change (see methods section 5.2) in neuronal firing rate (solid black lines in Fig 5.5). As before, we simulated the sub-networks having two strengths of coupling constants σ. We found that the response time critically depends on the relative position (in

frequency space) of driving frequency with respect to network resonant curve (Fig 5.5a). The network response time to the external input on the rising portion of the resonance curve (Fig 5.5b) is significantly faster than on the falling portions (Fig 5.5c,d). The shifted resonance curve of the heterogeneity (high σ) relative to the rest of the network (low σ) results in the rise and decline portions of their resonance curves to occur for different driving frequencies. Therefore, we observe that for driving frequencies where the resonance curves overlap (Fig 5.5c) and the neurons in the heterogeneity are on the upward sloping portion of their resonance and the neurons outside of the heterogeneity are on the downward portion, the response times are widely different. (Fig 5.5c inset).

This variation in the timescale for response times can be explained by the behavior of the network's mean phase coherence at different driving frequencies, and by the resonance frequency distribution. When the mean phase coherence is large and a significant number of neurons are active (i.e. they are in resonance), even a small perturbation in the current input drives a rapid network response, as the active neurons synchronously respond to perturbation. Here the response happens within a single cycle of the driving oscillation. However, if the neurons are largely desynchronized the rapid response to the current perturbation is not observed and the slow drift in the network response can be attributed to slow changes in the average cellular resonance frequencies due to the current input. This large variation in the response times potentially provides an additional mechanism of signal separation.

We have shown a potential mechanism for ensemble activation in simplified excitatory only networks. However, inhibition can potentially play an important role in further separating the activity of the functionally disparate network regions. To illustrate this we formed and coupled an additional network of 400 inhibitory Integrate-and-Fire[65]

neurons to the existing excitatory network such that the activity of the heterogeneity and rest of the network are mutually inhibitory. We varied the strength of the inhibitory coupling and found that inhibition enhances the separation between the activated patterns (Fig 5.6). This effect is not surprising as the inhibitory neurons are activated by the corresponding resonating excitatory population and inhibit other excitatory neurons, driving their resonance frequencies away from the driving frequency at the same time. To quantify the strength of inhibition in relation to the strength of excitation, we show the separation between activated patterns as a function of the ratio of the mean total inhibitory to excitatory inputs that the cells receive over time. The ratio of one corresponds to a balanced network (Fig 5.6).

Inhibition can play additional, critical role within this framework. For the resonance frequency shift mechanism to be a general coding strategy, it has to be successfully applied to separate multiple competing neuronal representations. We show that separate heterogeneities can be selectively activated and dynamically switched through the use of targeted lateral inhibition (see methods section 5.2). Excitatory neurons within competing heterogeneities mutually inhibit each other so that activation of one heterogeneity shifts the resonance of another heterogeneity away from the frequency of driving oscillation. Figure 5.7 shows an example network with two heterogeneities of identically enhanced synaptic coupling (σ=4). In this case, the heterogeneities do not overlap and share basic excitatory connectivity (σ=1) between each other and across the rest of the network. In addition, there are targeted inhibitory connections originating at one heterogeneity and targeting neurons in the other heterogeneity. Sub-threshold input applied to a subset of neurons within each heterogeneity selectively enhances the firing rate in that heterogeneity, but no enhanced firing occurs when input is applied to regions of the network outside of either heterogeneity

(Fig 5.7a,b). Thus, the heterogeneities can be selectively and dynamically activated. Similar strategy (targeted inhibition) can be applied to multiple and overlapping representations.

The resonance shift mechanism not only selectively activates competing heterogeneities, but also dynamically controls switching the activation between heterogeneities. Activation of one heterogeneity blocks the activation of the other in a winner takes all fashion (Fig. 5.7c). We change the fraction of stimulated neurons (i.e. the neurons are driven with additional sub-threshold dc current) in heterogeneity 2, while the number of stimulated neurons in heterogeneity 1 remains constant (Fig. 5.7c,d). The heterogeneity 1 remains activated without significant change until the number of stimulated neurons in heterogeneity 2 exceeds that of heterogeneity 1. At that time there is a rapid switch in activation between the heterogeneities as heterogeneity 1 completely deactivates while heterogeneity 2 is fully activated. Thus, resonance shifts facilitated by targeted inhibitory coupling can separate network activity patterns and dynamically switch between activated network regions through sub-threshold input bias. Finally, in Figure 5.7d, we show that these results are robust against independent network realizations.

Finally, we show that the neuronal representation can also be distributed throughout the network and the resonance frequency shift can act as a feature binding mechanism for such a distributed representation. We illustrate how such a representation can be formed based on external input and easily retrieved based on intrinsic network dynamics (Fig 5.8). Initially, for a network with no additional coupling (i.e. no stored memory), a small additional sub-threshold current bias is given to a population of neurons spatially distributed in the network. The source of this additional current could be activation from sensory input. This current shifts the resonance frequency of neurons receiving the additional current into resonance with the driving oscillation (Fig 5.8a). The

distributed population is activated, forming a functionally correlated ensemble. Learning rules can strengthen these connections creating a structural heterogeneity that can later be reactivated with the same resonance frequency shift mechanism when no biasing current is present. We heuristically show the effect by artificially strengthening the connectivity between the same neuronal populations (Fig 5.8b).

5.4 Discussion

It has long been assumed that input from our sensory environment affects neuronal activity, which alters the strength of the synaptic connections between neurons, forming an interactive feedback between network structure and its activity patterns. However, little is known about how large scale network activity results from modifications in neuronal coupling strength and network connectivity, or the role of oscillations in information processing. Here we provide a robust mechanism for spatial temporal pattern formation and separation based on the interaction of resonance phenomena in individual neurons, large scale oscillatory rhythms, and heterogeneities in network connectivity.

We demonstrated that regions of higher coupling can provide additional current to neurons within a network heterogeneity, shifting their resonance curves and leading to differential activation properties in their firing frequency and phase locking with dynamically changing sub-threshold input. In addition, the fast response times of the model networks to dynamically shifting resonances is similar to the timescales for enhanced firing frequencies observed in the brain during pattern identification tasks[140–142].

These networks do not need to be limited to excitatory connections only; in fact the separation mechanism is enhanced by interactions with inhibitory neurons, which can allow for separation and switched between multiple representations. The described

mechanism works well within known biological constraints of the brain[129,130] and reproduces a number of experimental findings in terms of neuronal dynamics during memory retrieval[133–135].

Until now two, to some extent competing, population coding strategies have been proposed: rate[143] and spike-timing (synchrony) dependent[47,124,144] coding mechanisms. Neuronal activity patterns indicative of both of these schemes have been observed. Rate-coding is generally easy to explain and intuitive to understand as greater supra-threshold input can provide higher frequency rates. While understanding of the spike-timing dependent mechanisms underlying the formation of content dependent, network wide, brief, and synchronous population bursts remains elusive. It is also unclear how rate coding can provide the content dependent, dynamic pattern separation[40] needed for brain information processing.

The mechanism that we propose, based on sub-threshold input dependent resonance frequency shift, provides the theoretical solution to these inconsistencies and, furthermore, it links the two coding mechanisms together. Neurons that are in resonance with a given input oscillation will fire with higher frequency rates and also will phase lock to the oscillation, generating increased synchrony among themselves. Thus an input dependent resonance frequency shift provides means for dynamic content dependent grouping in frequency as well as phase domains.

While it clearly remains to be seen whether this mechanism plays a role in brain's information processing, in general it is not limited to biological neuronal networks but it provides a universal dynamical mechanism for information processing that can be applied to any network with oscillatory nodes.

Finally, it is worth noting that we used a linear dependence of resonant frequency on input. There are indications that this dependence could be non-linear due to type of transition from spiking to non-spiking neuronal state, specifically for type II neuronal excitability (subcritical Hopf bifurcation)[145–147].

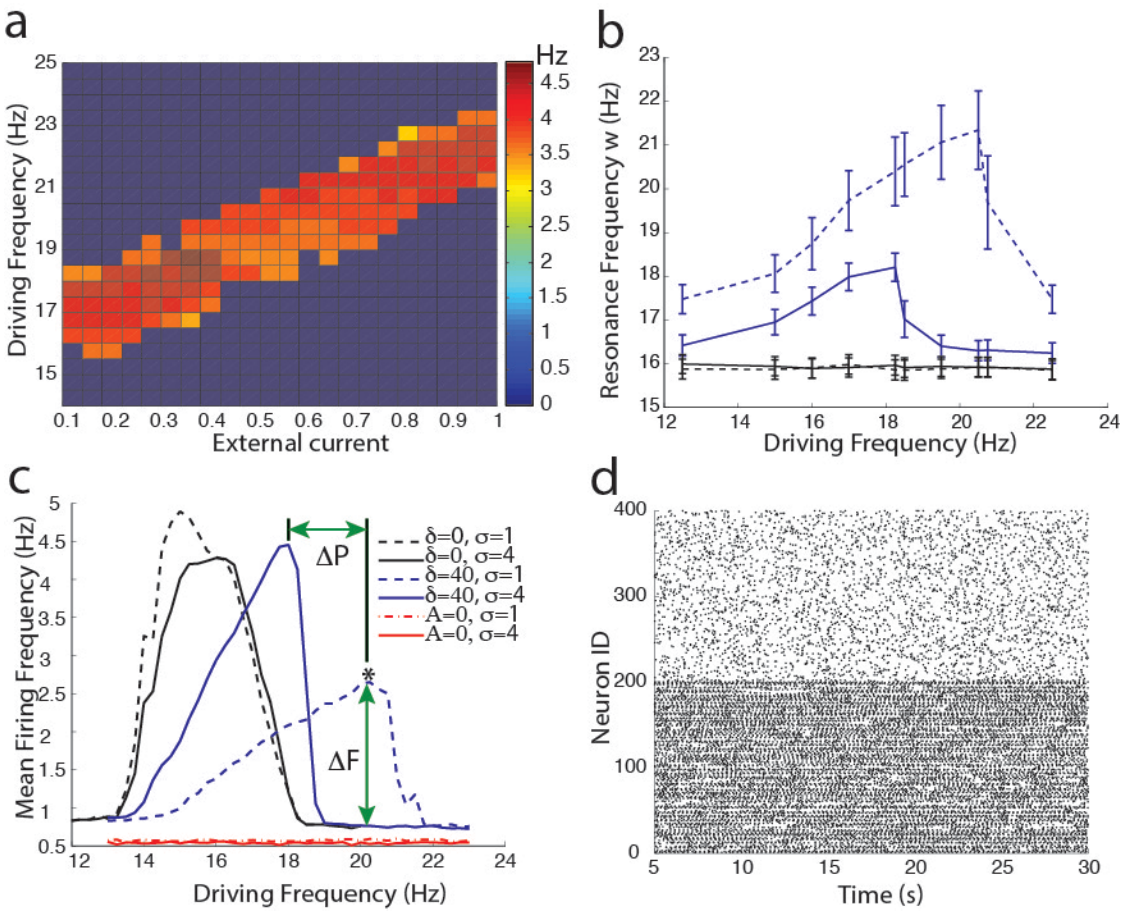

Figure 5.1. Intrinsic resonance frequency shifts is based on current input and allows for selective activation of regions of a network. (a) Single RF neuron firing frequency response to varying additional external current (I_{sub}) and driving frequency of sub-threshold current input. (b) The average resonance frequency ω in a network with (blue) and without (black) resonance frequency shift (δ=40 and δ=0, respectively). A sub-network (dashed lines) with additional coupling from synaptic multiplier (σ=4), has a shifted average resonance frequency from neurons outside of the heterogeneity (solid line). (c) Resonance curves of network firing across driving frequencies, shows a shift in resonance for the network heterogeneity (σ=4). For non-oscillatory current input (A=0), resonance is abolished. (d) Example raster plot of network activity for sub-threshold driving frequency of 20 Hz. A subset of the network, Neurons 1-200, have an enhanced coupling multiplier of σ=4 and are selectively activated by the sub-threshold oscillatory input.

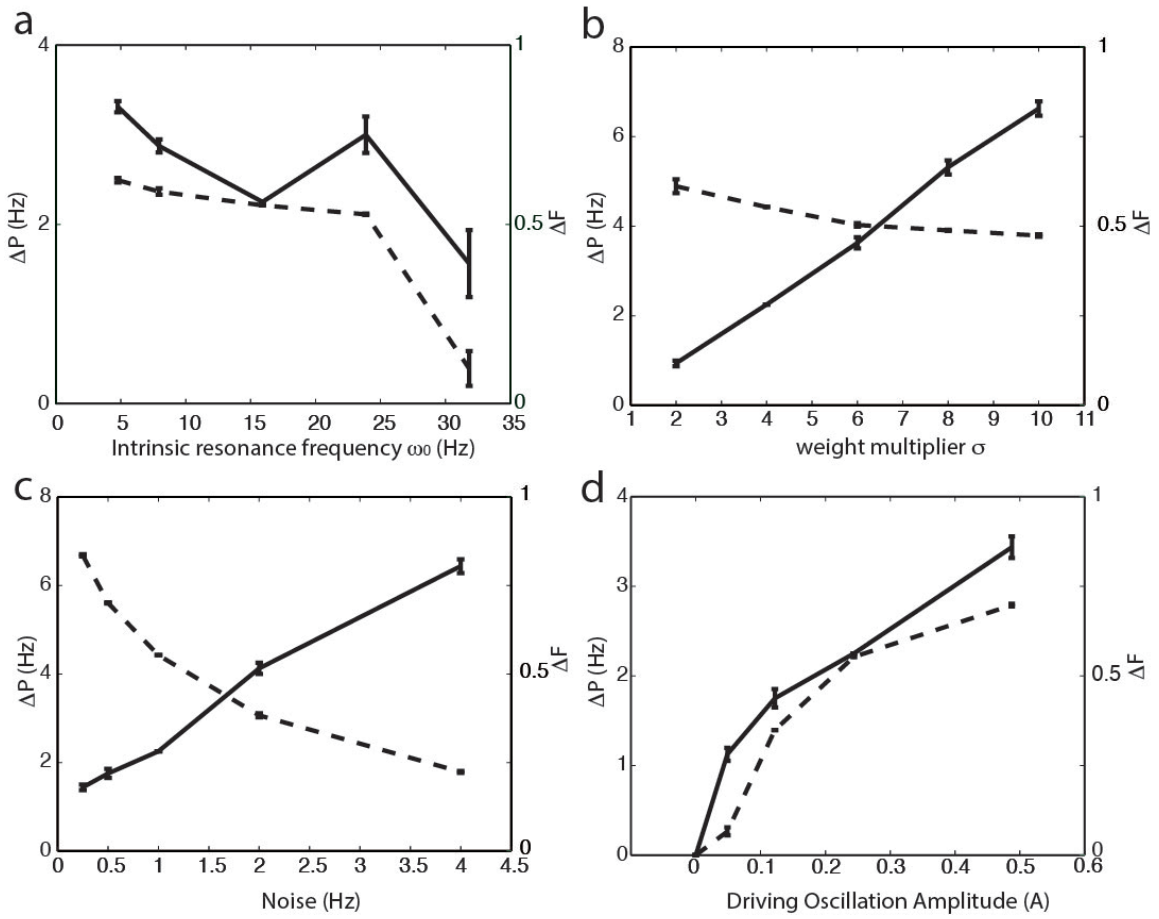

Figure 5.2. Robustness of the resonance based separation mechanism as a function of various system parameters for disconnected networks. Separation of signals is characterized with peak to peak distance ΔP (solid lines) and normalized firing frequency difference ΔF (dashed lines) for changing intrinsic cellular resonance frequencies ω_o (a), additional coupling weight σ (b), noise (c), and amplitude of sub-threshold oscillatory current A (d). For both ΔP and ΔF values above zero denote significant separation.

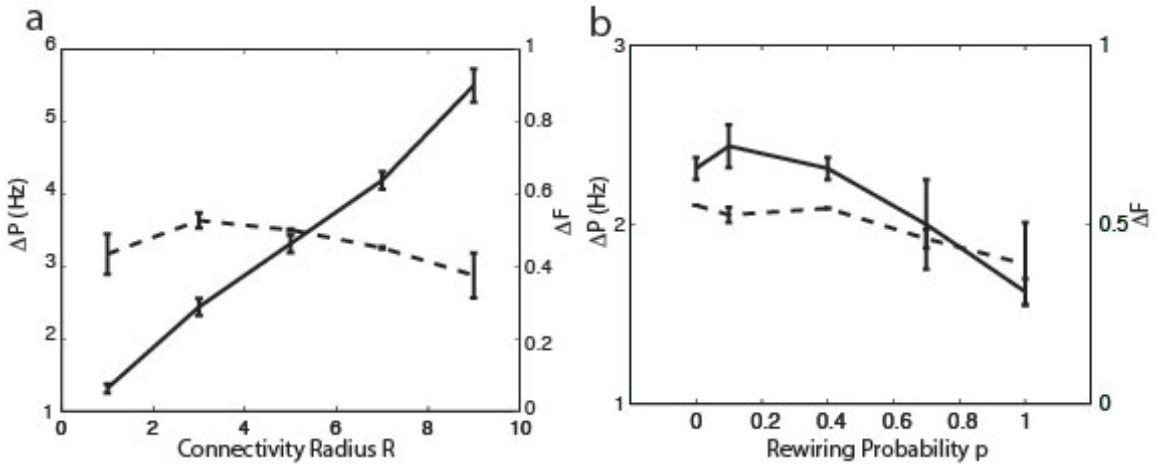

Figure 5.3. The influence of network topology on separation measures for connected network clusters. (a) Peak to peak separation ΔP (solid lines) increases for larger connectivity radius R. (B) Signal separation as a function of network topology (rewiring parameter p).

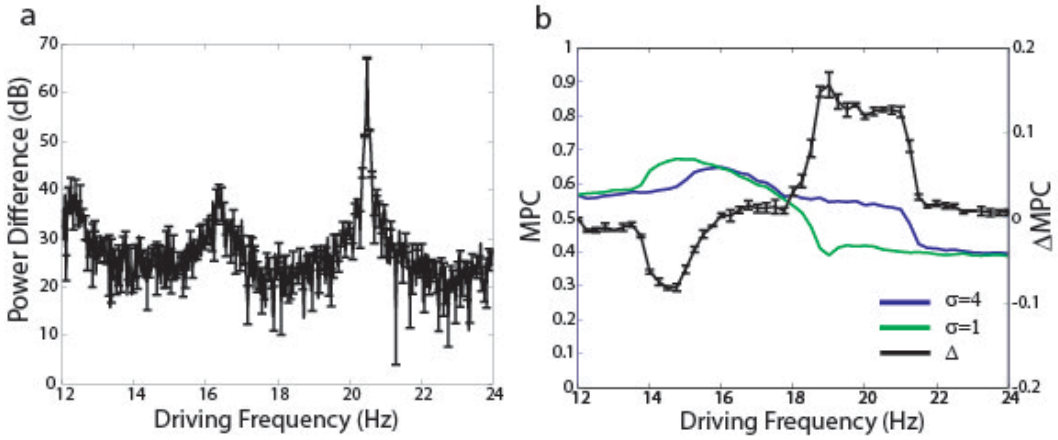

Figure 5.4. Total activity within heterogeneity shows separation in frequency content and increased phase coherence with the sub-threshold driving oscillation when in resonance. (a) Difference in power of total network activity (heterogeneity – outside heterogeneity) shows a peak in the power spectrum for resonant frequency of driving oscillation (marked with * in fig.1). (b) Difference in Mean Phase Coherence between sub-threshold oscillatory input and the activity signal formed within (blue) and outside (green) the heterogeneity.

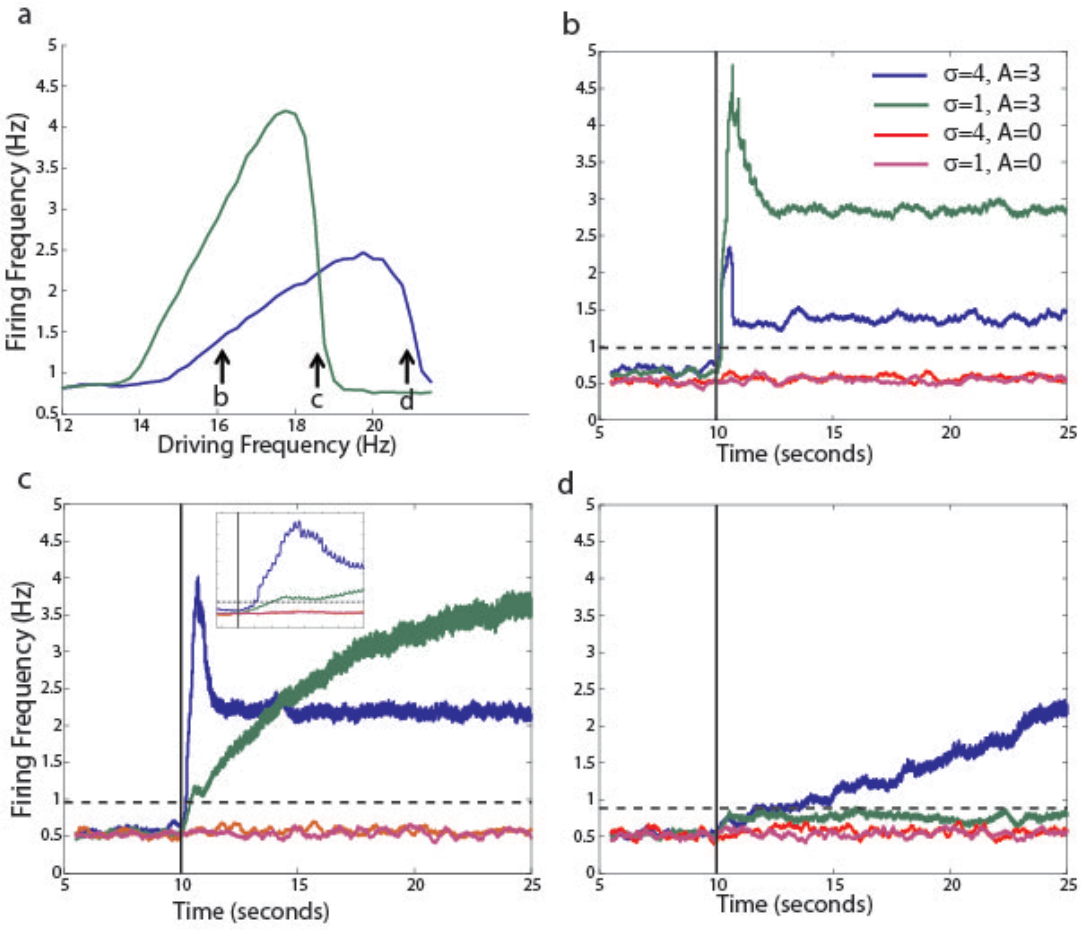

Figure 5.5. Response time to current induced resonance shift. a) Example resonance curves for a network after additional current input begins 10 seconds into the simulation. The current input shifts the resonance frequency of the neurons as marked by the arrows. (b-d) response times of the network depicted on (a) 16 Hz (b), 18.5 Hz (c), and 21 Hz (d). Solid black line marks the onset of additional sub-threshold current. The average instantaneous firing rate over time is plotted for neurons within and outside of the network heterogeneity (σ=4 and σ=1, respectively) and also for non-oscillatory current input (A=0). The inset in (c) shows the magnified timescale of firing onset. Black dashed lines mark 5 standard deviations above the baseline firing rate. All firing rate curves are averaged over 4 simulations.

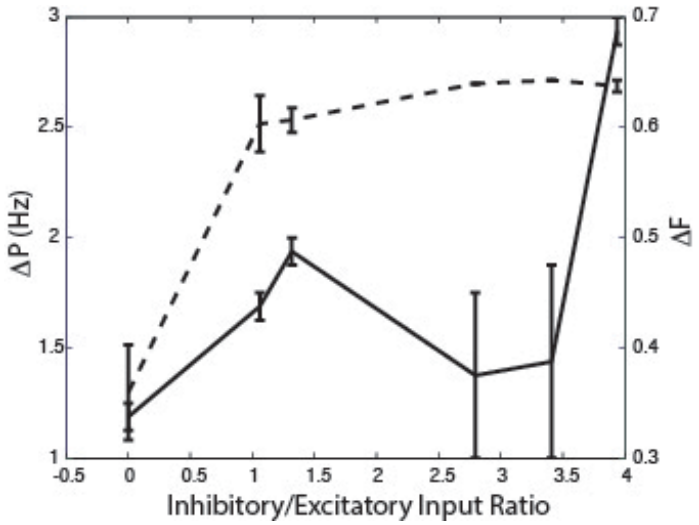

Figure 5.6. Firing rate difference ΔF (dashed line) and the peak-to-peak distance ΔP (solid line) as a function of inhibitory coupling strength. Inhibitory network strength is shown as a ratio of the inhibitory synaptic input to excitatory synaptic input (see methods). The separation mechanism is enhanced for networks in the balanced state (Inhib/Excit input ratio = 1), and also for larger inhibitory to excitatory input ratios, even with weaker resonance frequency shift (results shown are for $\delta = 10$). Values for Inhib/Excit input ratio are given for the peak of the resonance curve (18 Hz driving frequency).

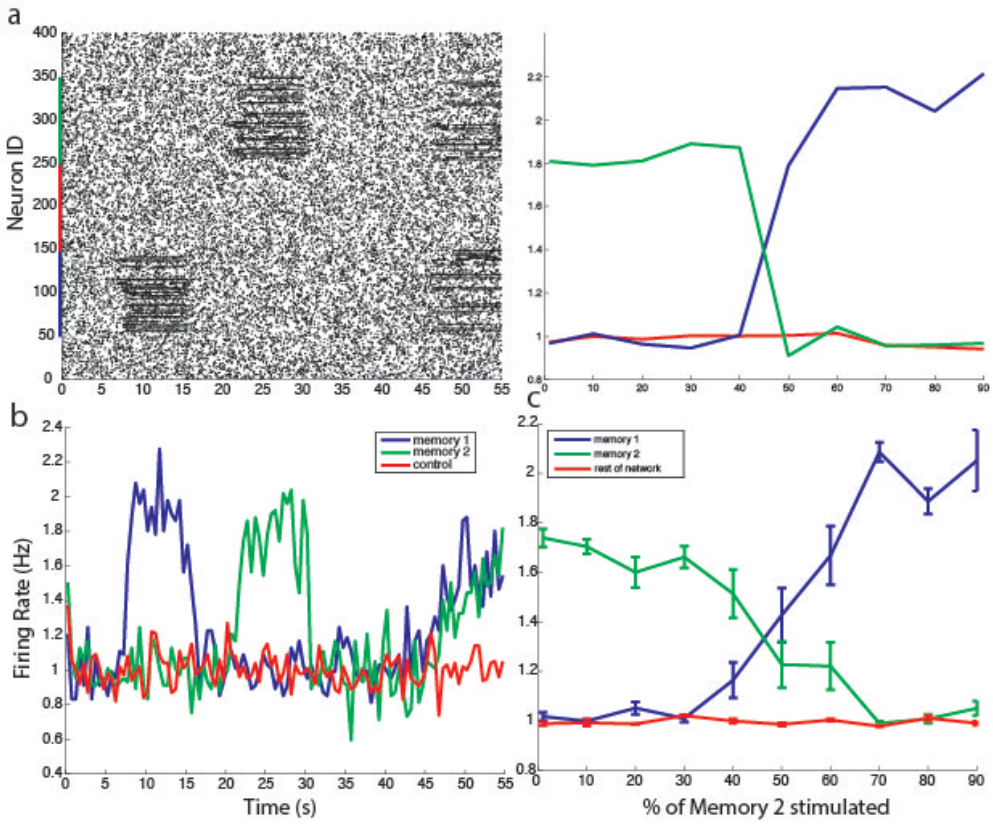

Figure 5.7. Resonance Frequency shift mechanism can selectively activate multiple competing heterogeneities through lateral inhibition. (a) Example raster plot shows selective switching between heterogeneities for a driving frequency of 25.5 Hz. Neurons with IDs 50 to 150 belong to one heterogeneity, while neurons with IDs 250 to 350 are in a second heterogeneity. Between 5 and 15 seconds of the simulation heterogeneity 1 is shifted into resonance with sub-threshold input applied a randomly chosen subset of 50% of neurons in that heterogeneity. Similarly, Heterogeneity 2 is shifted into resonance with sub-threshold input, between 20 and 30 seconds of the simulation. As a control, a region outside of both heterogeneities (IDs 150 to 250) receives identical sub-threshold input between 35 and 45 seconds in the simulation, and results in no enhanced firing rate. (b) Corresponding firing rate responses of regions of the network to sub-threshold input shows multiple heterogeneities can be selectively activated. (c) Targeted inhibition can dynamically and rapidly switch activation between heterogeneities. Heterogeneity 1 is activated by sub-threshold stimulation of 50% of neurons belonging to that heterogeneity; the x-axis denotes the percentage of stimulated cells in second heterogeneity. The activation of heterogeneities switches rapidly as number of stimulated neurons in heterogeneity 2 grows. (d) Same as (c) averaged over four network representations, and error bars represent 1 standard error of the mean. Example shown for driving frequency of 21.5 Hz.

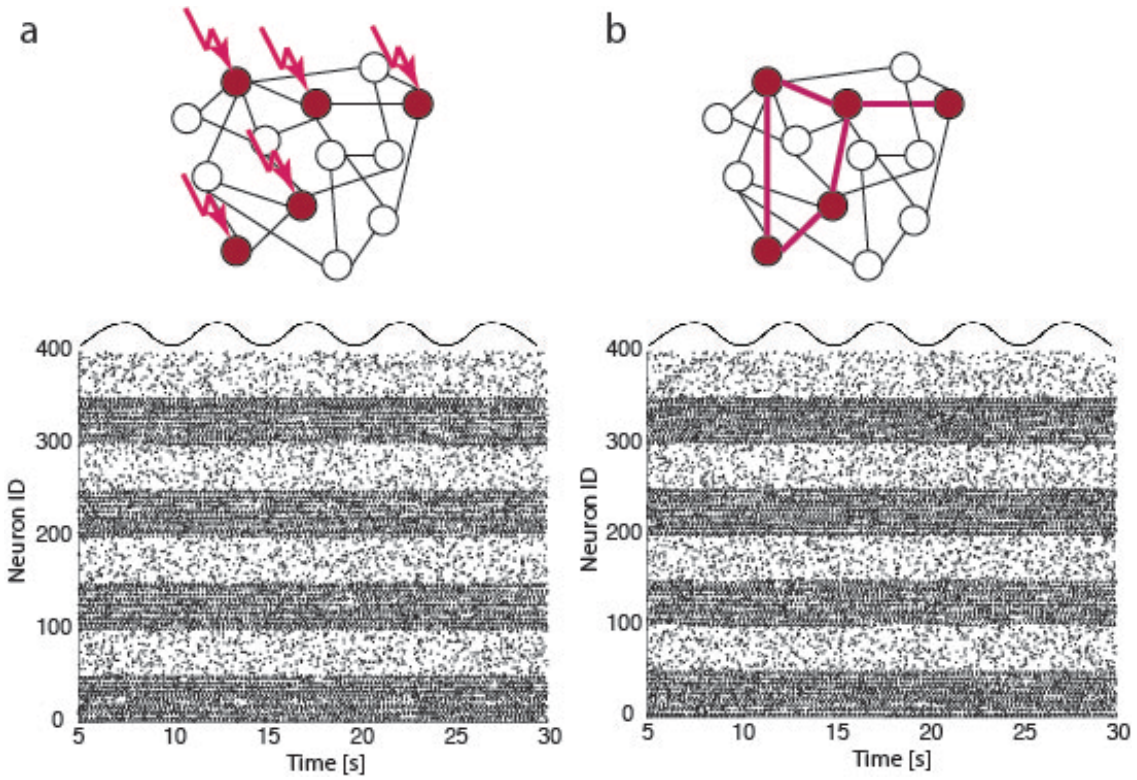

Figure 5.8. Resonance frequency shifts provide a mechanism for both functional and structural distributed network formation. (a) Sub-threshold input (arrows) driving a spatially distributed subset of the network (red circles), shifts the resonance frequency of those neurons creating a functional heterogeneity in the network, reflected in selective activation of functional clusters in the raster plot below. Learning mechanisms can strengthen these connections creating a distributed structural heterogeneity. (b) Distributed structural network heterogeneity (red circles) with additional coupling weight (thicker edges) is selectively activated based on the resonance frequency of sub-threshold input. Sub-threshold driving oscillations picture above raster plots are not to scale.

Chapter VI.

Summary and Conclusions

Neurons and glia are embedded and interconnected in complex networks. Networks of interacting components can self organize to form complex macroscopic processes, which emerge from local interactions between individual network components. The interactions between neurons through synaptic connections are dynamic and activity dependent. Chemical transmitter release from neurons can interact with astroctyes, particular types of glia, through activation of calcium signaling. In turn, calcium signaling can activate gliotransmission, which allows astrocytes to interact with both neurons and other astrocytes, in addition to the direction gap junction coupling between astrocytes. We see that the brain is composed of large numbers of interacting components, whose coordination and pattern formation underlies the emergent phenomena of brain function. This dissertation focuses on the interactions that can link activity patterns across microscopic to macroscopic scales, facilitating the emergence of brain function. I investigated mechanisms that can couple and coordinate collections of neurons in their patterns of activity, potentially causing interactions across spatial and temporal scales, which can underlie the powerful computational capabilities that emerge in the brain.

My work explored the coordination of network dynamics through pattern formation and synchrony in both experiments and simulations. Experimentally, I showed how networks of astrocytes form interconnected networks in the brain coupled via gap junctions. In Chapter III, we investigated modes of communication of astrocytes in mixed networks of glia and neurons. To do so, we imaged astrocyte calcium activity and quantified how perturbing the coupling between astrocytes influences astrocytic activity patterns in cultured networks. We reproduced the observed properties of the network calcium patterning and perturbations with a simple model that incorporates the two mechanisms of astrocyte communication: gap junction coupling (active coupling) and diffusive coupling of extracellular chemical release (passive coupling). We showed that gap junctions and extracellular chemical release interact in astrocyte networks to modulate the spatial temporal patterns of their calcium dynamics.

Chapter IV investigated how glial cells modulate neuronal dynamics and synchrony, through quantifying the spontaneous spiking patterns of neurons in dissociated rat hippocampal cultures. We studied cultures that were grown in two conditions: the first supporting glial cell growth (high glial group), and the second one inhibiting it (low glial group). We performed structural network studies as well as investigated the spatio-temporal activity patterns of the neurons. Differences in dynamics between the two groups could be linked to the impact of the glial network on the neuronal network as the cultures developed. We also implemented the Functional Clustering Algorithm (FCA) to obtain the resulting functional network structure. The FCA detects changes in functional structure that are consistent with expected dynamical differences due to the impact of the glial network. Cultures in the high glial group showed an increase in global synchronization as the cultures aged, while those in the low glial group remained locally synchronized. We additionally

used the FCA to quantify the amount of synchronization present in the cultures and showed that the total level of synchronization in the high glial group was stronger than in the low glial group. These results suggest an interaction between the glial and neuronal networks present in dissociated cultures, and that glial networks influence the coordination and synchrony among populations of neurons.

In Chapter V, I demonstrated in a computational model of how biophysical cellular properties, such as the resonance properties of individual neurons, interact with the network topology to influence pattern formation and separation. We investigated a theoretical mechanism for selective activation of diverse neural populations that is based on dynamically shifting cellular resonances in functionally or structurally coupled networks. We specifically showed that sub-threshold neuronal depolarization from synaptic coupling or external input can shift neurons into and out of resonance with specific bands of existing extracellular oscillations, and this can act as a dynamic readout mechanism during information storage and retrieval.

We found that this mechanism is robust and suggest it as a general coding strategy to facilitate the emergence of the computational abilities in the brain. The resonance shift mechanism supports both rate and temporal neural coding schemes. The mechanism was able to separate assemblies in both their firing rate and their coherence with the driving oscillation. In addition, the mechanism separated assemblies spatially by their enhanced connectivity domains and temporally in their timescale to form elevated firing rate patterns.

Mechanisms that can couple and coordinate collections of neurons in their patterns of activity can potentially cause interactions across spatial and temporal scales. Due to their ability to interact and modulate neurons and their synaptic connections, we investigated the

role of astrocyte networks as a potential source for coordinating neuronal assemblies. Astroctyes may play an additional role as they could potentially provide a source of additional depolarization in the resonance shift mechanism. In the work presented on the resonance shift mechanism, the source of depolarization is either from enhanced synaptic coupling or sub-threshold external input. This sub-threshold external input may arise due to sensory activation, neuromodulatory input from other brain regions, or potentially astrocyte network gliotransmission. Through release of transmitters, astrocytes may facilitate the resonance shift mechanism for coordinating and segmenting the activity patterns in collections of neurons both spatially and temporally. This mechanism could potentially unify the cellular substrates for coding with the emergence of information processing in brain networks. Further work needs to be done to verify if resonance shifts and astrocyte network calcium signaling can be linked to neuronal network function and computations. As experimental techniques advance, one hopes to test the proposed mechanism in awake behaving animal models to link the electrophysiology of individual neurons, the spatiotemporal activity patterns of neuronal networks, and the behavioral output.

BIBLIOGRAPHY

1. Nicolis, G. and Prigogine, I. Self-Organization in Non- Equilibrium Systems: From Dissipative Structures to Order Through Fluctuations. *Wiley* (1977).

2. Haken, H. Information and Self-organization: A Macroscopic Approach to Complex Systems. *Springer-Verlag, Berlin.* (1988).

3. Chaitin, G. J. Irreducible complexity in pure mathematics. *Arxiv Prepr. math/0411091.* (2004).

4. Anderson, P. W. More is different. *Science (80-.).* **177,** 393–396 (1972).

5. C., G. A general methodolgy for designing self-organizing systems. *Tech. Rep* (2005).

6. HEYLIGHEN, F. AND CAMPBELL, D. T. Selection of organization at the social level: Obstacles and facilitators of metasystem transitions. *World Futur. J. Gen. Evol.* **45,** 181–212 (1995).

7. Heylighen, F. Self-organization , Emergence and the Architecture of Complexity.

8. Strogatz, S. H. Nonlinear Dynamics and Chaos: With Applications to Physics, Biology, Chemistry and Engineering. *Perseus Books Gr.* **ISBN: 0738,**

9. Jeanson, R., Dussutour, A. & Fourcassié, V. Key factors for the emergence of collective decision in invertebrates. *Front. Neurosci.* **6,** 121 (2012).

10. F., H. The science of self-organization and adaptivity. *EOLSS Publ. Oxford* (2003).

11. Roces, F. Individual Complexity and Self-Organization in Foraging by Leaf-Cutting Ants. 306–313 (2002).

12. Segota, I., Boulet, L., Franck, D. & Franck, C. Spontaneous emergence of large-scale cell cycle synchronization in amoeba colonies. *Phys. Biol.* **11,** 036001 (2014).

13. Pearce, D. J. G., Miller, A. M., Rowlands, G. & Turner, M. S. Role of projection in the control of bird flocks. *Proc. Natl. Acad. Sci. U. S. A.* **111,** 10422–6 (2014).

14. López-Muñoz, F., Boya, J. & Alamo, C. Neuron theory, the cornerstone of neuroscience, on the centenary of the Nobel Prize award to Santiago Ramón y Cajal. *Brain Res. Bull.* **70,** 391–405 (2006).

15. Blank, H., Wieland, N. & von Kriegstein, K. Person recognition and the brain: Merging evidence from patients and healthy individuals. *Neurosci. Biobehav. Rev.* **47C,** 717–734 (2014).

16. Malsburg, von der C. The correlation theory of brain function. *Intern. Rep. 81-2. Max-Planck-Institut für Biophys. Chemie, Göttingen, Ger.* 1981 (1981).

17. Singer, W. & Gray, C. M. Visual feature integration and the temporal correlation hypothesis. *Annu. Rev. Neurosci.* **18,** 555–586 (1995).

18. Kandel E., S. J. Principles of Neural Science. *ISBN-10 0838577016 Ed. 4th* (2000).

19. Money, K. M. & Stanwood, G. D. Developmental origins of brain disorders: roles for dopamine. *Front. Cell. Neurosci.* **7,** 260 (2013).

20. Eppinger, B., Hämmerer, D. & Li, S.-C. Neuromodulation of reward-based learning and decision making in human aging. *Ann. N. Y. Acad. Sci.* **1235,** 1–17 (2011).

21. Lee, S.-H. & Dan, Y. Neuromodulation of brain states. *Neuron* **76,** 209–22 (2012).

22. Sarter, M., Hasselmo, M. E., Bruno, J. P. & Givens, B. Unraveling the attentional functions of cortical cholinergic inputs: interactions between signal-driven and cognitive modulation of signal detection. *Brain Res. Brain Res. Rev.* **48,** 98–111 (2005).

23. Sarter, M., Lustig, C., Howe, W. M., Gritton, H. & Berry, A. S. Deterministic functions of cortical acetylcholine. *Eur. J. Neurosci.* 1–9 (2014). doi:10.1111/ejn.12515

24. Parikh, V. & Sarter, M. Cholinergic mediation of attention: contributions of phasic and tonic increases in prefrontal cholinergic activity. *Ann. N. Y. Acad. Sci.* **1129,** 225–35 (2008).

25. Anderson, J., Rosenfeld, E. & Hebb, D. O. The Organization of Behavior. (1989).

26. Bi, G. & Poo, M. Synaptic Modifications in Cultured Hippocampal Neurons : Dependence on Spike Timing , Synaptic Strength , and Postsynaptic Cell Type. **18,** 10464–10472 (1998).

27. Lendvai, B., Stern, E. A., Chen, B. & Svoboda, K. Experience-dependent plasticity of dendritic spines in the developing rat barrel cortex in vivo. **404,** 1–6 (2000).

28. Boccaletti, S., Latora, V., Moreno, Y., Chavez, M. & Hwang, D. Complex networks: Structure and dynamics. *Phys. Rep.* **424,** 175–308 (2006).

29. Percha, B., Dzakpasu, R., Żochowski, M. & Parent, J. Transition from local to global phase synchrony in small world neural network and its possible implications for epilepsy. *Phys. Rev. E* **72,** 031909 (2005).

30. Watts, D. J. & Strogatz, S. H. Collective dynamics of "small-world" networks. **393,** 440–442 (1998).

31. Barabasi, A.-L. & Albert, R. Emergence of scaling in random networks. 11 (1999). at <http://arxiv.org/abs/cond-mat/9910332>

32. Bonifazi, P. *et al.* GABAergic Hub Neurons Orchestrate Synchrony in Developing Hippocampal Networks.

33. Beggs, J. M. & Plenz, D. Neuronal Avalanches in Neocortical Circuits. **23,** 11167–11177 (2003).

34. Rosenberg, T. *et al.* The roles of protein expression in synaptic plasticity and memory consolidation. *Front. Mol. Neurosci.* **7,** 86 (2014).

35. Mayo, J. P. & Sommer, M. A. Neuronal correlates of visual time perception at brief timescales. (2012). doi:10.1073/pnas.1217177110/-/DCSupplemental.www.pnas.org/cgi/doi/10.1073/pnas.1217177110

36. Miller, J. -e. K., Ayzenshtat, I., Carrillo-Reid, L. & Yuste, R. Visual stimuli recruit intrinsically generated cortical ensembles. *Proc. Natl. Acad. Sci.* **2014,** 1–9 (2014).

37. Hubel, D. H. & Wiesel, T. N. Receptive fields of single neurones in the cat's striate cortex. *J. Physiol.* **148,** 574–591 (1959).

38. Wang, X. & Walker, K. M. M. Neural mechanisms for the abstraction and use of pitch information in auditory cortex. *J. Neurosci.* **32,** 13339–42 (2012).

39. O'Keefe, J. & Recce, M. L. Phase relationship between hippocampal place units and the EEG theta rhythm. *Hippocampus* **3,** 317–30 (1993).

40. Gerstner, W., Kreiter, A. K., Markram, H. & Herz, A. V. M. Neural codes : Firing rates and beyond. **94,** 12740–12741 (1997).

41. Richmond, B. J. Temporal Encoding of Two-Dimensional Patterns by Single Units in Primate Inferior Temporal Cortex . I . Response Characteristics. *J. Neurophysiol.* **57,** 132–146 (1987).

42. Richmond, J. & Opttcan, M. Temporal Encoding of Two-Dimensional Patterns by Single Units in Primate Primary Visual Cortex . I . Stimulus-Response Relations. *J. Neurophysiol.* **64,** (1990).

43. Middlebrooks, J. C., Clock, A. E., Xu, L. & Green, D. M. Code for Sound Location by Cortical Neurons. *Science (80-.).* **264,** 842–844 (2014).

44. Abeles, M., Margalit, E. & Vaadia, E. Spatiotemporal Firing Patterns in the Frontal Cortex of Behaving Monkeys. *J. Neurophysiol.* **70,** 1629–1638 (1993).

45. Freeman, W. The Physiology of Perception. *Sci. Am.* 78–85 (1991).

46. Wagemans J, Elder JH, Kubovy M, Palmer SE, Peterson MA, Singh M, von der H. R. A Century of Gestalt Psychology in Visual Perception: I. Perceptual grouping and figure-ground organization. (2012).

47. Malsburg, C. Von Der. The What and Why of Binding : The Modeler ' s Perspective. **24,** 95–104 (1999).

48. Mason, A., Nicoll, A. & Stratford, K. Synaptic Transmission between Individual R & t Visual Cortex in vitro Pyramidal Neurons of the. *J. Neurosci.* **11,** 72–84 (1991).

49. Izhikevich, E. M. Resonate-and-fire neurons. *Neural Netw.* **14,** 883–94 (2001).

50. Sanhueza, M. & Bacigalupo, J. Intrinsic subthreshold oscillations of the membrane potential in pyramidal neurons of the olfactory amygdala. *Eur. J. Neurosci.* **22,** 1618–26 (2005).

51. Alonso, A. & Llinas, R. R. Subthreshold Na+ dependent theta-like rhythmicity in stellate cells of entorhinal coretex layer II. *Nature* **342,** 175 (1989).

52. Izhikevich, E. M. Dyamical Systems in Neuroscience, The Geometry of Excitabitilty and Bursting. *MIT Press.* 14 (2007).

53. Prescott, S. a, Ratté, S., De Koninck, Y. & Sejnowski, T. J. Pyramidal neurons switch from integrators in vitro to resonators under in vivo-like conditions. *J. Neurophysiol.* **100,** 3030–42 (2008).

54. Wang, W.-T. *et al.* Theta-frequency membrane resonance and its ionic mechanisms in rat subicular pyramidal neurons. *Neuroscience* **140,** 45–55 (2006).

55. Hu, H., Vervaeke, K. & Storm, J. F. Two forms of electrical resonance at theta frequencies, generated by M-current, h-current and persistent Na+ current in rat hippocampal pyramidal cells. *J. Physiol.* **545,** 783–805 (2002).

56. Fellin, T. Communication between neurons and astrocytes: relevance to the modulation of synaptic and network activity. *J. Neurochem.* **108,** 533–44 (2009).

57. Agulhon, C. *et al.* What is the role of astrocyte calcium in neurophysiology? *Neuron* **59,** 932–46 (2008).

58. Innocenti, B., Parpura, V. & Haydon, P. G. Imaging Extracellular Waves of Glutamate during Calcium Signaling in Cultured Astrocytes. **20,** 1800–1808 (2000).

59. Halassa, M. M., Fellin, T. & Haydon, P. G. The tripartite synapse: roles for gliotransmission in health and disease. *Trends Mol. Med.* **13,** 54–63 (2007).

60. Haydon, P. G. GLIA : LISTENING AND TALKING TO THE SYNAPSE. **2,** (2001).

61. Feldt, S. *et al.* Functional clustering in hippocampal cultures: relating network structure and dynamics. *Phys. Biol.* **7,** 046004 (2010).

62. Hales, C. M., Rolston, J. D. & Potter, S. M. How to culture, record and stimulate neuronal networks on micro-electrode arrays (MEAs). *J. Vis. Exp.* 1–7 (2010). doi:10.3791/2056

63. Potter, S. M. & DeMarse, T. B. A new approach to neural cell culture for long-term studies. *J. Neurosci. Methods* **110,** 17–24 (2001).

64. Wagenaar, D. a, Pine, J. & Potter, S. M. An extremely rich repertoire of bursting patterns during the development of cortical cultures. *BMC Neurosci.* **7,** 11 (2006).

65. Burkitt, a N. A review of the integrate-and-fire neuron model: I. Homogeneous synaptic input. *Biol. Cybern.* **95,** 1–19 (2006).

66. Sasai, Y. Cytosystems dynamics in self-organization of tissue architecture. *Nature* **493,** 318–26 (2013).

67. Westerhoff, H. V *et al.* Macromolecular networks and intelligence in microorganisms. *Front. Microbiol.* **5,** 379 (2014).

68. Stevens, B. Glia: much more than the neuron's side-kick. *Curr. Biol.* **13,** R469–R472 (2003).

69. Newman, E. a. Calcium Waves in Retinal Glial Cells. *Science (80-.).* **275,** 844–847 (1997).

70. Yuzo, T., Mriguchi, H., Kotani, K. & Jimbo, Y. Spontaneous Calcium Transients in Cultured Cortical Networks During Development. *IEE Trans. Biomed. Eng.* **56,** 2949–2956 (2009).

71. Sasaki, T., Kuga, N., Namiki, S., Matsuki, N. & Ikegaya, Y. Locally synchronized astrocytes. *Cereb. Cortex* **21,** 1889–900 (2011).

72. Koizumi, S. Synchronization of Ca2+ oscillations: involvement of ATP release in astrocytes. *FEBS J.* **277,** 286–92 (2010).

73. Ann, H., Steven, M., Mark, S. & Stephen, J. Glutamate Induces Calcium Waves in Cultured Astrocytes : Long-Range Glial Signaling (1990).

74. Henneberger, C., Papouin, T., Oliet, S. H. R. & Rusakov, D. a. Long-term potentiation depends on release of D-serine from astrocytes. *Nature* **463,** 232–6 (2010).

75. Giaume, C. Astroglial Wiring is Adding Complexity to Neuroglial Networking. *Front. Neuroenergetics* **2,** 1–7 (2010).

76. Maruyama, D. Competition and cooperation between active network processes and passive ones defined in the physical space. 1–11 (2014).

77. Nimmerjahn, A., Kirchhoff, F., Kerr, J. N. D. & Helmchen, F. Sulforhodamine 101 as a specific marker of astroglia in the neocortex in vivo. *Nat. Methods* **1,** 31–7 (2004).

78. Feldt Muldoon, S., Soltesz, I. & Cossart, R. Spatially clustered neuronal assemblies comprise the microstructure of synchrony in chronically epileptic networks. *Proc. Natl. Acad. Sci. U. S. A.* **110,** 3567–72 (2013).

79. Maruyama, D. & Zochowski, M. Competition and cooperation between active intra-network and passive extra-network transport processes. *Sci. Rep.* **4,** 5269 (2014).

80. Region, S., Koller, H., Siebler, M., Schmalenbach, C. & Muller, H. GABA and Glutamate Receptor Development of Cultured Neurons from Rat. **64,** 59–64 (1990).

81. Cerro, S. D. E. L., Garcia-estrada, J. & Garcia-segura, L. M. Neuroactive Steroids Regulate Astroglia Morphology in Hippocampal Cultures From Adult Rats. **6571,** (1995).

82. Tian, G.-F. *et al.* An astrocytic basis of epilepsy. *Nat. Med.* **11,** 973–81 (2005).

83. Tashiro, A., Goldberg, J. & Yuste, R. Calcium oscillations in neocortical astrocytes under epileptiform conditions. *J. Neurobiol.* **50,** 45–55 (2002).

84. Newman, M. E. J. Modularity and community structure in networks. *Proc. Natl. Acad. Sci. U. S. A.* **103,** 8577–82 (2006).

85. R. Fuimera, S. Mossa, A. Turtxchi, L. A. N. A. The worldwide air transportation network: Anomalous centrality, community structure , cities' global roles. *Natl. Acad. Sci.* **102,** 7794–7799 (2005).

86. Leicht, E. & Newman, M. Community Structure in Directed Networks. *Phys. Rev. Lett.* **100,** 118703 (2008).

87. Eldawlatly, S., Jin, R. & Oweiss, K. G. Identifying functional connectivity in large-scale neural ensemble recordings: a multiscale data mining approach. *Neural Comput.* **21,** 450–77 (2009).

88. Fingelkurts, A. a, Fingelkurts, A. a & Kähkönen, S. Functional connectivity in the brain--is it an elusive concept? *Neurosci. Biobehav. Rev.* **28,** 827–36 (2005).

89. Friston, K. J., Frith, C. D., Liddle, P. F. & Frackowiak, R. S. Functional connectivity: the principal-component analysis of large (PET) data sets. *J. Cereb. Blood Flow Metab.* **13,** 5–14 (1993).

90. Zhou, C., Zemanová, L., Zamora-López, G., Hilgetag, C. C. & Kurths, J. Structure–function relationship in complex brain networks expressed by hierarchical synchronization. *New J. Phys.* **9,** 178–178 (2007).

91. Breakspear, M., Sporns, O., Honey, C. J. & Ko, R. Network structure of cerebral cortex shapes functional connectivity on multiple time scales. (2007).

92. Honey, C. J. *et al.* Predicting human resting-state functional connectivity. **106,** 1–6 (2009).

93. Bowman, F. D., Zhang, L., Derado, G. & Chen, S. Determining functional connectivity using fMRI data with diffusion-based anatomical weighting. *Neuroimage* **62,** 1769–79 (2012).

94. Koch, M. a, Norris, D. G. & Hund-Georgiadis, M. An investigation of functional and anatomical connectivity using magnetic resonance imaging. *Neuroimage* **16,** 241–50 (2002).

95. Dichter, M. A. Rat cortical neurons in cell culture: culture methods, cell morphology, electrophysiology, and synapse formation. *Brain Res.* **149,** 279–293 (1978).

96. Shahaf, G. & Marom, S. Learning in Networks of Cortical Neurons. **21,** 8782–8788 (2001).

97. Segev, R., Benveniste, M., Shapira, Y. & Ben-Jacob, E. Formation of Electrically Active Clusterized Neural Networks. *Phys. Rev. Lett.* **90,** 168101 (2003).

98. Cohen, E., Ivenshitz, M., Amor-Baroukh, V., Greenberger, V. & Segal, M. Determinants of spontaneous activity in networks of cultured hippocampus. *Brain Res.* **1235,** 21–30 (2008).

99. Rolston, J. D., Wagenaar, D. a & Potter, S. M. Precisely timed spatiotemporal patterns of neural activity in dissociated cortical cultures. *Neuroscience* **148,** 294–303 (2007).

100. Baruchi, I., Volman, V., Raichman, N., Shein, M. & Ben-Jacob, E. The emergence and properties of mutual synchronization in in vitro coupled cortical networks. *Eur. J. Neurosci.* **28,** 1825–35 (2008).

101. Ham, M. I., Bettencourt, L. M., McDaniel, F. D. & Gross, G. W. Spontaneous coordinated activity in cultured networks: analysis of multiple ignition sites, primary circuits, and burst phase delay distributions. *J. Comput. Neurosci.* **24,** 346–57 (2008).

102. Raichman, N. & Ben-Jacob, E. Identifying repeating motifs in the activation of synchronized bursts in cultured neuronal networks. *J. Neurosci. Methods* **170,** 96–110 (2008).

103. Pasquale, V., Massobrio, P., Bologna, L. L., Chiappalone, M. & Martinoia, S. Self-organization and neuronal avalanches in networks of dissociated cortical neurons. *Neuroscience* **153,** 1354–69 (2008).

104. Ivenshitz, M. & Segal, M. Simultaneous NMDA-dependent long-term potentiation of EPSCs and long-term depression of IPSCs in cultured rat hippocampal neurons. *J. Neurosci.* **26,** 1199–210 (2006).

105. Li, Y., Zhou, W., Li, X., Zeng, S. & Luo, Q. Dynamics of learning in cultured neuronal networks with antagonists of glutamate receptors. *Biophys. J.* **93,** 4151–8 (2007).

106. Sombati, S. & Delorenzo, R. J. Recurrent Spontaneous Seizure Activity Networks in Culture in Hippocampal Neuronal. **73,** (1995).

107. Srinivas, K. V, Jain, R., Saurav, S. & Sikdar, S. K. Small-world network topology of hippocampal neuronal network is lost, in an in vitro glutamate injury model of epilepsy. *Eur. J. Neurosci.* **25,** 3276–86 (2007).

108. Furshpan, E. J. Seizure-like Activity in Rat Hippocampal and Cellular Damage Neurons in Cell Culture. (1989).

109. Wallace, L. & Johnson, M. Cytosine Arabinoside Kills Postmitotic Neurons : Evidence That Deoxycytidine May Have a Role in Neuronal Survival That Is Independent of DNA Synthesis. **9,** (1989).

110. Brewer, G. J., Torricelli, J. R., Evege, E. K. & Price, P. J. Optimized Survival of Hippocampal Neurons in B27-Supplemented Neurobasalm , a New Serum-free Medium Combination. **35567476,** (1993).

111. Pfrieger, F. W. & Barres, B. A. Synaptic Efficacy Enhanced by Glial Cells in Vitro. 2–6

112. Nett, W. J., Oloff, S. H., Carthy, K. E. N. D. M. C., Wolfgang, J. & Hip-, K. D. M. Hippocampal Astrocytes In Situ Exhibit Calcium Oscillations That Occur Independent of Neuronal Activity. 528–537 (2002).

113. Pasti, L., Volterra, A., Pozzan, T. & Carmignoto, G. Intracellular Calcium Oscillations in Astrocytes : A Highly Plastic , Astrocytes In Situ. **17,** 7817–7830 (1997).

114. Verderio, C. *et al.* Astrocytes are required for the oscillatory activity in cultured hippocampal neurons. *Eur. J. Neurosci.* **11,** 2793–2800 (1999).

115. Volman, V., Gerkin, R. C., Lau, P.-M., Ben-Jacob, E. & Bi, G.-Q. Calcium and synaptic dynamics underlying reverberatory activity in neuronal networks. *Phys. Biol.* **4,** 91–103 (2007).

116. Fellin, T. *et al.* Endogenous nonneuronal modulators of synaptic transmission control cortical slow oscillations in vivo. *Proc. Natl. Acad. Sci. U. S. A.* **106,** 15037–42 (2009).

117. Feldt, S., Waddell, J., Hetrick, V., Berke, J. & Żochowski, M. Functional clustering algorithm for the analysis of dynamic network data. *Phys. Rev. E* **79,** 056104 (2009).

118. Soussou, W. V, Yoon, G. J., Brinton, R. D., Berger, T. W. & Member, S. Neuronal Network Morphology and Electrophysiologyof Hippocampal Neurons Cultured on Surface-Treated Multielectrode Arrays. **54,** 1309–1320 (2007).

119. Chang, J. C., Brewer, G. J. & Wheeler, B. C. Neuronal network structuring induces greater neuronal activity through enhanced astroglial development. *J. Neural Eng.* **3,** 217–26 (2006).

120. Barahona, M. & Pecora, L. M. Synchronization in Small-World Systems. *Phys. Rev. Lett.* **89,** 054101 (2002).

121. Manor, Y. *et al.* Low-Amplitude Oscillations in the Inferior Olive : A Model Based on Electrical Coupling of Neurons With Heterogeneous Channel Densities plasticity Low-Amplitude Oscillations in the Inferior Olive : A Model Based on Electrical Coupling of Neurons With Hete. *J. Neurophysiol.* **77,** 2736–2752 (2014).

122. Ainsworth, M. *et al.* Rates and rhythms: a synergistic view of frequency and temporal coding in neuronal networks. *Neuron* **75,** 572–83 (2012).

123. Hutcheon, B. & Yarom, Y. Resonance , oscillation and the intrinsic frequency preferences of neuron. *Trends Neurosci.* **2236,** (2000).

124. Gray, C. M. & Singer, W. Stimulus-specific neuronal oscillations in orientation columns of cat visual cortex. *Proc. Natl. Acad. Sci. U. S. A.* **86,** 1698–702 (1989).

125. Murthy, V. N. & Fetz, E. E. Coherent 25- to 35-Hz oscillations in the sensorimotor cortex of awake behaving monkeys. *Proc. Natl. Acad. Sci. U. S. A.* **89,** 5670–4 (1992).

126. Laurent, G. & Davidowitz, H. Encoding of olfactory information with oscillating neural assemblies. *Science* **265,** 1872–5 (1994).

127. Thut, G. & Miniussi, C. New insights into rhythmic brain activity from TMS-EEG studies. *Trends Cogn. Sci.* **13,** 182–9 (2009).

128. Van Kerkoerle, T. *et al.* Alpha and gamma oscillations characterize feedback and feedforward processing in monkey visual cortex. *Proc. Natl. Acad. Sci.* **111,** 14332–14341 (2014).

129. Buzsáki, G. & Draguhn, A. Neuronal oscillations in cortical networks. *Science* **304,** 1926–9 (2004).

130. Anastassiou, C. a, Perin, R., Markram, H. & Koch, C. Ephaptic coupling of cortical neurons. *Nat. Neurosci.* **14,** 217–23 (2011).

131. Koepsell, K. *et al.* Retinal oscillations carry visual information to cortex. *Front. Syst. Neurosci.* **3,** 4 (2009).

132. Bi, G. & Poo, M. Synamptic modification by correlated activity: Hebb's postulate revisited. *Annu. Rev. Neurosci.* **24,** 139–66 (2001).

133. Sato, N. & Yamaguchi, Y. Theta synchronization networks emerge during human object-place memory encoding. *Neuroreport* **18,** 419–24 (2007).

134. Kaplan, R. *et al.* Medial prefrontal theta phase coupling during spatial memory retrieval. *Hippocampus* **24,** 656–65 (2014).

135. Benchenane, K. *et al.* Coherent theta oscillations and reorganization of spike timing in the hippocampal- prefrontal network upon learning. *Neuron* **66,** 921–36 (2010).

136. Watts, D. J. & Strogatz, S. H. Collective dynamics of "small-world" networks. *Nature* **393,** 440–2 (1998).

137. Buzsáki, G. Theta Oscillations in the Hippocampus. *Neuron* **33,** 325–340 (2002).

138. Jensen, R. V. Synchronization of driven nonlinear oscillators. *Am. J. Phys.* **70,** 607 (2002).

139. Mormann, F., Lehnertz, K., David, P. & E. Elger, C. Mean phase coherence as a measure for phase synchronization and its application to the EEG of epilepsy patients. *Phys. D Nonlinear Phenom.* **144,** 358–369 (2000).

140. Rey, H. G., Fried, I. & Quian Quiroga, R. Timing of single-neuron and local field potential responses in the human medial temporal lobe. *Curr. Biol.* **24,** 299–304 (2014).

141. Mukamel, R. & Fried, I. Human intracranial recordings and cognitive neuroscience. *Annu. Rev. Psychol.* **63,** 511–37 (2012).

142. Sederberg, P. B., Kahana, M. J., Howard, M. W., Donner, E. J. & Madsen, J. R. Theta and gamma oscillations during encoding predict subsequent recall. *J. Neurosci.* **23,** 10809–14 (2003).

143. Adrian, E. D. & Zotterman, Y. J.Physiol. *J Physiol* **61,** 151–171 (1926).

144. Di, F., Theunissen, R. I. C. & Miller, J. P. Temporal Encoding in Nervous Systems : A Rigorous Definition. **162,** 149–162 (1995).

145. Stiefel, K. M., Gutkin, B. S. & Sejnowski, T. J. Cholinergic neuromodulation changes phase response curve shape and type in cortical pyramidal neurons. *PLoS One* **3,** e3947 (2008).

146. Ermentrout, G. B. Type I membranes, phase resetting curves, and synchrony. 8: 979–1001. *Neural Comput* **8,** 979–1001 (1996).

147. Ermentrout, G. B., Pascal, M. & Gutkin, B. The effects of spike frequency adaptation and negative feedback on the synchronization of neural oscillators. *Neural Comput* **13,** 1285–1310 (2001).